Yale University
EliScholar – A Digital Platform for Scholarly Publishing at Yale

Yale Medicine Thesis Digital Library | School of Medicine

5-2004

Mechanistic and structure-function analysis of thymidylate synthase-dihydrofolate reductase from protozoal parasites: implications for the development of non-active site inhibitors

Chloé E. Atreya
Yale University.

Follow this and additional works at: http://elischolar.library.yale.edu/ymtdl

 Part of the Medicine and Health Sciences Commons

Recommended Citation
Atreya, Chloé E., "Mechanistic and structure-function analysis of thymidylate synthase-dihydrofolate reductase from protozoal parasites: implications for the development of non-active site inhibitors" (2004). *Yale Medicine Thesis Digital Library*. 2224.
http://elischolar.library.yale.edu/ymtdl/2224

This Open Access Dissertation is brought to you for free and open access by the School of Medicine at EliScholar – A Digital Platform for Scholarly Publishing at Yale. It has been accepted for inclusion in Yale Medicine Thesis Digital Library by an authorized administrator of EliScholar – A Digital Platform for Scholarly Publishing at Yale. For more information, please contact elischolar@yale.edu.

Mechanistic and structure-function analysis of thymidylate ...
Atreya, Chloe E.
ProQuest Dissertations and Theses; 2004; ProQuest

Mechanistic and Structure-Function Analysis of Thymidylate Synthase-Dihydrofolate Reductase from Protozoal Parasites:

Implications for the Development of Non-Active Site Inhibitors

A Dissertation

Presented to the Faculty of the Graduate School

of

Yale University

in Candidacy for the Degree of

Doctor of Philosophy

by

Chloé E. Atreya

Dissertation Director: Karen S. Anderson

May 2004

Reproduced with permission of the copyright owner. Further reproduction prohibited without permission.

Abstract

Mechanistic and Structure-Function Analysis of

Thymidylate Synthase-Dihydrofolate Reductase from Protozoal Parasites:

Implications for the Development of Non-Active Site Inhibitors

Chloé E. Atreya

2004

A major advance in the field of bifunctional thymidylate synthase-dihydrofolate reductase (TS-DHFR) is the recent crystallization of two apicomplexan TS-DHFR enzymes, from *Cryptosporidium hominis* and *Plasmodium falciparum*, which demonstrate significant structural differences from the well-known kinetoplastid TS-DHFR structure (*Leishmania major*). A principal finding of this dissertation research is that the significant structural differences between the apicomplexa and kinetoplastid bifunctional TS-DHFR enzymes translate as significant mechanistic differences between parasite classes and among parasites within the same class.

An in depth mechanistic analysis of *C. hominis* TS-DHFR and a preliminary analysis of the *P. falciparum* enzyme were completed. Results with *C. hominis* TS-DHFR mark a paradigm shift for TS activity and substrate channeling behavior. Despite a well-conserved active-site, *C. hominis* TS activity was found to be 10 to 40-fold faster than that of other TS enzymes characterized. *C. hominis* also represents the first bifunctional TS-DHFR enzyme for which there is clear evidence against substrate channeling, or direct transfer of dihydrofolate produced at TS to DHFR, where it serves as a substrate.

Reproduced with permission of the copyright owner. Further reproduction prohibited without permission.

Neither *C. hominis* nor another apicomplexan protozoa, *Toxoplasma gondii*, exhibit the TS-DHFR domain-domain communication observed with *L. major*.

In the second and third parts of this dissertation, two concurrent approaches are taken to assess the putative electrostatic channeling region in *L. major* TS-DHFR: site-directed mutagenesis of solvent-exposed basic residues and molecular docking. In order to test the electrostatic channeling hypothesis, 12 charge reversal or charge neutralization mutants were made, with up to 6 putative channel residues changed at once. The mutants were assessed for impaired channeling using two criteria: a lag in product formation at DHFR and an increase in H_2folate accumulation. Surprisingly, none of the mutations produced changes consistent with impaired channeling. Therefore, our findings do not support the electrostatic channeling hypothesis.

Molecular docking was also used to target the shallow groove between the two active sites of the *L. major* bifunctional enzyme. One of the predicted inhibitors, eosin B, was found to inhibit both the *L. major* TS and DHFR catalytic activities, without competing with substrates, suggesting that the non-active site region, unique to bifunctional enzymes, represents a valid therapeutic target.

Reproduced with permission of the copyright owner. Further reproduction prohibited without permission.

Mechanistic and Structure-Function Analysis of Thymidylate Synthase-Dihydrofolate Reductase from Protozoal Parasites:

Implications for the Development of Non-Active Site Inhibitors

A Dissertation

Presented to the Faculty of the Graduate School

of

Yale University

in Candidacy for the Degree of

Doctor of Philosophy

by

Chloé E. Atreya

Dissertation Director: Karen S. Anderson

May 2004

Reproduced with permission of the copyright owner. Further reproduction prohibited without permission.

© 2004 by Chloé E. Atreya

All Rights Reserved

Reproduced with permission of the copyright owner. Further reproduction prohibited without permission.

In Memorium

Thomas Angus Casey

1967-2002

Reproduced with permission of the copyright owner. Further reproduction prohibited without permission.

Acknowledgements

Thank you first and foremost to Dr. Karen S. Anderson for being a wonderful thesis advisor. I remember clearly my first meeting with Karen, when I was deciding whether to rotate in her lab. It was then that I discovered that the same aspects of science excite us: "*Everything is more interesting at the interface*". Here was a lab at the interface between biology and chemistry; basic science research and clinical applications. This approach has led to many fruitful collaborations, increasing the efficiency of our progress.

Consistently during my graduate studies Karen has provided valuable advice and, while we may not always agree initially, when we both get excited about an idea or approach it has proven to be worth pursuing. This precedent has helped to foster a spirit of communication and compromise. Karen is generous with her time: always approachable when I have interesting or confusing data, while at the same time respecting my preference not to discuss experimental results before the data are fully analyzed. Karen also recognizes that people do their best work when they are doing what they enjoy. I am grateful to her for allowing me to take an unusual approach in the lab, and to make time for artistic and clinical pursuits outside of the lab.

Karen is attentive to each of the individuals in her lab as human beings and cultivates a caring and cooperative lab environment. I thank her and the members of the lab for helping me to get through a very tough time. Each member of the Anderson lab has helped me in some way to further my research, as well as by providing comradery to

Reproduced with permission of the copyright owner. Further reproduction prohibited without permission.

make the experience more enjoyable. Thank you specifically to Eisuke Murakami for offering to read the first copy of my thesis.

Thank you to my Dissertation Committee: to Dr. Ed Chu, Dr. Keith Joiner, and Dr. Alan Sartorelli for helping to direct the course of my research, and to Dr. Larry Hardy for agreeing to be my outside reader. Thank you to the Department of Pharmacology faculty, staff and students; to the MD-PhD Program, including Dr. Jim Jamieson and Sue Sansone; and to the NIH Medical Scientist Training Program for providing financial support.

Thank you to everyone who has contributed to this project. In Chapter 3, "Kinetic Characterization of Bifunctional TS-DHFR from the Apicomplexan Protozoa *Cryptosporidium hominis*," thank you to Dr. Amy Anderson and her lab at Dartmouth College for helpful discussions and for participating in the free exchange of data (including the *C. hominis* TS-DHFR coordinates) prior to publication. Thank you to Dr. Rick G. Nelson and Dr. David S. Roos for gifts of plasmid, and to Dr.Worachart Sirawaraporn for generously providing *P. falciparum* TS-DHFR protein.

Research in Chapter 4, "Probing Electrostatic Channeling and Domain-Domain Communication in Bifunctional TS-DHFR Using Site-Directed Mutagenesis," was initiated as a collaboration between myself and Eric. F. Johnson, then a graduate student in the lab. Together, Eric and I resurrected the TS-DHFR project, begun by Dr. Po-Huang Liang. I am indebted to Eric for continuing with the project (working out the bugs) while I completed my medical school coursework so that, when I returned to lab, we were in full swing for data collection. I thank Eric for his patience and thoroughness in transferring his knowledge to me. Jessica Williamson contributed to analysis of the TS-

Reproduced with permission of the copyright owner. Further reproduction prohibited without permission.

dead mutant during her rotation in the lab. Thank you to Sing-Yang Chang, Dr. Po-Huang Liang, C.-C. Kan and Dr. Dave Matthews for gifts of plasmid.

In Chapter 5, "Use of Molecular Docking to Identify Non-Active Site Inhibitors of TS-DHFR," the DOCK screen was a collaboration between Antonia Dow during her rotation in the lab, and Dr. Brian K. Shoichet and John J. Irwin, now at UCSF. Eosin was tested in parasites by Valeska Stempliuk in Dr. Stephen Beverley's lab at Washington University; and Dr. Isabelle Coppens and Kristen Massimine in Dr. Keith A. Joiner's lab at Yale University. Interesting results with the apicomplexa parasites led to further collaborations and friendship with Kristen and Isabelle in the Joiner lab. Thank you to Leah M. Fohl in the laboratory of Dr. David S. Roos for sharing results of TS-DHFR localization studies. The GLIDE screening in the second part of the chapter was conducted by

Marina Udier Blagovic in Dr. Bill Jorgenson's lab at Yale University. Thank you to Marina for permission to include some of her figures. Oladapo Babatunde, a Yale undergraduate student, also contributed to the work in this section. Thanks to Dr. Dave Matthews, Dr. David Roos, Dr. Carl Frieden, Dr. Bob Matthews, and Dr. Frank Maley for generous gifts of plasmids or protein

Finally, thank you to my parents and to Jeffrey Benjamin for their love and support, to friends too numerous to mention, and to the New Haven arts community for enriching my time here.

Reproduced with permission of the copyright owner. Further reproduction prohibited without permission.

Table of Contents

Reproduced with permission of the copyright owner. Further reproduction prohibited without permission.

Reproduced with permission of the copyright owner. Further reproduction prohibited without permission.

Reproduced with permission of the copyright owner. Further reproduction prohibited without permission.

Reproduced with permission of the copyright owner. Further reproduction prohibited without permission.

Reproduced with permission of the copyright owner. Further reproduction prohibited without permission.

List of Figures

Chapter One

Chapter Two

Chapter Three

Reproduced with permission of the copyright owner. Further reproduction prohibited without permission.

Chapter Four

Reproduced with permission of the copyright owner. Further reproduction prohibited without permission.

Chapter Five

Reproduced with permission of the copyright owner. Further reproduction prohibited without permission.

List of Tables

Reproduced with permission of the copyright owner. Further reproduction prohibited without permission.

List of Abbreviations and Symbols

Abs	Absorbance
ACD	American Chemicals Database
ACD	Available Chemicals Directory
AIDS	Acquired Immune Deficiency Syndrome
Arg, R	Arginine
AU	Absorbance Units
BrdUMP	Brominated deoxyuridate
C. hominis	*Cryptosporidium hominis*
CH_2H_4folate	(6R)-L-5,10-Methylene tetrahydrofolate
CHO cells	Chinese Hamster Ovary cells
cm^{-1}	Per centimeter
CMC	Comprehensive Medicinal Chemistry
Cont.	Contaminant
C-terminal	Carboxy-terminal
DHFR	Dihydrofolate reductase
DMSO	Dimethyl sulfoxide= Me_2SO
dpm	Disintegrations per minute
dTMP	2'-Deoxythymidylate
DTT	DL-dithiothreitol
dUMP	2'-Deoxyuridate
E	Enzyme

Reproduced with permission of the copyright owner. Further reproduction prohibited without permission.

E. coli	*Escherichia coli*
EDTA	Ethylenediaminetetraacetic acid
Em	Emission
Ex	Excitation
FDA	Food and Drug Administration
FdUMP	5-Fluorodeoxyuridine-5'-monphosphate
FKBP	FK-506 binding protein
FMN	Flavin mononucleotide
FRET	Fluorescence Resonance Energy Transfer
Gln, Q	Glutamine
Glu, E	Glutamic Acid
h	Hour
HFF	Human foreskin fibroblast
H_4folate	Tetrahydrofolate
HIV	Human Immunodeficiency Virus
HPLC	High Performance Liquid Chromatography
H_2folate	7,8-Dihydrofolate
I, Int.	Intermediate
IC_{50}	Concentration at which 50% inhibition is observed
IdUMP	Iodinated deoxyuridate
k_{cat}	Pseudo-first order steady-state reaction constant, $V_{max}/[E]$
k_{chem}	Rate constant of chemical step, rate of chemistry
KCl	Potassium chloride

Reproduced with permission of the copyright owner. Further reproduction prohibited without permission.

K_d	Dissociation constant (k_{off}/k_{on})
K_i	Inhibition constant (concentration for half-maximal inhibitor binding)
K_m	Michaelis constant (concentration for half-maximal steady-state rate)
k_{obs}	Observed rate
k_{off}	First order dissociation-rate constant
KOH	Potassium hydroxide
k_{on}	Second order binding-rate constant
k_{ss}	Steady-state rate constant, rate constant of rate-limiting step
L. casei	*Lactobacillus casei*
L. major	*Leishmania major*
L. tropica	*Lieshmania tropica*
Lys, K	Lysine
M	Molar
M^{-1}	Per molar
MDDR	MDL Drug Data Report
MDR	Multiple drug resistance
Met, M	Methionine
$MgCl_2$	Magnesium chloride
min	Minute
mL	Milliliter
mm	Millimeter
mM	Millimolar
MRP	Human multidrug resistance protein

Reproduced with permission of the copyright owner. Further reproduction prohibited without permission.

MTX	Methotrexate
N	Normal
$NADP^+$	Nicotinamide adenine dinucleotide phosphate
NADPH	Nicotinamide adenine dinucleotide phosphate, reduced form
nm	Nanometer
nM	Nanomolar
P. falciparum	*Plasmodium falciparum*
PC	Personal Computer
PCR	Polymerase chain reaction
PDB	Protein data bank
PDDF	10-Propargyl 1-5, 8-dideazafolate
PECSS	Perkin Elmer Computerized Spectroscopy Software
s	Second
s^{-1}	Per second
SD	Standard deviation
SHMT	Serine Hydroxymethyl Transferase
T	Temperature
t	Time
T. gondii	*Toxoplasma gondii*
Tris	Tris[hydroxymethyl]aminomethane
TS	Thymidylate synthase
TS-DHFR	Thymidylate synthase-dihydrofolate reductase bifunctional enzyme
UV	Ultraviolet

Reproduced with permission of the copyright owner. Further reproduction prohibited without permission.

V_{max}	Maximum steady-state reaction velocity
ΔG	Change in Gibb's free energy
$\Delta\varepsilon_{rxn}$	Change in molar absorptivity (extinction coefficient) for a reaction
ε_{340}	Extinction coefficient at 340 nm
μCi	Microcurie
μM	Micromolar
°C	Degrees Celsius
[X]	Concentration of species X
^{14}C	Carbon 14
2x solution	Solution with components at twice the final concentration
^{3}H	Tritium

Reproduced with permission of the copyright owner. Further reproduction prohibited without permission.

Chapter One

Introduction to Bifunctional

Thymidylate Synthase-Dihydrofolate Reductase

(TS-DHFR)

Reproduced with permission of the copyright owner. Further reproduction prohibited without permission.

Bifunctional TS-DHFR[1]

Only in protozoal parasites and some plants are thymidylate synthase (TS) and dihydrofolate reductase (DHFR) found on the same polypeptide chain, as a single bifunctional enzyme, thymidylate synthase-dihydrofolate reductase (TS-DHFR). TS and DHFR are critical enzymes and established drug targets. In most species, including humans and protozoa, TS represents the only means of *de novo* synthesis of 2'-deoxythymidylate (dTMP) for DNA synthesis, producing dihydrofolate (H_2folate) in the process. DHFR catalyzes the reduction of H_2folate to generate tetrahydrofolate (H_4folate), used for one carbon unit transfer reactions in several biochemical processes, including thymidylate, purine nucleotide, and amino acid biosynthesis. Chemotherapeutic agents, notably 5-fluorouracil, target TS [1]; DHFR is targeted by anti-cancer agents including methotrexate, and anti-microbials such as trimethoprim and pyramethamine. It has been predicted that bifunctional TS-DHFR will serve as a target for new classes of antiparasitic drugs [2-5].

The studies presented here are distinctive in that they focus on the non-active site region, specific to bifunctional TS-DHFR, as a potential drug target. To this end, unique mechanistic features as well as functions exclusive to the bifunctional enzyme, including substrate channeling and domain-domain communication, will be explored. There are precedents for non-active site regions serving as effective infectious disease targets. Non-nucleoside inhibitors of HIV-1 reverse transcriptase, such as nevirapine and efavirenz, bind in a hydrophobic pocket remote from the active site, in contrast to phosphorylated

[1] TS-DHFR is a functional designation as dihydrofolate is produced at TS and used at DHFR. Elsewhere the bifunctional enzyme is referred to as DHFR-TS because DHFR resides at the N-terminal portion of the bifunctional enzyme.

Reproduced with permission of the copyright owner. Further reproduction prohibited without permission.

nucleoside inhibitors like AZT-TP that bind at the active site. One concern regarding these non-active site inhibitors was that residues outside the active site would have a greater propensity to mutate and develop resistance. Indeed, when used as monotherapy, drug resistance to nevirapine quickly develops in cell culture. Non-nucleoside compounds are typically used in combination with nucleosides however, and the combination therapy has proven more effective both in terms of inhibiting viral replication and decreasing the onset of drug resistance. Targeting non-active site regions specific to bifunctional TS-DHFR has the potential to produce more specific therapies, with fewer side-effects than traditional active-site directed medications, for protozoal diseases including malaria, toxoplasmosis, cryptosporidiosis, and leishmaniasis.

TS-DHFR from Select Protozoal Parasites

The protozoal parasites that serve as the focus of this study were chosen on the basis of 1) clinical relevance and 2) the availability of a crystal structure of bifunctional TS-DHFR from this organism. Until recently there was only one crystal structure available for the study of bifunctional TS-DHFR, that from the kinetoplastid protozoa *Leishmania major* [6], so all early mutagenesis and molecular docking studies focus on TS-DHFR from this species. In the Spring of 2003 however, structures of TS-DHFR from two relevant apicomplexan protozoa, *Plasmodium falciparum* and *Cryptosporidium hominis* (previously called *Cryptosporidium parvum*, type 1, [7]) were solved [8, 9], and the *Toxoplasma gondii* TS-DHFR structure is in the final stages of completion (personal communication, Dr. Amy C. Anderson, Dartmouth College). Therefore, later mechanistic

Reproduced with permission of the copyright owner. Further reproduction prohibited without permission.

work as well as additional mutagenesis and molecular docking studies focus on TS-DHFR from these clinically relevant apicomplexan protozoa.

1. Clinical Relevance. In the United States, *L. major*, *C. hominis*, and *T. gondii* have become particularly problematic in the era of AIDS, anti-cancer chemotherapy and organ transplantation [10-13]. Individuals harboring HIV are 500-fold more likely to become infected with *Leishmania*, and infection can produce severe cutaneous skin ulcerations as well as visceral leishmaniasis.

No effective treatments currently exist for cryptosporidiosis, caused by *C. hominis* infection and producing chronic diarrhea (often lasting >4 months) and the wasting disease of AIDS [7, 14-17]. *C. hominis* has been classified as an emerging infectious disease [16, 18], with outbreaks also occurring in otherwise healthy populations in daycare centers [18], water supplies [19], and among the elderly [20]. Due to its water- and food-borne modes of transmission [21], *C. hominis* has been added to the Center of Disease Control's list of potential bioterrorist threats.

T. gondii infection, or toxoplasmosis, is a cause of frequently lethal meningoenchephalitis in immunocompromised individuals, and can also produce severe congenital abnormalities [22]. Current therapies for acquired toxoplasmosis are subject to poor patient tolerance and emerging resistance [23]. The standard treatment is the co-administration of pyramethamine and a sulfonamide, but cross-reactivity with the human DHFR active site yields a narrow therapeutic window for pyramethamine [24]. AIDS patients are particularly susceptible to severe hypersensitivity reactions with sulfonamide therapy, but pyrimethamine cannot be used alone due to the rapid onset of resistance. A

Reproduced with permission of the copyright owner. Further reproduction prohibited without permission.

low-dose regimen, often used as prophylactic treatment, can also select over time for resistant parasites.

P. falciparum, the causative agent of the most severe form of malaria, is responsible annually for approximately 500 million cases of malaria and 2 million fatalities worldwide [25]. Furthermore, the parasite has developed resistance to virtually all currently available antimalarial drugs, including those targeting the DHFR active site [26, 27].

High or growing rates of infection, combined with emerging resistance, ineffective therapies, and unacceptable side-effects prove that there is a real and urgent need not only for new drugs to treat protozoal infections, but also for the identification of new chemotherapeutic targets. A new class of non-active site inhibitors may be beneficial in several ways. First, combination therapy may allow for lower doses of more toxic drugs, such as the sulfonamides, to be used; decreasing overall toxicity. By analogy to the synergy observed between HIV reverse transcriptase nucleoside and non-nucleoside inhibitors, it is possible that non-active site TS-DHFR inhibitors will be synergistic with active site agents, lowering the therapeutic dose requirements. Synergy has also been observed between inhibitors of sequential steps of the folate metabolic pathway such as the DHFR inhibitor, trimethoprim, and sulfamethoxazole (given in combination as TMP-SMZ or bactrim). Second, targeting multiple sites can prevent the onset of resistance. Thus even if non-active site inhibitors do not alone result in parasite death, they may be extremely valuable as combination therapy agents.

2. TS-DHFR Crystal Structures. For almost a decade, the crystal structure of TS-DHFR from *L. major* (2.9 Å resolution, [6]) was the only one available for study of

Reproduced with permission of the copyright owner. Further reproduction prohibited without permission.

the bifunctional enzyme (Fig 1.0 A). In the Spring of 2003, however, the TS-DHFR structures from two apicomplexan protozoa were solved: *P. falciparum*, at 2.8 Å resolution, but with disordered electron density among residues 232-280 in the junctional region [8]; and *C. hominis*, complete structure at 2.8 Å resolution [9] (Fig 1.0 B-C)). The apicomplexan TS-DHFR structures bear similarities to each other, but are significantly different from the *L. major* structure that had previously been our model. Although there was likely a single TS-DHFR gene fusion event, the apicomplexan protozoa belong to a separate class from leishmania (Fig 1.1A). The apicomplexa are classified as Alveolata whereas the kinetoplastids, including leishmania and the trypanosomes, are Euglenozoa [9, 28].

Solution of the crystal structures of the two apicomplexa enzymes followed by sequence alignment revealed that the TS-DHFR enzymes from the Alveolata protozoa, including the apicomplexa, belong to a structural family that is distinct from that of the Euglenozoa protozoa, including *L. major* [9]. *L. major* TS-DHFR contains only 2 linker or junctional amino acids between the TS and DHFR domains and has a 22 amino acid N-terminal tail that extends from DHFR and wraps the TS domain. By contrast, the apicomplexan protozoa have extensive linker regions but lack an N-terminal tail that contacts TS. The junctional region is 89-93 amino acids in *P. falciparum*, 58 amino acids in *C. hominis*, and 72 amino acids in *T. gondii*. TS exists as a dimeric enzyme: in the apicomplexan protozoa a donated or cross-over α-helix in the junctional region makes extensive contacts with the DHFR domain of the opposite half of the TS-DHFR dimer, bringing the two DHFR domains closer together. Accordingly, it has been proposed that there exist 2 families of bifunctional TS-DHFR structures: a short linker family with an

Reproduced with permission of the copyright owner. Further reproduction prohibited without permission.

Fig. 1.0 Crystal structures of bifunctional TS-DHFR . *A*, *L. major* TS-DHFR with TS in red and DHFR in blue. *P. falciparum* TS-DHFR (1J3I) and *C. hominis* TS-DHFR (1QZF), both with TS in red and pink; DHFR in dark and light blue (*B-C*, respectively).

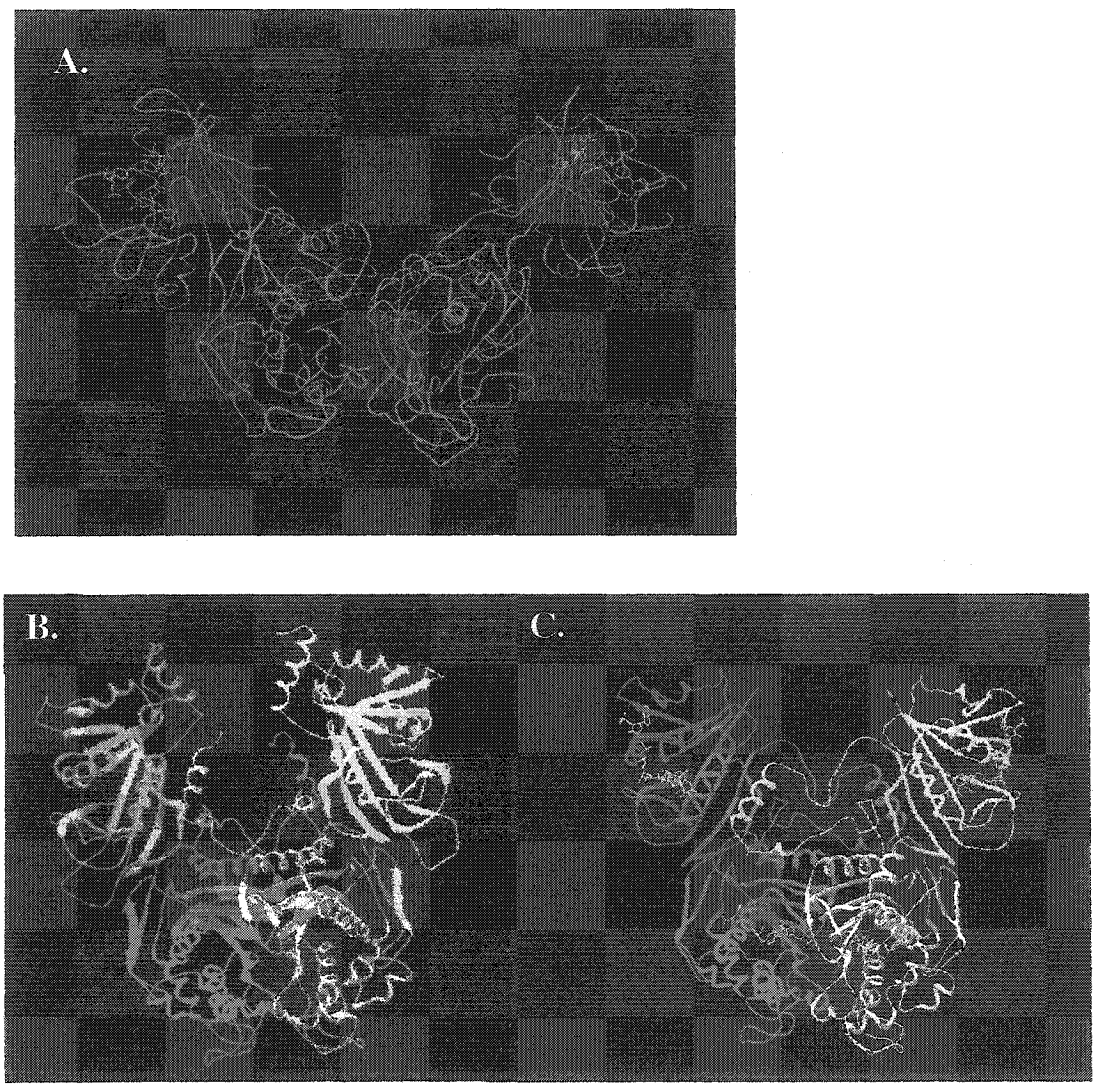

Reproduced with permission of the copyright owner. Further reproduction prohibited without permission.

Fig 1.1 *A*, Evolutionary origins of bifunctional TS-DHFR and *B*, Cartoon diagrams of the long- and short-linker families of TS-DHFR structures. *A*, Evolutionary tree rooting the TS-DHFR gene fusion event. Protist species in the Alveolata grouping constitute the long-linker TS-DHFR family, whereas species in the Euglenozoa grouping fit in the short-linker family. *B*, TS is shown in purple; DHFR in green; the letter N denotes the N-terminus. Active sites are indicated as cavities if on the front side of the protein, or as outlined circles if on the back side. For clarity, the linker between TS and DHFR is diagrammed in only one monomer. *a*, Side view of the long-linker family with the cross-over helix in blue; *b*, top view of the long-linker family; *c*, side view of the short-linker family; *d*, top view of the short-linker family. Used with author's permission [9].

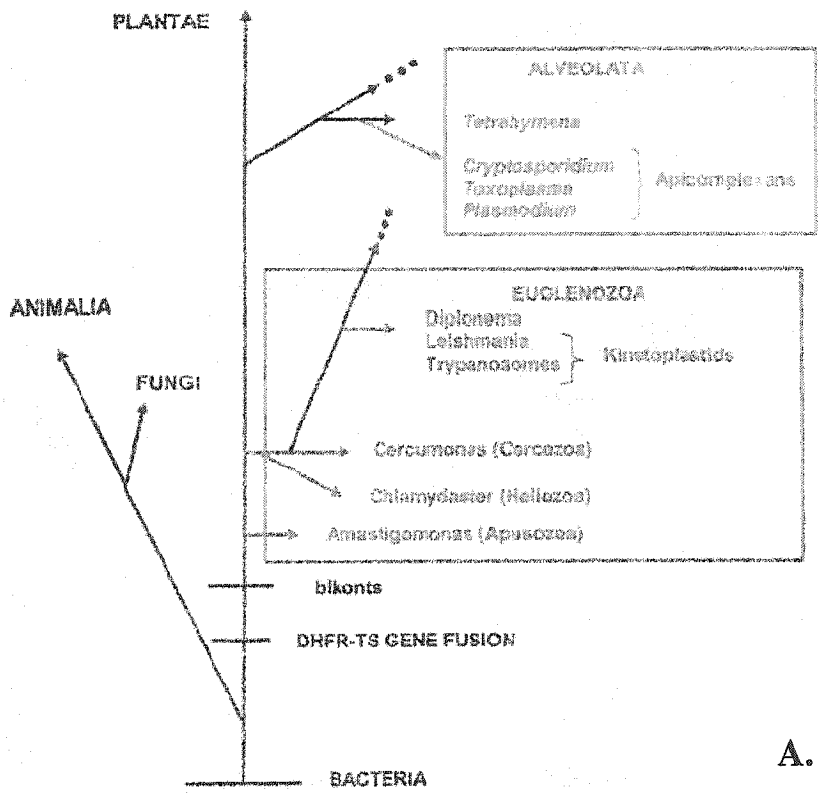

Reproduced with permission of the copyright owner. Further reproduction prohibited without permission.

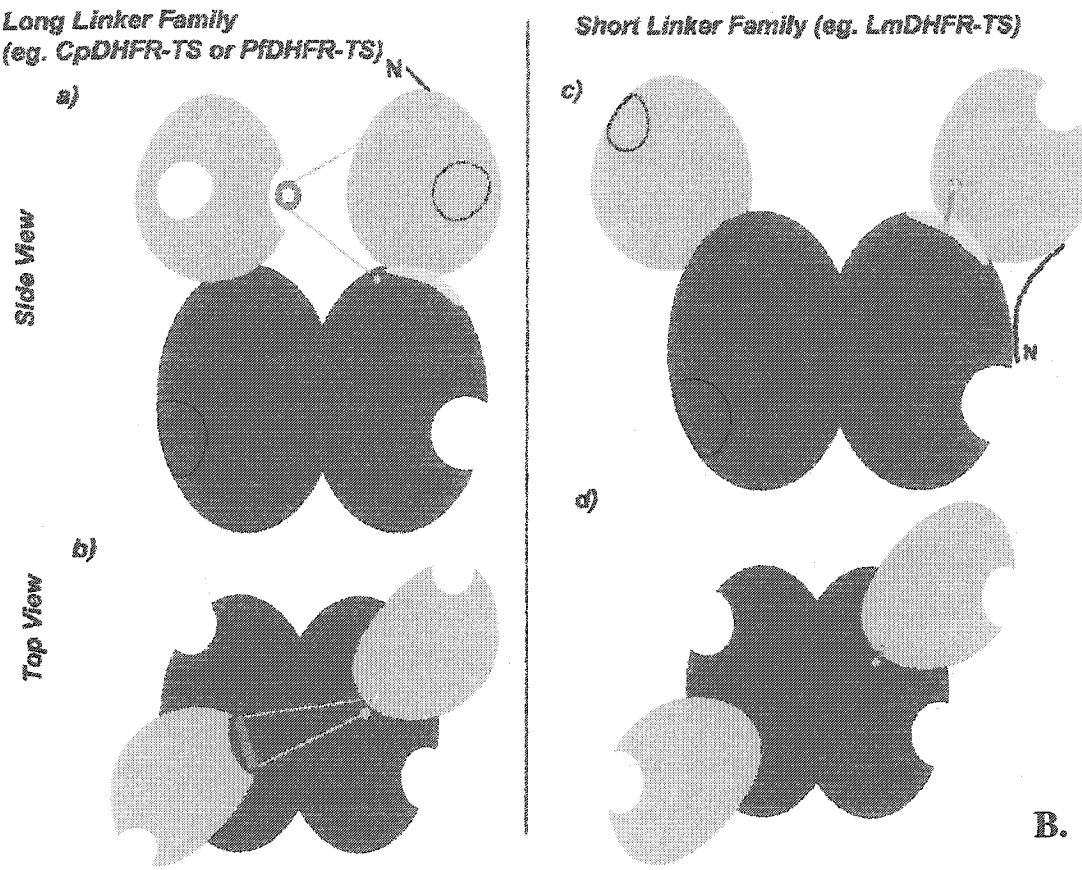

Reproduced with permission of the copyright owner. Further reproduction prohibited without permission.

N-terminal tail, as in *L. major*; and a long linker family with a cross-over helix, as in the apicomplexa parasites (Fig. 1.1B, [9]).

When the crystal structure of *L. major* TS-DHFR was solved it was observed that there is a path of solvent exposed basic residues between the TS and DHFR active sites: it was proposed that these residues may compose a 40 Å "electrostatic highway" for directional substrate channeling of negatively charged H_2folate produced at TS to the DHFR active site, without equilibration in bulk solution [6, 29]. Relative to *L. major* TS-DHFR, basic residues are more scattered over the apicomplexa protein surface, making electrostatic channeling improbable. Furthermore, the TS active site of one half of the apicomplexa dimer is orthogonal to the DHFR active site of the same peptide chain, making an alternate, dynamic channeling hypothesis, whereby a conformational change brings the active sites in closer proximity [29], less feasible (Fig. 1.1 B).

While we were able to conduct mechanistic studies on *T. gondii* TS-DHFR prior to solution of the crystal structure, none of the unique structural features were predicted by homology modeling [30]. Thus, the availability of the crystal structures is crucial to our ability to conduct structure-function studies aimed at development of new non-active site inhibitors to treat apicomplexan infections.

Mechanistic Features of TS and DHFR

TS represents the only means of *de novo* synthesis of dTMP in most species, via reductive methylation of 2'-deoxyuridate (dUMP) with methylene tetrahydrofolate (CH_2H_4folate), producing H_2folate in the process. DHFR catalyzes the reduction of H_2folate by NADPH to generate H_4folate and $NADP^+$ (Fig 1.2). A third enzyme, serine

Reproduced with permission of the copyright owner. Further reproduction prohibited without permission.

Fig 1.2 *A*, Schematic of the TS-DHFR reaction and *B*, Chemical structures of TS and DHFR reactants and products

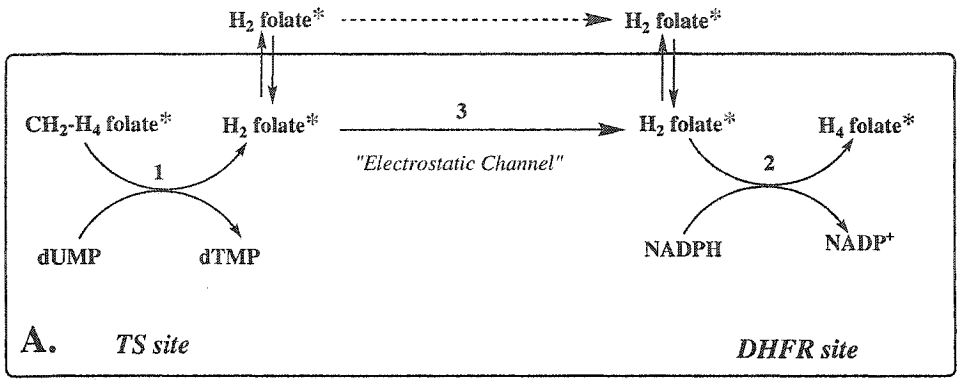

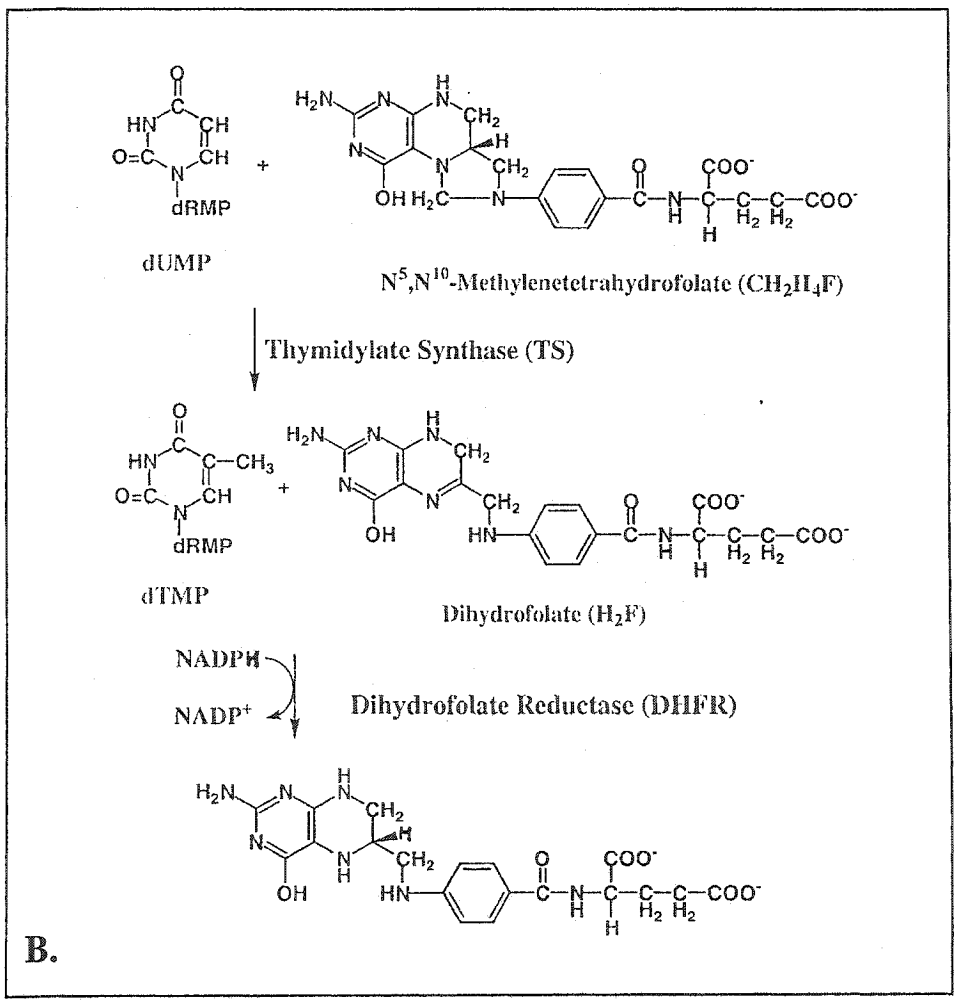

Reproduced with permission of the copyright owner. Further reproduction prohibited without permission.

hydroxymethyl transferase (SHMT), completes the cycle: producing CH_2H_4folate from H_4folate. It was recently discovered that some non-symbiotic microbes contain a structurally and sequence-unrelated enzyme for thymidylate synthesis, Thy-X. These organisms typically lack Thy-A (the form of TS studied here), DHFR, and thymidine kinase for thymidine salvage [31]. Both human TS and DHFR, as well as bifunctional TS-DHFR from *P. falciparum* have been shown to participate in translational autoregulation, whereby mRNA coding for the protein binds to it, repressing translation until a signal triggers mRNA release [32-36].

1. Thymidylate Synthase. First crystalized in 1987 by Larry Hardy *et al.* [37], TS is a highly conserved enzyme, making the identification of species specific TS active-site inhibitors challenging. The overall sequence identity at the TS domain between *L. major* and *T. gondii* is 59 %; it is 50% between *L. major* and *C. hominis*, and 53% between *T. gondii* and *C. hominis*. All known TS enzymes, including those in bifunctional TS-DHFR, exist as obligate TS dimers (although the structurally unrelated Thy-X variant is tetrameric). One amino acid (Arg 126 in *E. coli*; Arg 380 in *L. major*) participates in the catalytic site of the opposite half of the dimer; mutation of this residue to glutamic acid in both halves of the dimer results in a TS-dead enzyme [38]. When the *E. coli* R126E mutant is combined with another TS-lethal mutant to form a heterodimer, however, full TS activity is restored. In the heterodimer, one half of the dimer effectively has 2 mutations (R126E contributes to the opposite half), but the TS subunit containing R126E is catalytically active, as a normal R126 is contributed by the other mutant form of TS. The fact that full activity is restored when only one half of the TS dimer is

Reproduced with permission of the copyright owner. Further reproduction prohibited without permission.

functional is one indication that TS is a half-the-sites activity enzyme, meaning that at any given time, only one half of the TS dimer is kinetically competent [38, 39].

In TS catalysis dUMP binds first, then CH_2H_4folate [40, 138]. This ordered binding is followed by movement of the C-terminus over the substrates to form a "closed" active site cavity, shielded from solvents, required for catalysis to proceed [41-43] (Fig. 1.3; Fig 1.4, step 1). Formation of a closed complex at one half of the TS dimer renders the other half in an unfavorable conformation for ligand binding, greatly reducing ligand affinity at the opposite subunit, and providing a structure-function explanation for TS half-the-sites reactivity [38, 39, 43-45].

A dUMP-CH_2H_4folate-enzyme ternary complex is formed at the first TS subunit [46, 47]. It has been proposed that ternary complex formation involves an iminium ion intermediate, linking the bridge methylene and N-5 of CH_2H_4folate (Fig. 1.4, step 2) [42, 136]. It was observed that a C-terminal valine deletion mutant of *Lactobacillus casei* TS, while TS dead, still binds dUMP and CH_2H_4folate [139]. A crystal structure of the C-terminal valine deletion mutant suggested the presence of hydroxymethylene tetrahydrofolate, a hydrolytic product of the putative TS iminium ion intermediate [48]. In the wild-type TS enzyme, iminium ion formation is followed by several steps in rapid equilibrium, leading up to an overall rate-limiting chemistry step involving hydride transfer to form the products, dTMP and H_2folate (Fig. 1.4, steps 3-6, [41]).

Reproduced with permission of the copyright owner. Further reproduction prohibited without permission.

Fig 1.3 Role of the C-terminus in TS catalysis. When cofactor binds TS monomer A, the C-terminus closes the active site cavity and a catalytic cysteine forms a covalent bond with dUMP. These conformational changes are transferred to monomer B, impeding covalent bond formation. The conformational changes also result in the hydrogen bonds between TS and dUMP being broken in monomer B, yielding a misoriented dUMP and preventing both folate binding and catalysis. CB3717, also known as propargyl dideazafolate (PDDF) is a TS-specific folate analog. Figure used with author's permission [43].

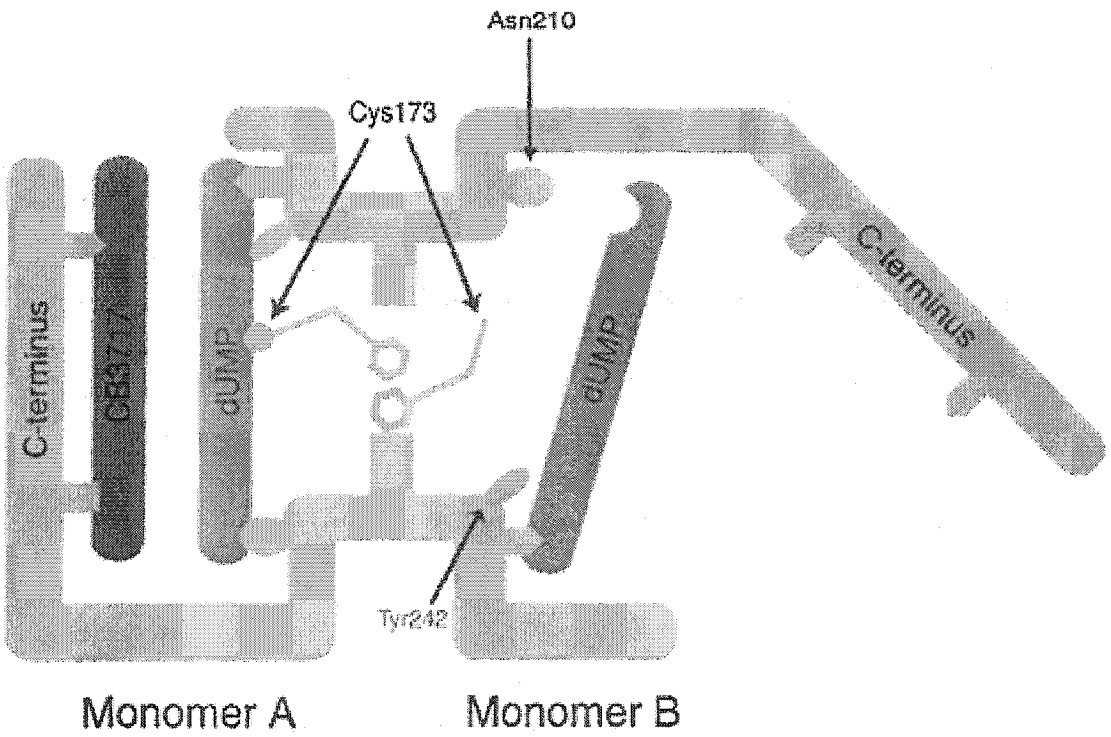

Reproduced with permission of the copyright owner. Further reproduction prohibited without permission.

Fig 1.4 Catalytic mechanism of TS. Modified version of a figure created by Eric F. Johnson that appeared in Johnson, E.F., Hinz, W., Atreya C.E., Maley, F. and Anderson, K.S. (2002). *J. Biol. Chem.* **277** (45), 43126-43136.

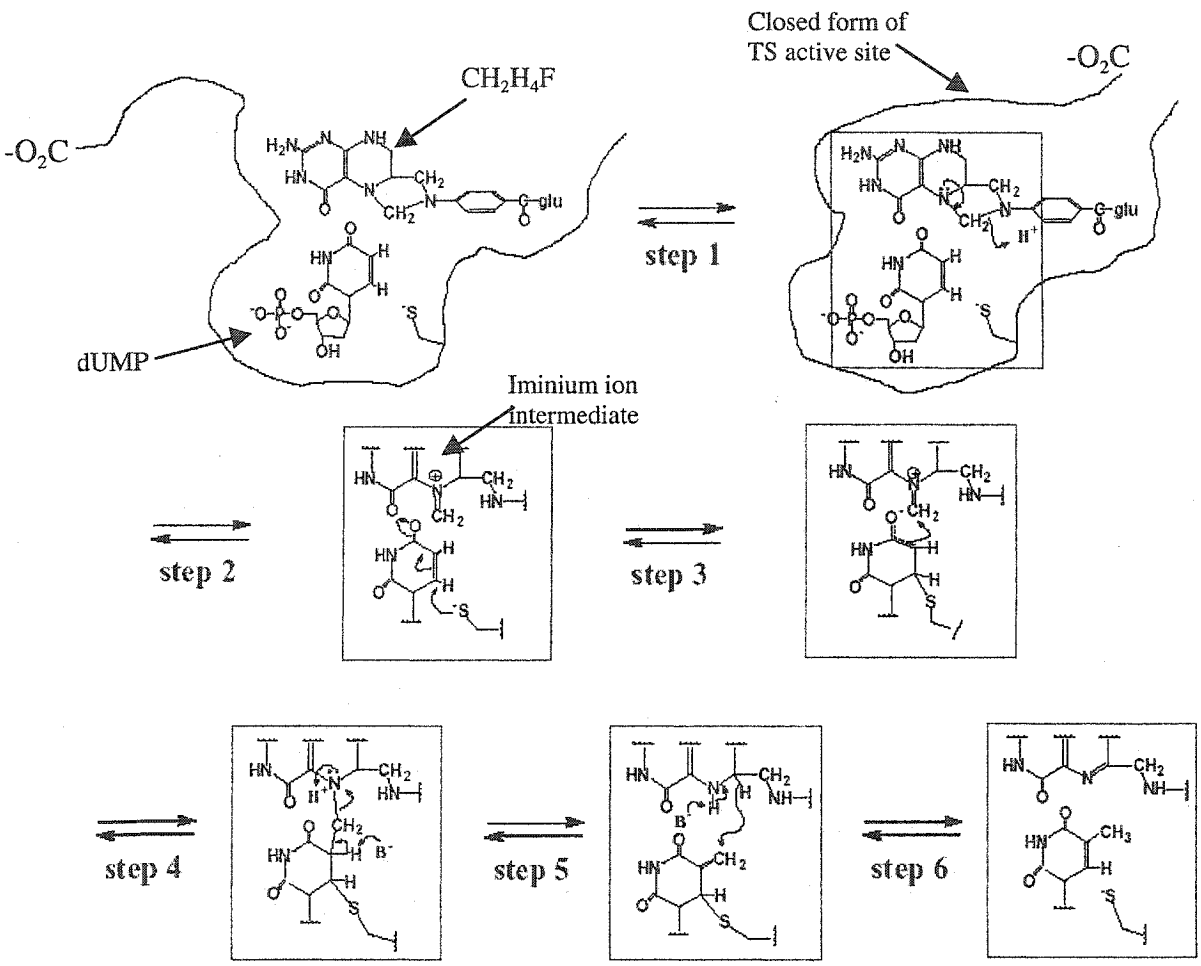

Reproduced with permission of the copyright owner. Further reproduction prohibited without permission.

2. Dihydrofolate Reductase. DHFR is much less conserved than TS, possibly because the simple reaction catalyzed can be accomplished by many different protein sequences [49]. Species specific variation makes DHFR a more popular active site drug target, but this site is also more prone to develop resistance-conveying mutations [49]. The sequence identity at the DHFR domain between *L. major* and *T. gondii* is 22 %; it is 16 % between *L. major* and *C. hominis*, and 25 % between *T. gondii* and *C. hominis*. Studies of monofunctional DHFR enzymes from multiple species indicate, however, that DHFR typically exhibits high functional homology despite low primary sequence identity.

The DHFR substrates NADPH and H_2folate bind synergistically and in a random order [50-53]. A DHFR-NADPH-H_4folate ternary complex is formed upon reduction of H_2folate and displacement of $NADP^+$ by NADPH [54]. With *E. coli* DHFR, H_4folate product dissociation from the DHFR-NADPH-H_4folate ternary complex is rate-limiting at low pH. At high pH, hydride transfer of NADPH is the rate-limiting step.

Mechanistic differences between the *L. major* and *T. gondii* DHFR domains have already been observed: one major distinction between the two enzymes is that there is no activation of *T. gondii* DHFR activity upon ligand binding at the TS site (Fig. 1.5, [30, 55]). Unlike with *L. major,* where formation of the ternary complex at TS accelerates the DHFR rate from 6.4 s^{-1} to 120 s^{-1} [56], *T. gondii* DHFR activity is maximal (180 s^{-1}), even when TS is in an unliganded state [30]. In addition, there is a difference in the location of the rate-limiting step in each enzyme pathway. With *T. gondii*, the rate-limiting step occurs after NADPH binding, whereas with *L. major* it occurs after $NADP^+$ release from the TS-DHFR-$NADP^+$-H_4folate ternary complex. Finally, product release is kinetically

Reproduced with permission of the copyright owner. Further reproduction prohibited without permission.

Fig. 1.5 Comparison of the *T. gondii* and *L. major* DHFR mechanisms. Figure appeared as Scheme 4 in Johnson, E.F., Hinz, W., Atreya C.E., Maley, F. and Anderson, K.S. (2002). *J. Biol. Chem.* **277** (45), 43126-43136 [30].

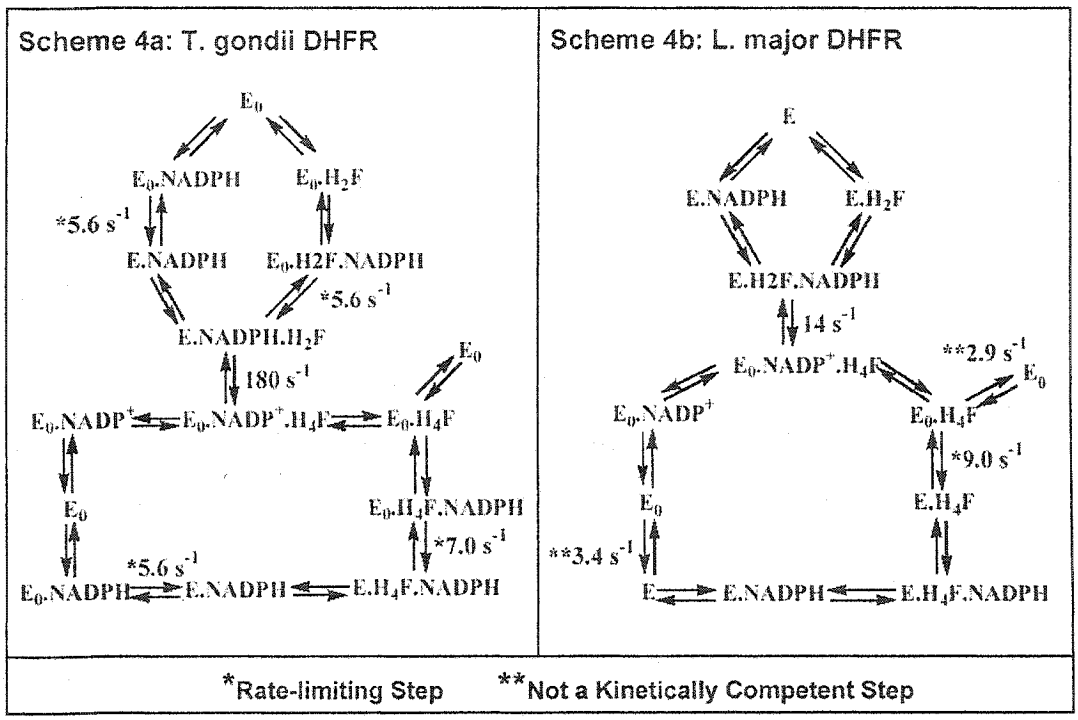

Reproduced with permission of the copyright owner. Further reproduction prohibited without permission.

restricted to one path with *L. major*, whereas the *T. gondii* DHFR mechanism includes multiple kinetically competent paths for product release [30].

Unique Prospects for Bifunctional TS-DHFR: Substrate Channeling and Domain-Domain Communication.

With the ultimate goal to develop non-active site inhibitors in mind, special attention was paid to possible functions unique to bifunctional TS-DHFR, notably substrate channeling and domain-domain communication.

1. Substrate Channeling. H_2folate is the product of TS and the substrate of DHFR: it has been proposed that H_2folate is channeled from the TS active site to the DHFR active site, without equilibration in bulk solution. More specifically, when the crystal structure of *L. major* TS-DHFR was solved, a shallow, basic residue-rich groove connecting the two enzyme active sites was observed [6]. Based on this structural finding, it was hypothesized that the negatively charged H_2folate produced at the TS active site is handed-off along a series of solvent-exposed lysine and arginine residues, or electrostatically channeled, to the DHFR active site, where it is converted to H_4folate [6, 56].

There are precedents for channeling among bifunctional enzymes, of which tryptophan synthase from *Salmonella typhimurium* is one of the best characterized examples [57-63]. Tryptophan synthase is an $\alpha_2\beta_2$ enzyme complex: the α subunit catalyzes the aldolytic cleavage of indole-3-glycerol phosphate to indole and glyceraldehyde-3-phosphate, whereas the β subunit catalyzes the condensation of indole with serine to form tryptophan. Solution of the crystal structure of tryptophan synthase

Reproduced with permission of the copyright owner. Further reproduction prohibited without permission.

from *S. typhimurium* revealed a 25 Å hydrophobic tunnel connecting the active sites [57]. There is also kinetic evidence for a conformational change following formation of the aminoacrylate intermediate at the β subunit, which accelerates the rate of catalysis at the α subunit by approximately 150-fold [59]. Build-up of indole is only observed in single enzyme turnover of the αβ reaction when channeling is obstructed by site-directed mutagenesis [60, 61]. A tryptophan synthase channeling impaired *E. coli* strain displayed severely compromised growth due to buildup of the indole intermediate [64].

Although there is no obvious hydrophobic tunnel through *L. major* TS-DHFR, there is kinetic evidence for substrate channeling, notably the absence of a lag in product formation at DHFR and a lack of build-up of H_2folate [56, 65]. Also similar to tryptophan synthase, in bifunctional TS-DHFR, the second enzyme (DHFR) is faster than the first (TS). Steady-state kinetics indicates that there is a lag in formation of the products of the DHFR reaction ($NADP^+$ and H_4folate) when monofunctional TS and DHFR enzymes are combined, but not in the case of bifunctional TS-DHFR from *L. tropica* [65]. This suggests that, in the case of the bifunctional enzyme only, H_2folate produced at the TS site is directly transferred to the DHFR site, rather than first equilibrating in bulk solvent. Direct evidence for substrate channeling has been obtained by transient kinetic analysis. It was shown by rapid chemical quench that, in single enzyme turnover experiments with *L. major*, there is no lag in H_4folate production and little H_2folate accumulation is observed, again suggesting direct transfer of H_2folate from TS to DHFR [56].

Prior to this research there was no direct evidence for electrostatic guidance of H_2folate as the mechanism by which channeling occurs. There are however, precedents for electrostatic steering in other enzyme systems, including superoxide dismutase and

Reproduced with permission of the copyright owner. Further reproduction prohibited without permission.

acetylcholinesterase [66-70]. Structural analysis and Brownian dynamics simulation techniques applied to TS-DHFR also provide support for the electrostatic channeling hypothesis [6, 71, 72]. Structural analysis elucidated a highly positively charged electrostatic potential surface forming the solvent exposed path connecting TS and DHFR, with a generally negatively charged surrounding surface [6]. Brownian dynamics simulation predicts that, in the presence of electrostatic effects, 95% of substrate with charge –2 (the charge on H_2folate; polyglutamylated folate substrates found in nature are even more highly negatively charged), exiting the TS site would reach the DHFR site, whereas only 6% of substrate would channel in the absence of electrostatics [67].

2. Domain-Domain Communication. There is evidence from studies with *L. major* TS-DHFR of domain-domain communication, or conformational changes induced upon ligand binding at one active site that affect activity at the active site of the other enzyme. With *L. major*, formation of the ternary complex at TS accelerates the DHFR rate from 6.4 s^{-1} to 120 s^{-1} [56]. The presence of the DHFR ligand NADPH changes the shape of the *L. major* TS burst from one that fits a single exponential burst of 1 s^{-1} to a double exponential burst with rates of 210 s^{-1} and 5.4 s^{-1}; adding a DHFR inhibitor, methotrexate, results in a 4-fold slower TS single turnover rate [55]. Like substrate channeling, communication between active sites suggests that the region between active sites plays a crucial role.

Reproduced with permission of the copyright owner. Further reproduction prohibited without permission.

Overview of Research Presented

This research comes at an exciting time in the field of bifunctional TS-DHFR, marked by the recent solution of the two apicomplexa structures that deviate significantly from our kinetoplastid model. Since targeting the non-active site of a protein for inhibition requires a more in-depth understanding of the interplay of mechanism and structure than targeting the active site, mechanistic and structure-function studies are the focus of the research presented. These studies rely primarily on a transient kinetic approach, described in Chapter 2. All of the experimental methods used are also detailed in Chapter 2.

Following the solution of the crystal structures of *C. hominis* and *P. falciparum* TS-DHFR, an in depth mechanistic analysis of *C. hominis* TS-DHFR and a preliminary analysis of the *P. falciparum* enzyme were performed, presented in Chapter 3. This research was conducted last but is presented first both to highlight the novelty of its findings and because mechanistic analysis is the foundation on which all future structure-function research is built.

Previous research in the lab focused on mechanistic characterizations of *L. major* and *T. gondii* TS-DHFR, conducted primarily by Po Huang Liang and Eric F. Johnson, respectively. Since *L. major* TS-DHFR was until recently, the only available bifunctional crystal structure, my project focused initially on further assessment of the putative channel region in the *L. major* enzyme. Two concurrent approaches were taken to assess the putative electrostatic channeling region in *L. major* TS-DHFR: site-directed mutagenesis of solvent-exposed basic residues (Chapter 4) and molecular docking (Chapter 5). In the case of tryptophan synthase, where substrate channeling occurs

Reproduced with permission of the copyright owner. Further reproduction prohibited without permission.

through a hydrophobic tunnel, mutation alone was sufficient to obstruct channeling [61]. With TS-DHFR we sought also to use targeted molecular docking searches to identify small molecules that bind within the shallow electrostatic groove and to examine their ability to inhibit enzymatic activity as well as parasite growth in cell culture.

The second parts of Chapters 4 and 5 respectively, describe preliminary studies involving point mutations in regions of *T.gondii* and *C. hominis* TS-DHFR hypothesized to participate in domain-domain communication, and molecular docking into a novel non-active site pocket in *C. hominis* TS-DHFR, as well as plans for creation of a bifunctional *T. gondii* TS-DHFR inhibitor. Conclusions and future directions of this research are presented in the final chapter, Chapter 6.

Reproduced with permission of the copyright owner. Further reproduction prohibited without permission.

Chapter Two

Experimental Methods

Reproduced with permission of the copyright owner. Further reproduction prohibited without permission.

Overview: Rapid Transient Kinetics

Enzyme kinetics can be studied using either a steady-state or rapid transient (pre-steady-state) kinetic approach. Steady-state methodologies are widely used because they require a minimal amount of enzyme and can allow one to quickly and easily determine general features of enzyme activity and mechanism. Steady-state analysis is an indirect method from which one can infer information about the rate-limiting step of an enzymatic reaction, as well as determine maximum velocity of the multi-turnover reaction (V_{max}), apparent affinity of substrates (K_m), affinity of inhibitors (K_i), order of substrate binding, order of product release, and reaction reversibility. While the kinetic parameters obtained through steady-state experiments can be useful, particularly for screening purposes, they are complex functions and, as such, offer little insight into the individual steps in a kinetic pathway or the reaction kinetics of intermediate formation at the enzyme active site.

By contrast, rapid transient kinetic analysis allows one to directly measure discrete events occurring at the enzyme active site. These include the rates of ligand binding and release, rates of individual chemical steps, rates of conformational changes occurring during catalysis, and rates of formation and decay of any transient intermediates at the enzyme active site. Transient kinetics also has several advantages for investigation of substrate channeling because, in principle, this technique enables one to directly monitor chemical catalysis at each active site as well as the transit of the putative intermediate from one active site to another [63, 105].

For the reasons detailed above, steady-state kinetic analysis was reserved primarily for the screening of inhibitors predicted by molecular docking searches. The

Reproduced with permission of the copyright owner. Further reproduction prohibited without permission.

majority of experiments instead employed rapid transient kinetics methodologies under single enzyme turnover or pre-steady-state burst conditions. Single enzyme turnover conditions represent the most definitive way to examine the reactions at the active site and to detect transient enzyme intermediates. This type of experiment requires enzyme to be in sufficient excess over substrate that binding or product release is not rate-limiting, and essentially only one enzyme turnover occurs upon initiation of the reaction. The reaction proceeds (typically on a millisecond timescale) with consumption of substrate and corresponding product formation at a single exponential rate equal to the rate of the chemical step, or a rate-limiting step prior to chemistry, such as conformational change.

A complementary type of experiment is the pre-steady-state burst in which both the first enzyme turnover and multiple subsequent turnovers are evaluated to determine the concentration of functional active sites, and to detect and measure a rate-limiting step after chemical catalysis, such as product release. Here substrate is in 3 to 5-fold excess over enzyme, allowing one to observe multiple turnovers. If a rate-limiting step follows a faster chemical step, a "burst" will be observed, with the initial fast rate (also called the burst rate) corresponding to the rate of chemistry detected during the first enzyme turnover. If a step after chemistry is rate-limiting, the reaction will encounter a bottleneck following the first turnover that will limit all subsequent turnovers. As a result, the fast phase will be followed by a slow phase and subsequent turnovers will be observed at a linear, steady-state rate. Alternatively, a burst may be observed if the rate of formation of an intermediate species is faster than chemistry. Since the burst corresponds to the first reaction turnover, the amplitude of the burst represents the concentration of functional enzyme active sites and burst experiments are often employed to obtain this information.

Reproduced with permission of the copyright owner. Further reproduction prohibited without permission.

If on the other hand, chemistry or a step prior to chemistry is rate-limiting, no burst will be observed; instead the reaction will simply proceed at the linear steady-state rate. In this case, another methodology, such as following fluorescence changes accompanying ligand titration, will be required to determine the percentage of functional active sites.

Steady-state kinetics is monitored on a time scale of seconds or minutes and thus assays can be conducted using a UV/Vis spectrophotometer (manually initiating and mixing), or by manually quenching a reaction with radiolabeled substrates (bench-top quench experiments). A single enzyme turnover proceeds over a millisecond time course, however, requiring the use of specialized equipment: a rapid chemical quench box or stopped flow fluorescence/absorbance instrument. In rapid chemical quench experiments, enzyme is mixed with radiolabeled substrate for a programmed millisecond time interval and then quenched with a chemical agent such as base to stop the enzymatic reaction. Quantification of the conversion of radiolabeled substrates to products is accomplished by High Performance Liquid Chromatography (HPLC) analysis interfaced with an in-line radioactivity flow detector.

Stopped-flow fluorescence/absorbance experiments can provide rates of enzyme catalysis, information about substrate or inhibitor binding (e.g. on and off rates), and also evidence of enzyme conformational change. Here, substrate or inhibitor ligand is rapidly mixed with enzyme and a change in fluorescence or absorbance is monitored as equilibrium is reached. In the case of the bifunctional TS-DHFR enzyme, changes in intrinsic protein fluorescence (excitation at 280 nm and emission at 340 nm) as well as fluorescence resonance energy transfer (FRET) from NADPH (excitation at 280 nm and emission at 450 nm) at the DHFR site, and from the folate analog PDDF (excitation at

Reproduced with permission of the copyright owner. Further reproduction prohibited without permission.

287 nm and emission at 380 nm) at the TS site, serve as useful spectroscopic signals to monitor the kinetic reactions. Stopped-flow absorbance experiments also provide information by monitoring the decrease in absorbance at 340 nm corresponding to the consumption of NADPH. These and other methodologies employed in this research are detailed follows.

Fig. 2.0 Rapid chemical quench box. Portrait by Jeffrey Benjamin.

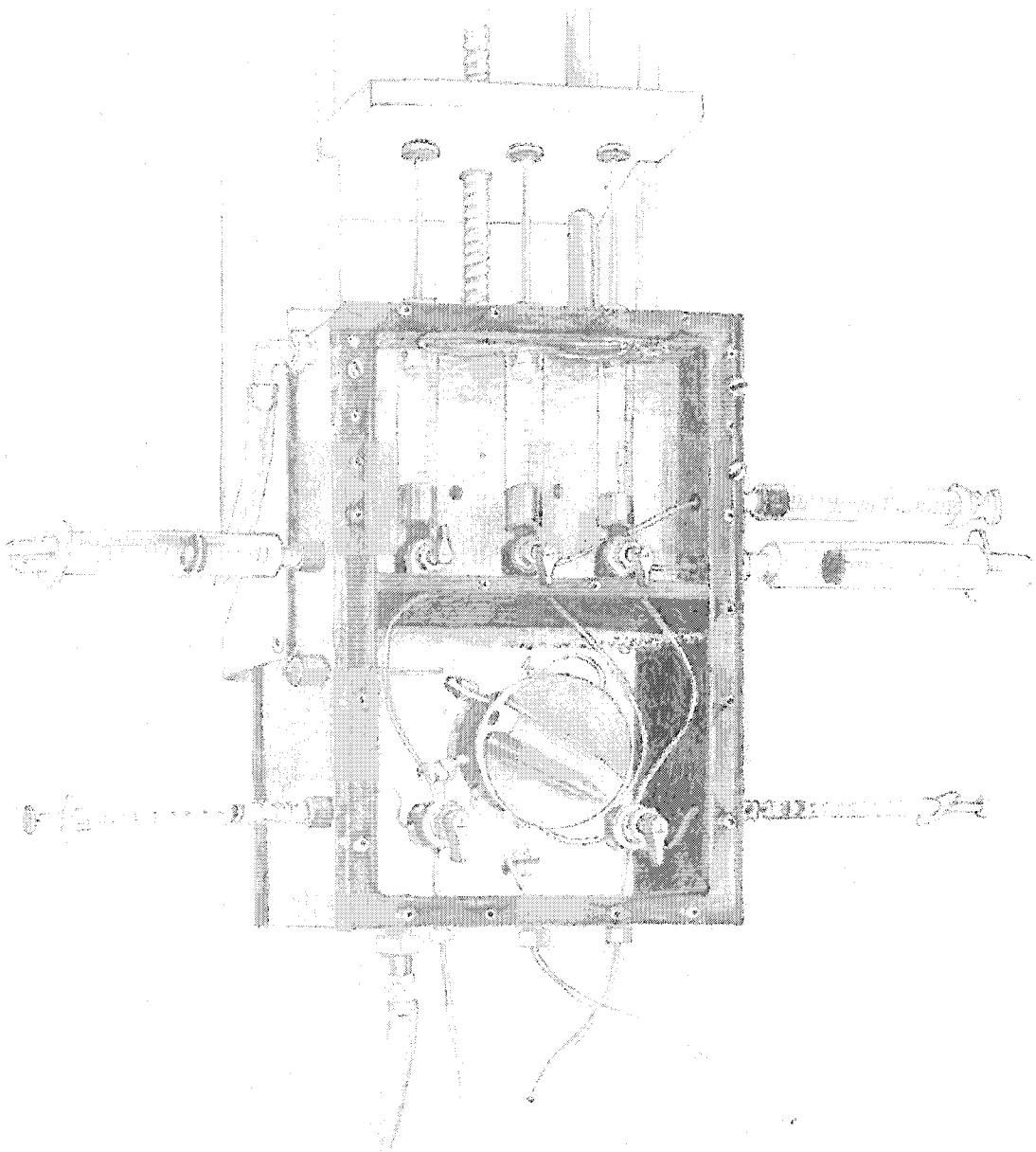

Reproduced with permission of the copyright owner. Further reproduction prohibited without permission.

Chemicals and Reagents

All buffers and other reagents employed were of the highest chemical purity. Millipore ultrapure water was used for all solutions. CH_2H_4folate, H_2folate, and pteroylpenta-Y-L-glutamic acid were purchased from Schircks Laboratories (Switzerland). H_4folate was synthesized by reduction of folic acid with sodium borohydride. Unlabeled or tritium-labeled H_2folate and CH_2H_4folate were synthesized using unlabeled or tritiated folic acid as a starting material. The [3',5',7,9-^{3}H] folic acid, as well as ^{14}C labeled dUMP and FdUMP (5-fluorodeoxyuridine-5'-monphosphate, [2-^{14}C]), were obtained from Moravek Biochemicals (Brea, CA). Tritium-labeled H_2folate was chemically prepared from the reduction of folate by sodium hydrosulfite [73]. Tritiated CH_2H_4folate was prepared enzymatically: tritium-labeled H_2folate was converted to tritiated H_4folate by *L. major* TS-DHFR + NADPH (DHFR reaction), and condensed with formaldehyde to form CH_2H_4folate [74]. The natural (6R)-L-CH_2H_4folate enantiomer was used exclusively in the studies. Both H_2folate and CH_2H_4folate were purified using a DE-52 anion exchange resin (Whatman Co., Maidstone, England); eluted with a linear gradient of triethylammonium bicarbonate [75]. Concentrations of H_2folate, H_4folate and CH_2H_4folate were determined using molar extinction coefficients of 28,000 M^{-1} cm^{-1} at 282 nm [76]; 28,000 M^{-1} cm^{-1} at 297 nm [77]; and 32,000 M^{-1} cm^{-1} at 290 nm [78], respectively. H_2folate and CH_2H_4folate solutions were stored in argon purged vials at –80°C.

NADPH, dUMP, methotrexate, trimethoprim, fluorescein, phenolphthalein, steptonigrin, and flavin mononucleotide were purchased from Sigma. The concentration of NADPH was determined by using a molar extinction coefficient of 6220 M^{-1} cm^{-1} at

Reproduced with permission of the copyright owner. Further reproduction prohibited without permission.

340 nm. Eosin B was purchased from ABCR (A Better Choice for Research Chemicals, Karlsruhe, Germany); the tetra-bromo derivative of eosin B (benzoic acid, 2-(2,4,5,7-tetrabromo-8a,10a-dihydro-6-hydroxy-3-oxo-3H-xanthen-9-yl)-(9Cl)) was purchased from Specs (Rijswijk, The Netherlands). F1092-1772 and F0917-7119 were purchased from Ambinter (Paris, France)

Protein Expression, Purification, and Mutagenesis

The clone of the wild-type bifunctional TS-DHFR enzyme from *L. major*, in a pO2CLSA-4 plasmid and *E. coli* Rue 10 expression vector, was a generous gift from C.-C. Kan and D. Matthews, then at Agouron Pharmaceuticals. The *T. gondii* TS-DHFR coding sequence in a PET15b expression vector was kindly provided by David S. Roos. *P. falciparum* TS-DHFR protein was generously sent by Dr. Worachart Sirawaraporn at a concentration of 1.5 mg/ml in a storage buffer containing 50 mM TES, pH 8.0, 0.1 mM EDTA, 10 mM DTT, 50 mM KCl and 20% glycerol. *C. hominis* TS-DHFR was purified from a single colony of pTrc99A-rHCp (the "genotype 1" TS-DHFR gene derived from a human parasite isolate) in *E. coli* strain PA414 (*dhfr-)* on an LB Amp/Kan petri plate kindly provided by Dr. Richard G. Nelson and Amy C. Anderson. We are grateful to Sydney Hoeltzli and Carl Frieden for an *E. coli* DHFR clone; to Louise Wallace and Bob Matthews for *E. coli* DHFR protein; and to Frank Maley for *E. coli* TS protein.

These clones were used to obtain protein of high purity by previously described methods for purification, including a methotrexate column (Sigma) and elution with H_2folate [5, 56]. The protein was further purified using an Amersham Biosciences Superdex 75 Highload (26/60) gel filtration column to get rid of residual H_2folate. The purified *C. hominis* enzyme contains negligible H_2folate and approximately 5% of DHFR

Reproduced with permission of the copyright owner. Further reproduction prohibited without permission.

active sites have NADPH bound. The *T. gondii* V610Am (Amber stop codon) mutant was generated using a QuikChange Mutagenesis kit (Stratagene, La Jolla, CA) with 5'-CCAGATGGAGATGGCTTAGTGCGGAAATACAGAAGC-3' and its reverse complement as mutagenic primers; the underlined TAG amber stop codon replaces the wild-type GTC. Plasmid containing the desired mutation, as confirmed by nucleic acid sequencing, was used to transform competent BL21 *E. coli* cells and protein was purified in a manner similar to wild-type.

L. major channel and *C. hominis* cross-over helix mutants were similarly created, using a QuikChange Mutagenesis kit (Stratagene). Preliminary enzyme activity assays were conducted on small-scale and full-scale growths prior to purification. Large growths, typically 22 L, were necessary to obtain sufficient protein from the more impaired mutants. Mutation of *L. major* K73 or R74 led to very low yields of active enzyme (0-0.5 mgs per liter) and large amounts of insoluble enzyme by gel analysis of the cell pellet (data not shown).

Determination of Enzyme Concentrations

The TS-DHFR protein concentration was estimated spectrophotometrically at 280 nm using extinction coefficients of 67,800 $M^{-1}cm^{-1}$ for *L. major*; 78,800 $M^{-1}cm^{-1}$ for *T. gondii*; and 80,722 $M^{-1}cm^{-1}$ for *C. hominis*.

To rule out the possibility that differences in rates between *L. major* wild-type and mutant enzymes were a result of having different numbers of functional active sites at the same protein concentration, TS active site titrations were performed. One μM PDDF (10-propargyl-5, 8-dideazafolate =CB3717, a folate analog that binds at the TS active site) was titrated with enzyme, and the change in intensity of a fluorescence resonance energy

Reproduced with permission of the copyright owner. Further reproduction prohibited without permission.

transfer (FRET) peak at 396 nm was recorded on a SLM 4800 fluorimeter (Urbana, IL) with the excitation set to 280 nm. Active site titrations were carried out by adding enzyme in small aliquots to minimize any dilution effects, and with constant stirring in a 3 ml quartz cuvette at 25°C. Fluorescence measurements were recorded as an average of four 10 s readings within 15-30 s of enzyme addition, and the recorded fluorescence intensities were corrected for dilution [4]. The inflection point of the curve, obtained by plotting intensity versus enzyme concentration, approximates the amount of enzyme required to fully bind 1 μM PDDF. One μM wild-type *L. major* TS-DHFR; R64Q; R283E; and the K282E, R283E double mutant fully bound 1 μM PDDF. When the starting concentration of PDDF was doubled (2 μM), the inflection point occurred when 2 μM wild-type *L. major* TS-DHFR had been added (Fig. 2.1).

Spectroscopic Enzyme Activity Assays

TS activity was monitored by following the increase in absorbance at 340 nm that accompanies the conversion of substrates dUMP and CH_2H_4folate to dTMP and H_2folate [61]. The DHFR activity was determined by following the decrease in absorbance at 340 nm that accompanies the conversion of substrates NADPH and H_2folate to products $NADP^+$ and H_4folate [65] . The wild-type *L. major* protein has TS and DHFR activities similar to those previously reported: 6.4 $mM^{-1}cm^{-1}$ and -12.8 $mM^{-1}cm^{-1}$, respectively [4, 5, 65]. TS-DHFR activity was determined by following the decrease in absorbance at 340 nm that accompanies the conversion of substrates NADPH and H_2folate (produced at TS) to products $NADP^+$ and H_4folate.

Reproduced with permission of the copyright owner. Further reproduction prohibited without permission.

Fig. 2.1 Active-site concentrations of *L. major* wild-type TS-DHFR and the K282E, R283E double mutant measured by titrating 1 μM or 2 μM PDDF with enzyme. Recorded as intensity of the PDDF FRET peak at 396 nm as a function of enzyme concentration. The inflection point when 1 μM PDDF is titrated with either wild-type (●) or the K282E, R283E mutant (▼) is found near 1 μM enzyme, whereas the inflection point is close to 2 μM when wild-type TS-DHFR is titrated with 2 μM PDDF (■), indicating that TS active-site concentration is similar to protein concentration.

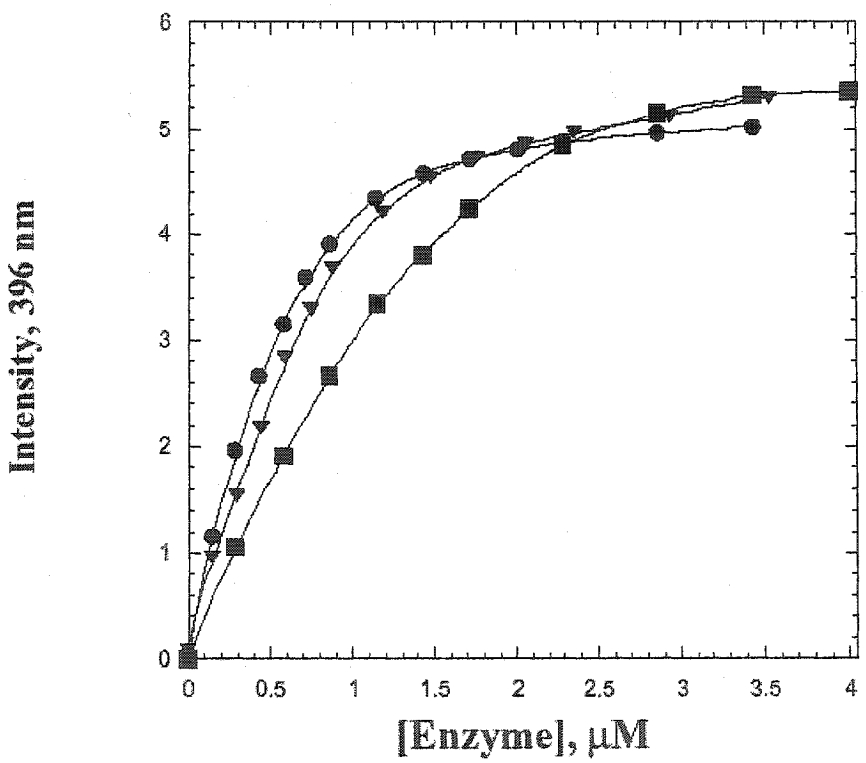

Reproduced with permission of the copyright owner. Further reproduction prohibited without permission.

Rapid Chemical Quench Experiments

Rapid quench experiments were performed using a Kintek RFQ-3 Rapid Chemical Quench Apparatus (Kintek Instruments, Austin, TX). The single enzyme turnover reaction was initiated by mixing the 15 µl enzyme solution (enzyme + 2x reaction buffer: 1mM EDTA, 50 mM $MgCl_2$, 50 mM Tris, at pH 7.8) with the tritiated substrates (15 µl, approx 20,000 dpm); in all cases, concentrations of enzyme and substrates cited in the text are those after mixing. The TS-DHFR single enzyme turnover reaction was monitored by addition of tritiated CH_2H_4folate to enzyme + NADPH and dUMP. Since CH_2H_4folate is more stable under basic conditions, triethylammonium bicarbonate was added to maintain a pH of 9.5 until mixing with enzyme; the final pH during the reaction was 7.8. The DHFR reaction was monitored by addition of tritiated H_2folate to enzyme + NADPH. In experiments to test the effect of inhibitors, fresh stocks of 25 mM inhibitor in DMSO were made prior to each experiment. Four percent of the final reaction volume was reserved for the inhibitor (1 mM inhibitor, final) or DMSO (control). The enzymatic reactions were terminated by quenching with 67 µl of 0.78 N KOH to give a final concentration of 0.54 N KOH and a pH of 12.6 [56]. The quench solution also contained 10% sodium ascorbate and 200 mM 2-mercaptoethanol to prevent oxidative degradation of H_2folate. Degradation was also minimized by storing samples at –80° C until just prior to use.

The TS reaction was also monitored under burst conditions: 7.5 µM enzyme + 250 µM CH_2H_4folate mixed with 90 µM [^{14}C] dUMP. TS reactions utilizing radiolabeled dUMP were quenched with 67 µl of 0.4 N HCl.

Reproduced with permission of the copyright owner. Further reproduction prohibited without permission.

The rate constants for individual single-turnover rapid chemical or burst quench experiments were estimated by fitting the data to a single exponential or burst curve using the curve fitting program, Kaleidagraph.

HPLC Analysis

Tritiated products of the rapid quench experiments were quantified by HPLC in combination with a radioactivity flow detector. The HPLC separation was performed using a BDS-Hypersil C18 reverse phase column (250 mm x 4.6 mm, Keystone Scientific, Bellefonte, PA) with a flow rate of 1 ml/min. An isocratic separation using a solvent system of 10% methanol in 180 mM triethylammonium bicarbonate at pH 8.0 was employed. The elution times were as follows: H_4folate, 9 min; H_2folate, 18 min; CH_2H_4folate, 20 min. For separation of dUMP and dTMP, an isocratic separation using a solvent system of 200 mM triethylammonium bicarbonate was used. The elution times were as follows: dUMP, 11 min; dTMP 21.5 min. The HPLC effluent from the column was mixed with liquid scintillation cocktail (Monoflow V, National Diagnostics) at a flow rate of 5 ml/min. Radioactivity was monitored continuously using a Flo-One radioactivity-flow detector (Packard Instruments, Downers Grove, IL). The analysis system was automated using a Waters 712B WISP (Milford, MA) autosampler.

Stopped-flow Absorbance/Fluorescence Measurements

Stopped-flow measurements were performed using a Kintek SF-2001 apparatus (Kintek Instruments, Austin, TX) as detailed previously [56]. In the absorbance experiments designed to measure the burst in CH_2H_4folate consumption in the TS reaction, absorbance at 340 nm was monitored when 25 μM enzyme was pre-incubated

Reproduced with permission of the copyright owner. Further reproduction prohibited without permission.

with 1 mM dUMP and buffer (1 mM EDTA, 50 mM $MgCl_2$, 50 mM Tris, at pH 7.8) and then mixed with 500 μM CH_2H_4folate. For TS, protein conformational change upon substrate binding was followed by setting the monochrometer to 287 nm on the input and monitoring the change in intrinsic enzyme fluorescence with an output filter at 340 nm (7.5 μM enzyme was pre-incubated with 100 μM FdUMP and buffer and then mixed with 50 μM CH_2H_4folate). For DHFR, NADPH coenzyme fluorescence resonance energy transfer (FRET) experiments were carried out with a 290 nm excitation and an output filter at 450 nm. In DHFR burst experiments, 7.5 μM enzyme was pre-incubated with 50 μM H_2folate and buffer and then mixed with 500 μM NADPH. In single enzyme turnover experiments, 50 μM enzyme was pre-incubated with 500 μM NADPH and buffer and then mixed with 10 μM H_2folate.

In the fluorescence experiments designed to measure dissociation rate constants, the trapping ligand (L2) was used at a concentration of ≥5-fold excess over that of L1 to allow for analysis as a pseudo-first-order rate constant. Fluorescence changes were monitored following excitation at 287 nm and emission at 340 nm. In experiments involving enzyme and PDDF, however, the monochromator was set at 287 nm on the input and the FRET was monitored with an interference filter at 380 nm to determine k_{on} and a 340 nm cut-off filter to measure k_{off}. The data were collected over a given time interval using a PC and software provided by Kintek Instruments. An average of 4-7 runs was used for data analysis: rate constants were obtained by fitting the data to a single or double exponential by nonlinear regression analysis.

Reproduced with permission of the copyright owner. Further reproduction prohibited without permission.

Kinetic Simulation

The KinTekSim kinetic simulation program (V. 3.0.3) was used to model the *C. hominis* TS-DHFR kinetic data [56, 78]. As a starting point, measured *C. hominis* rate constants were substituted into the minimal kinetic mechanism derived for *T. gondii* TS-DHFR [30]. The resulting model and estimated rate constants are presented in Fig. 3.5.

Spin-Column Binding Assays

Bio-Spin P-30 columns (Biorad) were washed with 10 mM Tris, and twice with 1x rapid chemical quench reaction buffer (each wash 1ml). Columns were loaded with 30 µL enzyme (50 µM) + ligands in reaction buffer; centrifuged for 1 min at 2000 rpm; an additional 30 µL reaction buffer was added to the column, and the centrifugation step was repeated. It was shown by UV absorbance that virtually all of the enzyme added to the column was recovered in the flow-through. The amount of enzyme-bound radiolabeled ligand in the flow-through was quantified by adding the 60 µL flow-through to 7 ml of Ultima Gold scintillation cocktail (Packard), and counting on an LS7000 scintillation counter (Beckman). Only 1% of total FdUMP counts came through the column in the absence of enzyme: these background counts were subtracted from the total recovered in the presence of enzyme.

Steady-State Spectroscopic Channeling Assays

The steady-state reaction was monitored spectroscopically using a procedure similar to that of Meek *et al.*, 1985 [65]. Meek *et al.* observed a lag in formation of the products of the DHFR reaction ($NADP^+$ and H_4 folate) when monofunctional TS and DHFR enzymes were combined, but not in the case of bifunctional TS-DHFR from *L.*

Reproduced with permission of the copyright owner. Further reproduction prohibited without permission.

tropica, suggesting that only in the case of the bifunctional enzyme, H_2folate produced at the TS site was directly transferred to the DHFR site. The predicted change in absorbance was very small, therefore, a 10 cm pathlength quartz observation cell was used to enhance sensitivity. The assay mixture (25 ml) containing buffer (50 mM Tris, pH 7.8, 1 mg/ml of BSA, 1 mM EDTA, 5 mM formaldehyde, 75 mM 2-mercaptoethanol), 10 nM enzyme, and 28 μM CH_2H_4folate was incubated with 20 μM NADPH until the OD at 340 nm stabilized, indicating enzymatic consumption of endogenous traces of H_2folate. The reaction was then initiated with 100 μM dUMP (final concentration), and the decrease in NADPH absorbance at 340 nm was monitored in the absence of added H_2folate. Experiments were performed using a Perkin Elmer Lambda 2 UV/Vis Spectrophotometer and running PECSS (Perkin Elmer Computerized Spectroscopy Software), Version 4.0.

Steady-state Quench Experiments to Determine Inhibitor IC_{50}

The reactions were initiated by mixing the 15 μl enzyme solution (enzyme; 2x reaction buffer: 1 mM EDTA, 50 mM Mg Cl_2, 50 mM Tris, at pH 7.8; saturating NADPH and dUMP; and inhibitor in DMSO or DMSO alone as control) with the 15 μl CH_2H_4folate. Four percent of the final reaction volume was reserved for eosin or the tetra-bromo derivative (1 mM inhibitor, final) or DMSO (control). A final concentration of 10 μM tritiated CH_2H_4folate (approximately 20,000 dpm) was supplemented with unlabeled substrate. In all cases, concentrations of enzyme and substrates cited in the text are those after mixing. The reactions were manually terminated by quenching with 67 μL of 0.78 N KOH to give a final concentration of 0.54 N KOH.

Reproduced with permission of the copyright owner. Further reproduction prohibited without permission.

Molecular Docking[2]

All docking calculations for the *L. major* enzyme were performed with the December 1999 development version of NWU DOCK, a version derived from UCSF DOCK 3.5. This version incorporates the ensemble method of ligand flexibility for up to 2000 conformations per molecule [79]. The polar and non-polar close contact limits used in the steric grids were 2.3 and 2.6 Å [80]. The AMBER united atom charge set, distributed with Delphi, was used for all receptor electrostatic calculations. CHEMGRID was used to calculate a van der Waals potential for the enzyme using standard potentials [81]. Chemical labeling was used [82] in the matching calculation. This involves labeling site positions or atoms by chemical properties to speed the docking calculation. Here, five labels were employed: positive, negative, hydrogen bond donor, hydrogen bond acceptor, and neutral. All water molecules and counterions were removed from the receptor model.

We used the *L. major* TS-DHFR coordinates provided to us by Dr. David Matthews [6]. A dielectric of two for the protein interior [83] and 78 [84] for the water phase were used in the DelPhi calculations. The internal and external dielectrics in the hydration calculation were also set to 2 and 78. In the DelPhi calculation the probe size was set to 1.4 Å. Atomic van der Waals radii for the protein and the ligand were taken from Rashin [84]. In the Delphi calculation, the ionic exclusion radius was set to 2 Å and the ionic molarity was set to 0.1 M. The proper values of ligand and protein dielectrics, probe, van der Waals, and ionic radii are active areas of research; we have not tried to

[2] Procedures related to DOCK were performed and contributed by John Irwin in Dr. Brian K. Shoichet's lab, now at UCSF. Procedures related to GLIDE were performed and contributed by Marina Udier Blagovic and Oladapo Babatunde in Dr. William Jorgenson's lab at Yale University.

Reproduced with permission of the copyright owner. Further reproduction prohibited without permission.

optimize these terms. In the receptor potential calculation, three-step focusing [85] was used with protein containment iteratively set to 20, 60, and 90% with a 65.3 A3 lattice.

All data base searches used the same 152,571 molecule subset of the 1995.2 release of the ACD [86]. These molecules were selected based on our ability to calculate partial atomic charges [81] and included most of the molecules in the ACD-3D. Partial atomic charges were calculated by the method of Gasteiger and Marsili (22). Ligand solvation corrections were calculated using HYDREN [80].

The shallow groove region between the TS and DHFR-binding sites was explored using sets of spheres to describe the channel. Spheres were prepared starting from the sphgen program and filtered through the cluster program [81, 87], and then edited by hand using Midas [88]. Thirty-seven receptor spheres were used. The mean number of orientations per molecule was 3000. Eosin B, ACD code MFCD00005041, scored 14.2 kcal/mol in run 7, placing its rank as 198 of 152,571 molecules. The best energy score in the same run was 37 kcal/mol.

In later studies, *C. hominis* TS-DHFR was targeted using a second generation docking program, *GLIDE v.2.5* [89], in conjunction with the enzyme crystal structure. *GLIDE v.2.5* implements a novel algorithm for rapid chemical generation: the best binding mode was identified by exploring the target site using flexible ligand minimization and Monte Carlo sampling of an energy grid. The ligands were then optimized and roughly scored by a function that takes into account major interactions such as hydrogen bonding and Leonard Jones Forces. Libraries screened included the CMC (Comprehensive Medicinal Chemistry) Database and a propriety database from Schrödinger Chemicals.

Reproduced with permission of the copyright owner. Further reproduction prohibited without permission.

Evaluation of Inhibition of Parasite Replication in Cell Culture [3]

1. Evaluation of *In Vitro* Activity Against *T. gondii*.

Cell lines and culture conditions: Chinese hamster ovary (CHO) cells were grown as monolayers at 37°C in an atmosphere of 5% CO_2 in minimum essential medium supplemented with 2 mM L-glutamine and penicillin/ streptomycin (100 units/ml per 100 μg/ml).

Parasite cultivation: The RH strain tachyzoite of *T. gondii* was used and maintained by *in vitro* culture in HFF (Human foreskin fibroblast) cells as previously described [90].

Determination of parasite viability: CHO cells were seeded in triplicate at a density of $2x10^4$ cells/ml in a 24-well plate, allowed to attach for 24 h, and then infected with *T. gondii*. Parasite cultures were synchronized by removal of parasites that had not yet invaded 4 h after their inoculation into confluent cells. After incubation with various concentrations of eosin B for 24 h, *T. gondii* viability was evaluated 24 h post-infection by measurement of [^{3}H]uracil incorporated into the parasite nucleic acids. Briefly, 1 μCi of radiolabel was added to each well for 2 h before the monolayers were fixed with trichloroacetic acid, rinsed, and counted as described [91].

2. Evaluation of *In Vitro* Antimalarial Activity. Effects of eosin B on *P. falciparum* (FCR-3) were assessed by measuring the incorporation of the radiolabeled nucleic acid precursor, [^{3}H] hypoxanthine (Amersham Life Science) [92]. The test compound (eosin B) was initially dissolved in DMSO and subsequently 2-fold serially diluted in a 96-well flat-bottomed micro-titer plate (Falcon) with culture medium (RPMI-1640, 10% A+

[3] Procedures in this section were performed and contributed by Dr. Isabelle Coppens (*T. gondii*) and Kristen Massimine (*P. falciparum*), both then in Dr. Keith A. Joiner's lab at Yale University

Reproduced with permission of the copyright owner. Further reproduction prohibited without permission.

human plasma, 40 μg/mL gentamycin) to render final concentrations of 0.05 μM-100 μM eosin B. Parasitized erythrocytes (5% parasitemia and 5% hematocrit) synchronized to the ring stage were added to various inhibitor concentrations. The plates were then placed in a gas-tight box that was flushed with a gas mixture of 5% O_2 and 5% CO_2 balanced with 90% N_2, sealed, and incubated at 37°C. After 24 h, [^{3}H] hypoxanthine (0.5 μCi/well) diluted in culture medium was added to each well; following a further 18 h incubation, the cells were harvested onto glass fiber filters with a semi-automatic cell harvester and incorporation of [^{3}H]hypoxanthine into DNA was measured by liquid scintillation counting. IC_{50} values were determined as the amount of test compound required to inhibit [^{3}H] hypoxanthine uptake by 50% compared to the control, which consisted of complete medium as a substitute for the test compound. Values obtained are a result of triplicate experiments.

3. Measurement of Substrate Transport by the Oil-stop Technique. Transport experiments were carried out with varying concentrations of either labeled folic acid or leucovorin (50 nM to 50 μM) in HEPES-buffered saline medium (20 mM HEPES, 140 mM NaCl, 5 mM KCl, 2 mM $MgCl_2$, 5 mM glucose and 5 mM ATP, pH 7.4) for various times (30 sec to 10 min) at 37°C, to determine the apparent kinetic parameters (K_m and V_{max}) for both compounds. To initiate uptake, a 100 μl sample of parasites (between $5x10^6$ to $3x10^7$ cells) was added to 100 μl of transport buffer containing either radioactive folate or leucovorin. Substrate uptake was halted by centrifuging cells through an inert oil layer as described [93]. The quantity of radioactivity incorporated into *T. gondii* was normalized with parasite cell number. The form of radioactivity in the cell pellet fraction of the oil stop was determined by filtering this fraction (45 micron syringe filter) and then

Reproduced with permission of the copyright owner. Further reproduction prohibited without permission.

injecting it on the BDS-Hypersil C18 reverse phase HPLC column, using HPLC conditions described above. The elution times for folinic acid and folic acid were 11 and 16.5 min. Tritiated compounds from sonicated parasites were matched to non-radiolabeled standards (OD 296 nm).

4. Light and Electron Microscopy. Light and epifluorescence microscopy were performed on infected cells seeded on sterile coverslips in 24-well culture dishes using a Microphot FXA microscope (Nikon Inc., Melville, NY). Images were captured on a Photometrics SenSys CCD camera, processed using Image-Pro Plus software (Media Cybernetics, Silver Spring, MD), and scanned (Hewlett Packard, ScanJet IIcx) into Adobe Photoshop software (Adobe Systems Inc.). For thin-section transmission electron microscopy (TEM), cells were fixed in 2.5% glutaraldehyde (EM Science) and 0.1 M sodium cacodylate buffer (pH 7.4) for 1 h at room temperature. They were then washed 3 times in 0.1 M cacodylate buffer and then postfixed for 1 h in 1% osmium tetroxide (EM Science) in the same buffer at room temperature. After 3 washes in water, the samples were stained for 1 h at room temperature in 2% uranyl acetate (EM Science), washed again in water and dehydrated in a graded series of ethanol. Samples were then embedded in Embed-812 epoxy resin (EM Science). Ultrathin (50-60 nm) sections were cut using a Reichert Ultracut ultramicrotome and collected on formvar- and carbon-coated nickel grids, stained with 2% uranyl acetate and lead citrate before examination with a Philips 410 Electron Microscope (Eindhoven, the Netherlands) under 80 kV. For immunoelectron microscopy, samples were fixed, LR White embedded and immunolabeled as described [94] by using anti-TS-DHFR antibodies (diluted 1:10) revealed by protein A-gold particles (18 nm). Immunofluorescence microscopy

Reproduced with permission of the copyright owner. Further reproduction prohibited without permission.

analysis was performed as detailed previously [95]: HFF monolayers grown on coverslips were infected with *T. gondii*; a 1:50 dilution of rabbit anti-TS-DHFR antibodies was used.

5. Visualization of Eosin B Accumulation. To visualize where eosin B associated within *T. gondii*, both infected cells and extracellular parasites were respectively incubated in culture medium containing different concentrations of eosin B. Coverslips with live cells were directly observed with an epifluorescence microscope. To measure the kinetics of eosin B association with the parasite, intravacuolar parasites were incubated with the compound for varying times, purified by density gradient using Nycodenz as described [90] and analyzed by spectrofluorimetry at 525 nm (eosin B excitation 460 nm; emission 550 nm).

Reproduced with permission of the copyright owner. Further reproduction prohibited without permission.

Chapter Three

Kinetic Characterization of Bifunctional TS-DHFR from the Apicomplexan Protozoa *Cryptosporidium hominis*

Reproduced with permission of the copyright owner. Further reproduction prohibited without permission.

Part A. Kinetic Characterization of Bifunctional TS-DHFR from C. hominis: A Paradigm Shift for TS Activity and Channeling Behavior

INTRODUCTION

Almost a decade of research on bifunctional TS-DHFR from protozoal parasites has relied on the only available TS-DHFR crystal structure, that from the kinetoplastid protozoa *Leishmania major* [6]. The recent solution of the crystal structures of TS-DHFR enzymes from two clinically relevant apicomplexan protozoa, *Plasmodium falciparum* and *Cryptosporidium hominis*, however, has revealed unanticipated deviations from the kinetoplastid model [8, 9]. An obvious next question is whether these significant structural differences manifest in significant mechanistic differences between parasite classes. Part A of this chapter we seek to address this question through a detailed kinetic characterization of TS-DHFR from *C. hominis*, again yielding surprising results.

A major conclusion of the recent solution of the apicomplexan TS-DHFR structures is that there exist two families of bifunctional TS-DHFR structures: a short linker family with an N-terminal tail, as in the kinetoplastids (a class which includes *Leishmania* and the trypanosomes), and a long linker family with a donated or cross-over helix, as in the apicomplexan parasites (which include *P. falciparum, C. hominis* and *Toxoplasma gondii*) [9]. Are these large structural differences correlated with mechanistic or functional differences? To address this question we have applied a transient kinetic approach to the study of TS-DHFR from *C. hominis*. We focused our

Reproduced with permission of the copyright owner. Further reproduction prohibited without permission.

efforts in three areas: determination of the *C. hominis* TS-DHFR kinetic mechanism, substrate channeling, and communication between the TS and DHFR domains.

TS is more highly conserved than DHFR. When the *C. hominis* TS-DHFR nucleic acid sequence was ascertained, it was noted that there exist unique residues in the DHFR domain analogous to mutations conferring resistance to anti-folate therapies in other species. It was postulated that these intrinsic differences may explain why *C. hominis* is refractory to the anti-folate drugs that are standard therapy for other apicomplexan infections. In the case of the TS domain, a change in a single conserved residue of unknown significance was mentioned [7]. The *C. hominis* crystal structure revealed a nine-stranded rather than the usual eight-stranded beta sheet in the DHFR domain, and a TS domain strongly resembling that from most eukaryotes [9]. These findings, combined with the fact that we had previously observed mechanisic differences between *T. gondii* and *L. major* DHFR but not TS [30], led us to speculate that unique features in the *C. hominis* mechanism would most likely involve the DHFR domain.

Our second objective was to explore the possibility of substrate channeling. An attractive hypothesis to explain the advantage of a having a bifunctional TS-DHFR enzyme is that H_2folate produced at TS is directly channeled to the DHFR active site, without equilibration in bulk solution [6, 29]. Indeed, there is evidence for substrate channeling with both *L. major* and *T. gondii* TS-DHFR. In the case of these bifunctional enzymes, unlike with the combination of monofunctional TS + DHFR, H_2folate produced at the TS active site does not substantially accumulate in solution and there is no lag in product formation at DHFR, suggesting that the TS product does not leave the protein and enter bulk solution before binding at DHFR [30, 56, 96]. Steady-state spectroscopic

Reproduced with permission of the copyright owner. Further reproduction prohibited without permission.

analysis, used to detect the presence or absence of a lag in $NADP^+$ production via the DHFR catalyzed reduction of H_2folate formed at TS, also supports substrate channeling by both *L. major* and *T. gondii* TS-DHFR [65, 97]. As detailed in Chapter 1, the *L. major* TS-DHFR crystal structure lends itself to the possibility of substrate channeling, whereas the scattered basic residues and orthogonal active-site orientations in the apicomplexa structures pose a challenge to the channeling hypothesis. We sought to determine whether or not there was mechanistic evidence for substrate channeling by *C. hominis* TS-DHFR.

Finally, the most striking differences between the *L. major* and apicomplexa structures exist in non-active site regions: the N-terminal tail in the case of *L. major*, and the long-linker region in the case of the new structures. Do these structural differences in non-active site regions result in differences in domain-domain communication, or conformational changes induced by ligand binding at one active site that affect activity at the other active site of the bifunctional enzyme? There is evidence with *L. major* TS-DHFR for domain-domain communication, summarized in Chapter 1. Unlike *T. gondii* DHFR where activity is maximal even when TS is in an unliganded state [30], with *L. major*, formation of a dUMP-CH_2H_4folate-enzyme ternary complex at TS accelerates the DHFR rate 20-fold [56]. There is further evidence of reciprocal communication in *L. major* in that an additional conformational change at TS occurs in the presence of the DHFR ligand, NADPH. Addition of the DHFR folate inhibitor, methotrexate, results in a 4-fold slower *L. major* TS single enzyme turnover rate [56]. Complementary ligand-binding studies, reported here, have been conducted with *C. hominis* and *T. gondii* TS-DHFR to probe communication between domains.

Reproduced with permission of the copyright owner. Further reproduction prohibited without permission.

RESULTS

Transient Kinetic Analysis to Assess TS, DHFR and TS-DHFR Activity

The *C. hominis* TS and DHFR steady-state rates were found to be 2.4 s^{-1} and 2.3 s^{-1}, respectively, in a spectroscopic activity assay (340 nm). Since the specific activity of DHFR is typically significantly higher than that of TS, steady-state kinetics provided the first clue that *C. hominis* TS-DHFR is unusual. We followed up this initial steady-state experiment with a thorough transient kinetic analysis, including both single enzyme turnover and pre-steady-state burst conditions.

Single enzyme turnover experiments, which measure the rate of chemical conversion of substrate to product at the active site under conditions where enzyme concentration is sufficiently high that substrate binding is not rate-limiting, were performed using a rapid chemical quench apparatus. To monitor the TS reaction, the bifunctional enzyme (78 μM) was pre-incubated with a saturating concentration of dUMP (500 μM) and then mixed with a limiting amount of radiolabeled CH_2H_4folate (11 μM). All reported concentrations are final, after mixing. *C. hominis* TS was found to be remarkably fast: 45 s^{-1} (data not shown). The TS single enzyme turnover rate is typically significantly slower than that of DHFR, so the TS rate limits and is equivalent to that of TS-DHFR: it was confirmed that the rate of CH_2H_4folate consumption in the TS-DHFR reaction is also 45 s^{-1} (Fig. 3.0 A).

The *C. hominis* DHFR reaction was monitored by stopped-flow fluorescence (Ex 290 nm, Em 450 nm): bifunctional enzyme (40 μM) was pre-incubated with a saturating concentration of NADPH (500 μM) and then mixed with a limiting amount of H_2folate (10 μM). Like with *T. gondii* but not *L. major*, DHFR appears to be in an "activated"

Reproduced with permission of the copyright owner. Further reproduction prohibited without permission.

state even in the absence of TS ligands: the DHFR rate for *C. hominis* was found to be 130 s^{-1} (Fig. 3.1A). This DHFR rate was confirmed in a rapid chemical quench experiment under similar conditions.

To monitor the TS-DHFR reaction, the bifunctional enzyme (45-78 μM) was pre-incubated with saturating concentrations of dUMP (500 μM) and NADPH (500 μM) and then mixed with a limiting amount of radiolabeled CH_2H_4folate (11-13.5 μM). As mentioned above, the rate of CH_2H_4folate consumption was found to be 45 s^{-1} (Fig. 3.0 A). The TS-DHFR reaction also provided HPLC evidence for a TS intermediate and a large accumulation of H_2folate, further discussed in subsequent sections. Even at 1 min, 13% of radioactivity was contained in a peak corresponding to H_2folate. In a side-by-side experiment, using the same CH_2H_4folate substrate, 0-4% of radiolabel corresponded to H_2folate after a 1 min TS-DHFR reaction using the *T. gondii* enzyme. No H_2folate was present in the no enzyme control.

Stopped-flow and rapid chemical quench experiments were also performed under pre-steady-state burst conditions (substrate in slight excess over enzyme). Similar to the other bifunctional enzymes studied, a DHFR burst was visualized by stopped-flow fluorescence (Ex 290 nm, Em. 450 nm; 7.5 μM TS-DHFR; 50 μM H_2folate, 500 μM NADPH) using *C. hominis* TS-DHFR (Fig. 3.1B). The *C. hominis* DHFR burst has a fast rate (~100 s^{-1}), followed by a slow rate matching the steady-state rate obtained in the steady-state activity assay. Results of burst experiments aimed at elucidating the *C. hominis* TS mechanism are reported in the next section.

Reproduced with permission of the copyright owner. Further reproduction prohibited without permission.

Fig. 3.0 *C. hominis* TS-DHFR single turnover reaction time courses.

C. hominis TS-DHFR reaction: CH_2H_4folate (■); H_2folate + intermediate (▲); H_4folate (●). *A*, When 78 μM bifunctional enzyme is reacted with 13 μM tritiated CH_2H_4folate, the rate of CH_2H_4folate consumption is 45 s^{-1} and maximum accumulation of H_2folate is 65% of tritiated product. *B*, Magnification of early time points from (*A*) reveals that H_2folate + intermediate accumulates before there is significant conversion to H_4folate. H_4folate production is fit to two curves: top curve is single exponential fit from (*A*), but points fit better to a slow followed by a fast phase (heavy line). *C*, KinTekSim model of the *C. hominis* TS-DHFR single enzyme turnover reaction superimposed on rapid chemical quench data. H_2folate and the TS intermediate are plotted together to simulate the experimental data, but are modeled separately in the inset (same axis labels implied).

Reproduced with permission of the copyright owner. Further reproduction prohibited without permission.

Fig. 3.0

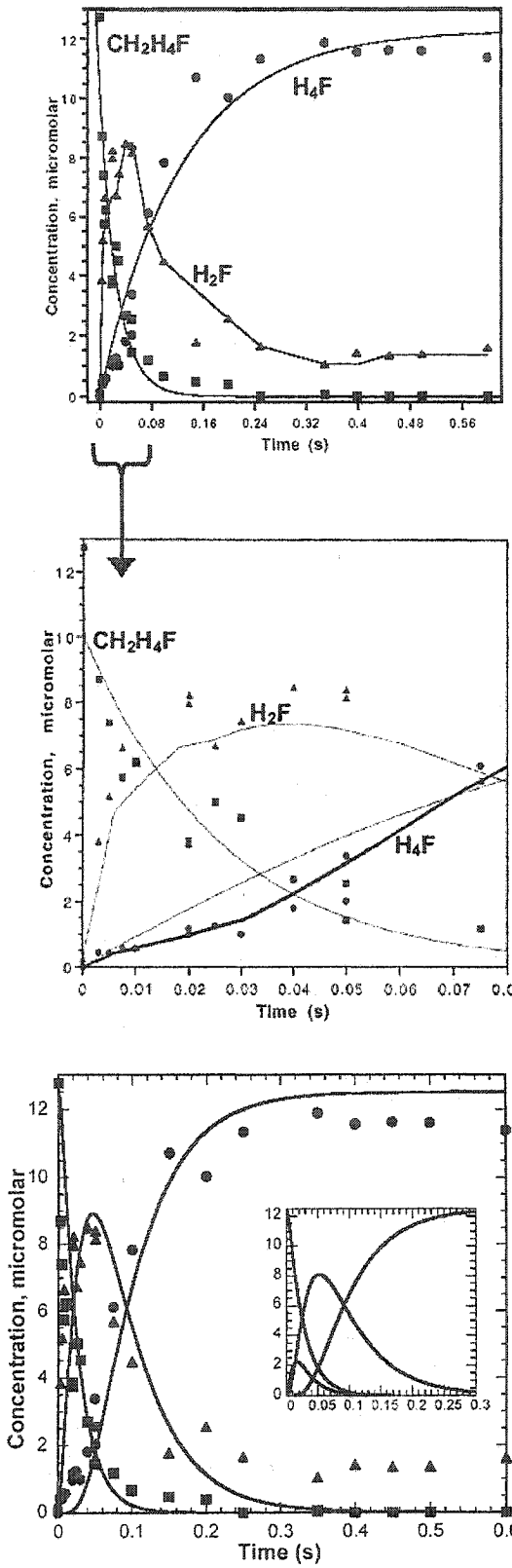

Reproduced with permission of the copyright owner. Further reproduction prohibited without permission.

Fig 3.1 DHFR single enzyme turnover and pre-steady state burst rates as measured by coenzyme fluorescence energy transfer. Averaged stopped-flow fluorescence traces (Ex 290 nm; Em 450 nm). *A*, Single enzyme turnover conditions: mixing of *C. hominis* TS-DHFR (40 μM) and H_2folate (10 μM) with NADPH (500 μM) reveals a time dependent rate of $NADP^+$ formation of 130 s^{-1}. *B*, Pre-steady state burst conditions: 7.5 μM *C. hominis* TS-DHFR; 50 μM H_2folate; 500 μM NADPH. Rates for the fast and slow phases are ~ 100 s^{-1} and 2.5 s^{-1} respectively.

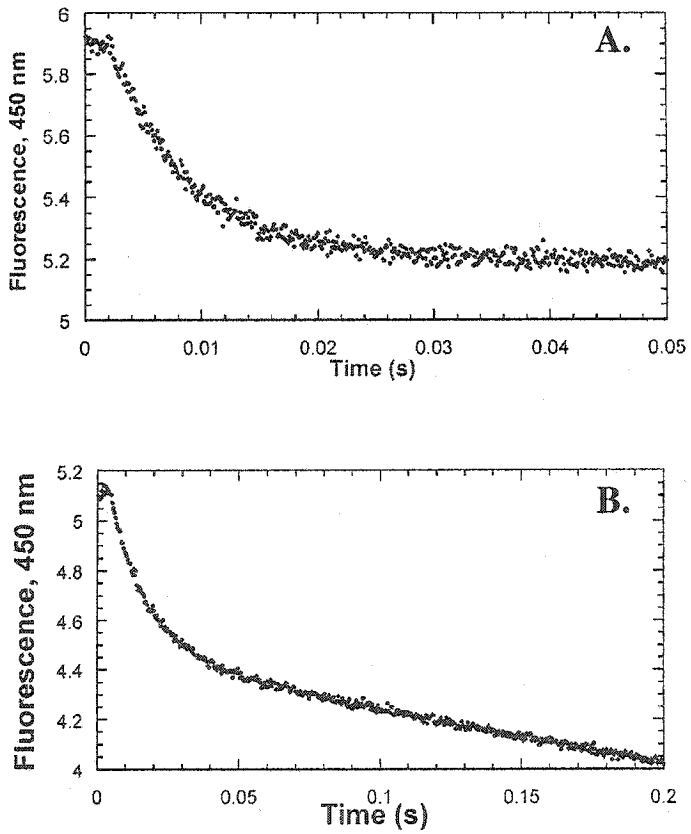

Reproduced with permission of the copyright owner. Further reproduction prohibited without permission.

Further Analysis of *C. hominis* TS Activity

1. Determination of the Rate-Limiting Step in the TS Reaction. Under pre-steady-state burst conditions, where *C. hominis* TS-DHFR (45 μM) was pre-incubated with excess [^{14}C]dUMP (200 μM) prior to mixing with a large excess of CH_2H_4folate (1 mM), no burst was observed (Fig. 3.2 A). The absence of a burst in dTMP formation is consistent with chemistry being overall rate-limiting at TS.

2. Presence of a TS intermediate. *C. hominis* TS-DHFR is surprising in that the TS activity is very fast and there is a large accumulation of H_2folate (Fig. 3.0). Furthermore, HPLC analysis of TS and TS-DHFR rapid chemical quench samples yielded clear evidence of a TS intermediate (Fig. 3.3). The intermediate is present at very early time points; peaks at 22 milliseconds, where it is fully separable from H_2folate and represents 18% of radioactive material; and is no longer observable at 40 ms. H_2folate is also present at very early time points, but peaks at 40-50 ms, where it represents 65% of tritiated material, leveling out by 200 ms. (Fig. 3.0A). The intermediate peak, seen previously in *T. gondii* TS and TS-DHFR reactions [30] but not observed with *L. major*, was hypothesized to represent a breakdown product of the TS iminium ion intermediate, perhaps hydroxymethylene tetrahydrofolate [48].

L. major and *T. gondii* were also observed to exhibit a pre-steady-state burst for consumption of the cofactor, CH_2H_4folate [30, 96]. The burst in CH_2H_4folate consumption is thought to correspond to the presence of a TS intermediate with a rate of formation that is faster than chemistry. Stopped flow absorbance (340 nm; 25 or 40 μM TS-DHFR, 1mM dUMP, 0.5 or 1 mM CH_2H_4folate) and fluorescence (Ex. 287 nm, Em. 340 nm; 7.5 μM TS-DHFR, 100 μM FdUMP, 50 μM CH_2H_4folate) were used to look for

Reproduced with permission of the copyright owner. Further reproduction prohibited without permission.

Fig. 3.2 TS pre-steady-state burst experiments: no burst in dTMP formation or CH_2H_4folate consumption observed with *C. hominis* TS-DHFR. *A*, Rapid chemical quench TS burst experiment where *C. hominis* TS-DHFR (25 μM) is pre-incubated with excess [^{14}C]dUMP (90 μM) prior to mixing with a large excess of CH_2H_4folate (250 μM). *B-C*, Stopped-flow absorbance at 340 nm monitored when TS-DHFR (25 μM) is preincubated with a large excess of dUMP (1mM) and then mixed with CH_2H_4folate (500 μM). *B, C. hominis* TS-DHFR (representative trace; several conditions were tested) *C*, *T. gondii* TS-DHFR control.

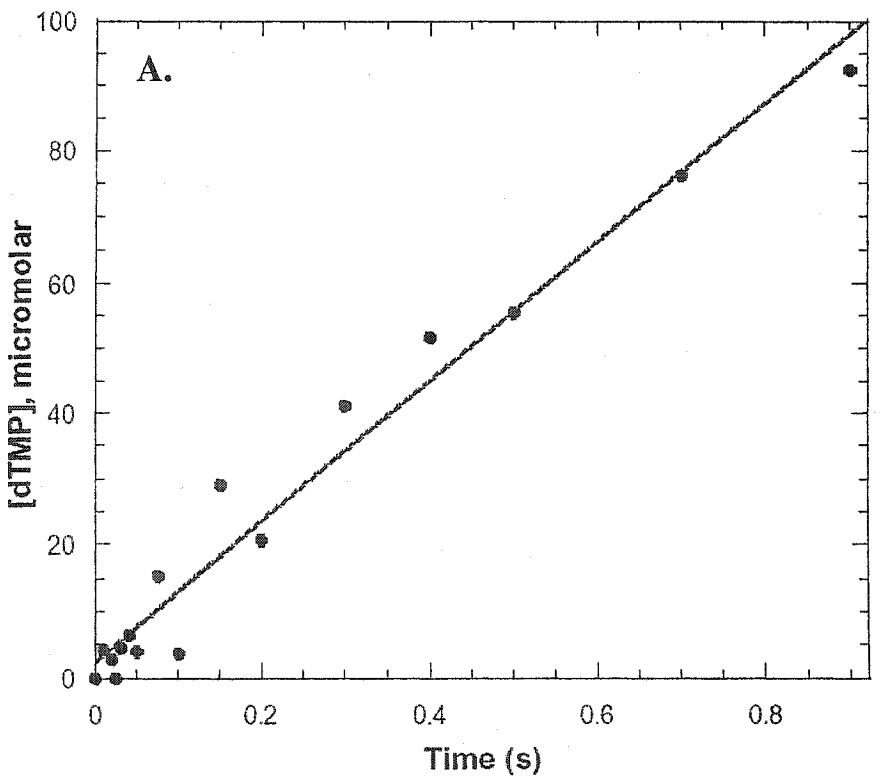

Reproduced with permission of the copyright owner. Further reproduction prohibited without permission.

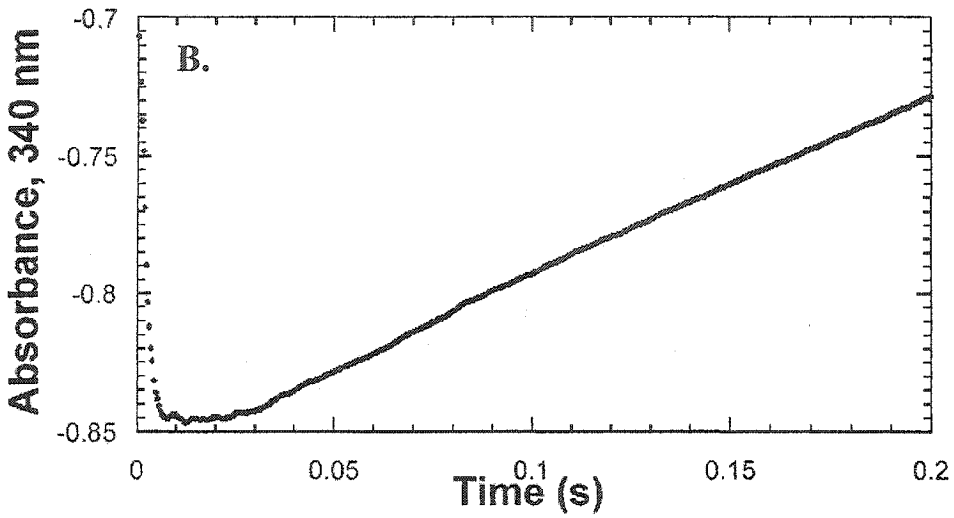

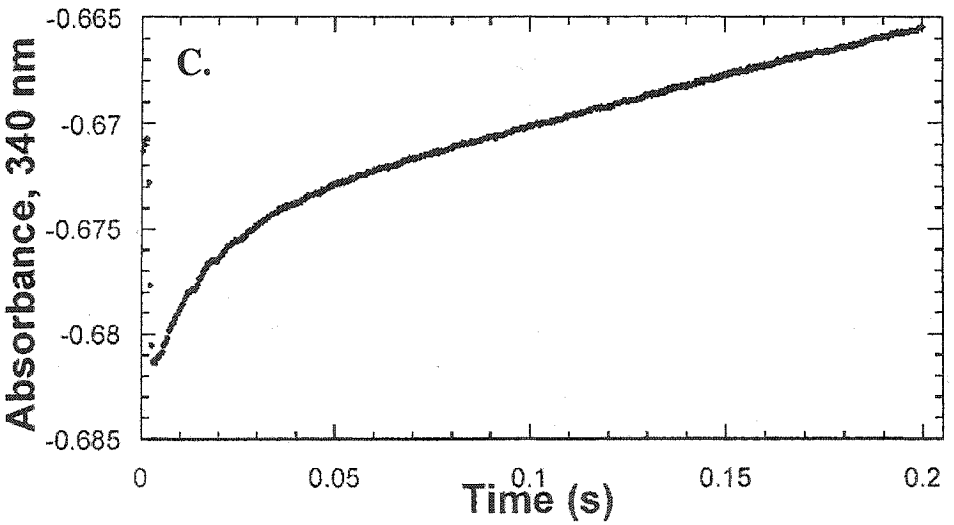

Reproduced with permission of the copyright owner. Further reproduction prohibited without permission.

Fig 3.3 HPLC analysis of *C. hominis* TS single enzyme turnover reaction: evidence for a TS intermediate. Radioactivity trace reveals the presence of a TS intermediate in a 22 millisecond rapid chemical quench time point (*top*). A H_2folate standard was added to the sample and is visualized at 13 min in the UV trace (282 nm, *middle*). The lower panel shows a representative UV trace of the reaction mixture in the absence of added H_2folate standard (buffer + quench solution only). There is a 30 s delay between the UV and radioactivity detectors.

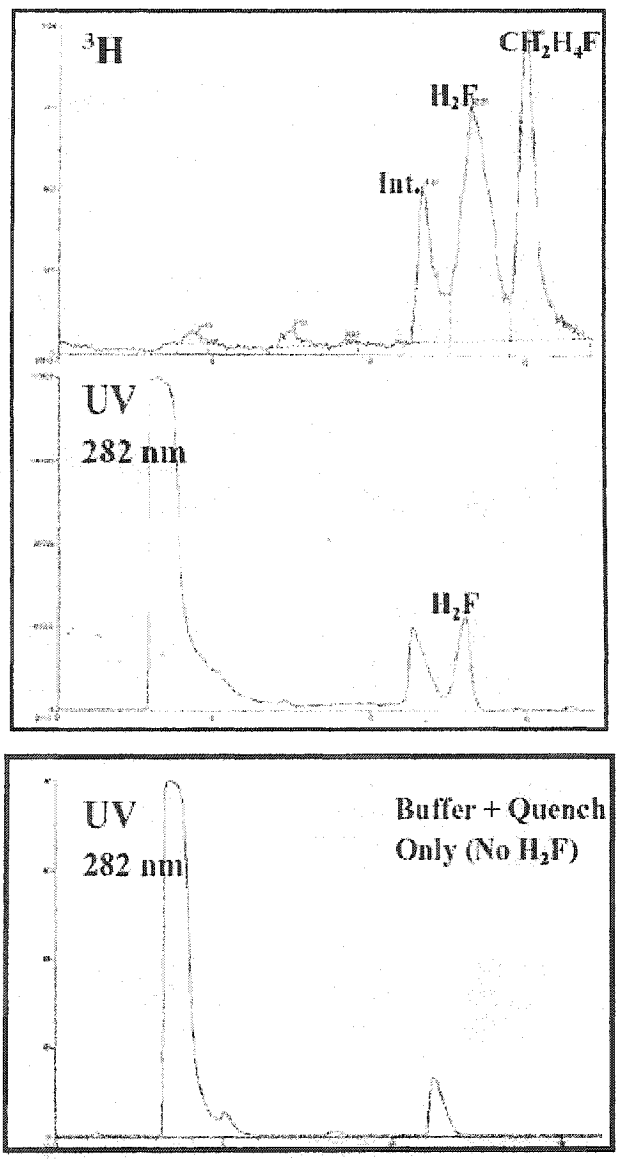

Reproduced with permission of the copyright owner. Further reproduction prohibited without permission.

a burst in CH_2H_4folate consumption, but no TS burst was observed with *C. hominis* TS-DHFR at any of the conditions tested (Fig. 3.2B). *T. gondii* TS-DHFR was used as a positive control (Fig. 3.2C).

3. Characterization of the dUMP Binding Site. *C. hominis* dUMP binding affinity was determined by stopped flow analysis. The k_{on} was obtained by titrating 0.5 μM *C. hominis* TS-DHFR with increasing amounts of dUMP in the presence of 10 μM PDDF (propargyl dideazafolate) in both syringes, and plotting k_{obs} (s^{-1}) versus concentration of dUMP added: $k_{obs} = k_{on}[dUMP] + k_{off}$. Due to the fast dUMP off rate, the folate analog PDDF was employed as a trapping ligand. An independent and more precise way to measure the k_{off} for dUMP is to measure the rate when dUMP is competed with an excess of a ligand that binds at the same site. This was accomplished by competing 20 μM dUMP with 200 μM FdUMP in the presence of 10 μM *C. hominis* TS-DHFR. For the *C. hominis* enzyme, k_{off} was found to be 90 ± 10 s^{-1} and k_{on} was 2.3 $s^{-1}\mu M^{-1}$; $K_d = k_{off}/k_{on} \approx 35$ μM (Fig. 3.4D). This dUMP K_d is significantly weaker than that observed by the same methods with *L. major* and *T. gondii* TS-DHFR, 0.18 μM and 4.5 μM, respectively [56, 30].

4. Characterization of the TS Folate Binding Site. It has been shown previously that increased affinity for folate substrates can alter the TS mechanism [98], so we sought to determine the relative affinities for folates of the *C. hominis* and *T. gondii* TS active sites. As it is not possible to directly measure the rate of CH_2H_4folate binding by stopped-flow absorbance or fluorescence, we took advantage of a FRET peak produced upon binding of a folate analog, PDDF, to enzyme. The k_{on} was obtained by titrating 100 nM *C. hominis* or *T. gondii* TS-DHFR with increasing amounts of PDDF and plotting k_{obs} (s^{-1})

Reproduced with permission of the copyright owner. Further reproduction prohibited without permission.

versus concentration of PDDF added (Fig. 3.4 B-C). Interestingly, in the case of *C. hominis* but not *T. gondii*, the data used to calculate k_{on} were biphasic, fitting a double exponential equation with a fast PDDF concentration-dependent phase (k_{obs}) followed by a slower PDDF concentration-independent phase of 5.7 s^{-1}. The slow PDDF concentration-independent phase is likely to represent a conformational change following PDDF binding. The k_{off} for PDDF was measured by competing 5 μM PDDF with 100 μM CH_2H_4folate in the presence of 200 nM *C. hominis* or *T. gondii* TS-DHFR (Fig. 3.4 A). For the *C. hominis* enzyme, k_{off} was found to be 2.3 s^{-1} and k_{on} was 48.6 $s^{-1}\mu M^{-1}$; $K_d = k_{off}/k_{on}$= 47.3 nM for folate cofactor binding. For *T. gondii* TS-DHFR, k_{off} was found to be 1.1 s^{-1} and k_{on} was 126.1 $s^{-1}\mu M^{-1}$, so the K_d for PDDF was 8.5 nM (data not shown).

A Kinetic Model of the *C. hominis* TS-DHFR Reaction

The mechanistic and rate information obtained in this study were used to simulate reaction time courses using the program KinTekSim (Fig 3.5). The minimal kinetic mechanism that approximates experimental data obtained with *C. hominis* TS-DHFR differs from the *T. gondii* mechanism in that it requires fast conversion of the TS intermediate to H_2folate, followed by a slow conformational change (predicted by the PDDF binding studies), with subsequent fast product release at TS. The KinTekSim model of the TS-DHFR single enzyme turnover reaction superimposed on experimental data is presented in Fig. 3.0 C. H_2folate and the TS intermediate are plotted separately in the figure inset.

Reproduced with permission of the copyright owner. Further reproduction prohibited without permission.

Fig. 3.4 Stopped-flow fluorescence experiments to measure the binding affinity of *C. hominis* TS-DHFR for PDDF and dUMP. *A*, Representative stopped-flow trace for the measurement of the dissociation of PDDF: *C. hominis* TS-DHFR (200 nM) was preincubated with PDDF (5 μM) prior to mixing with an excess of CH_2H_4folate (100 μM). *B*, Representative biphasic stopped-flow trace of fluorescence at 380 nm versus time, observed upon mixing *C. hominis* TS-DHFR (100 nM) with PDDF (0.5 μM). *C*, Plot of concentration dependent rate (k_{obs}) versus PDDF concentration. *D*, Plot of concentration dependent rate (k_{obs}) versus dUMP concentration.

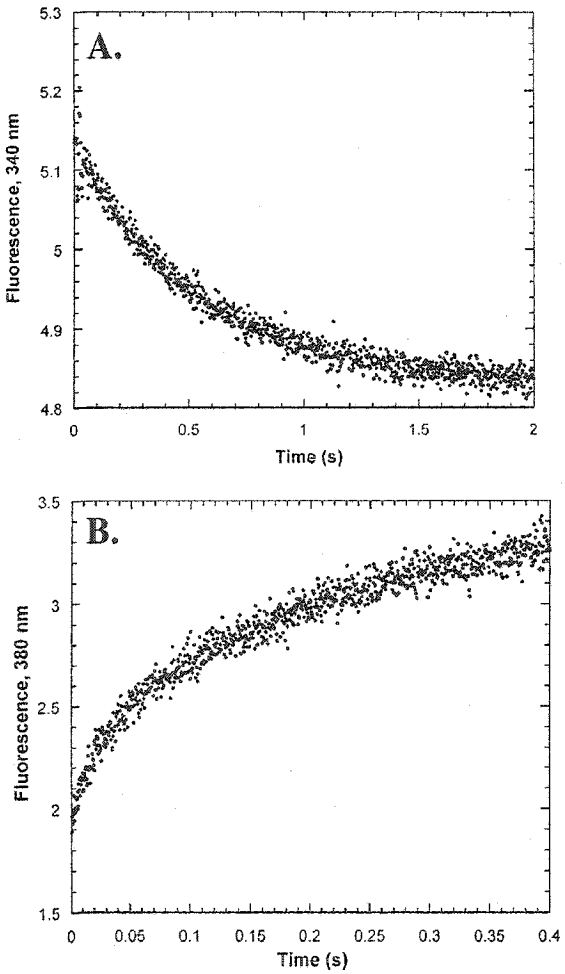

Reproduced with permission of the copyright owner. Further reproduction prohibited without permission.

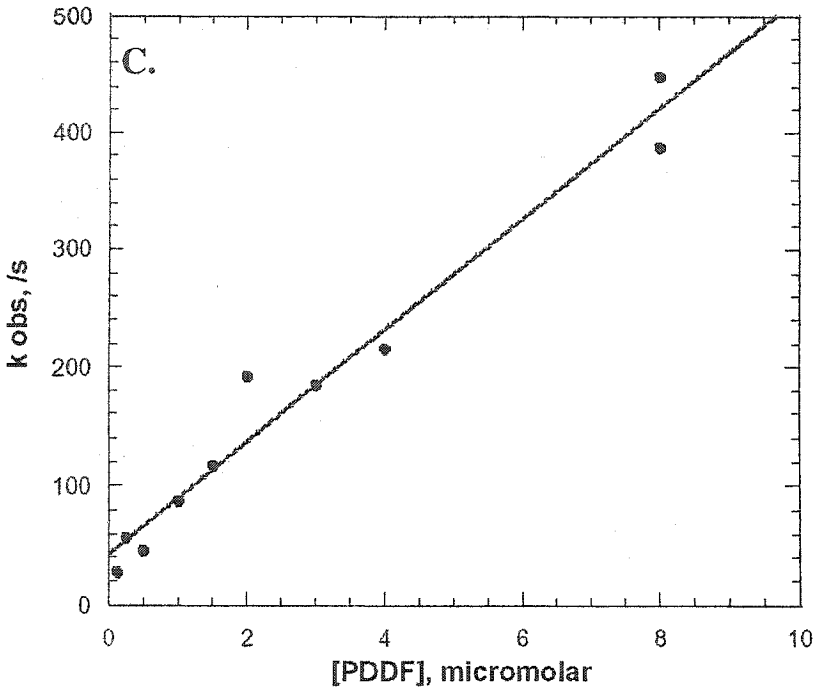

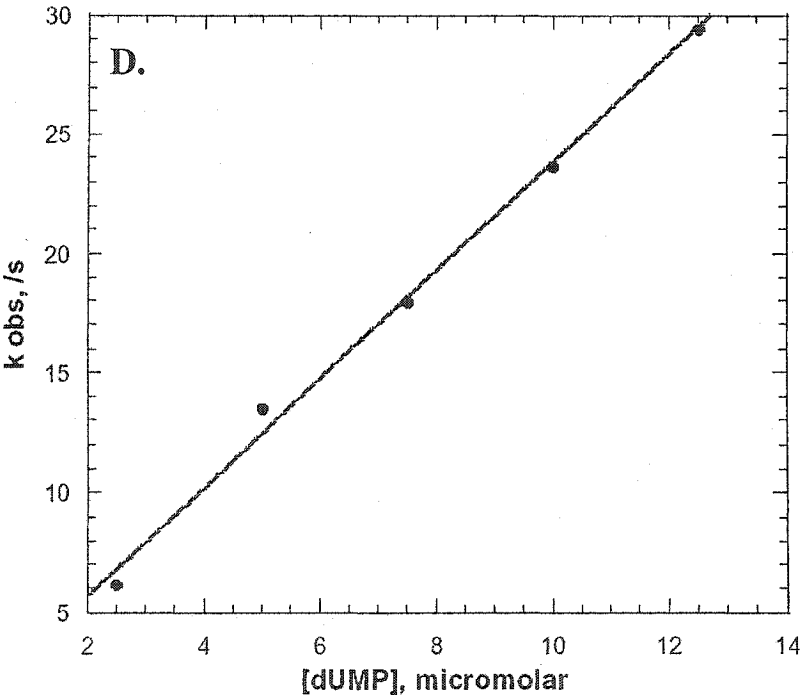

Reproduced with permission of the copyright owner. Further reproduction prohibited without permission.

Fig 3.5 Minimal kinetic mechanism and rate constants used to simulate *C. hominis* TS-DHFR

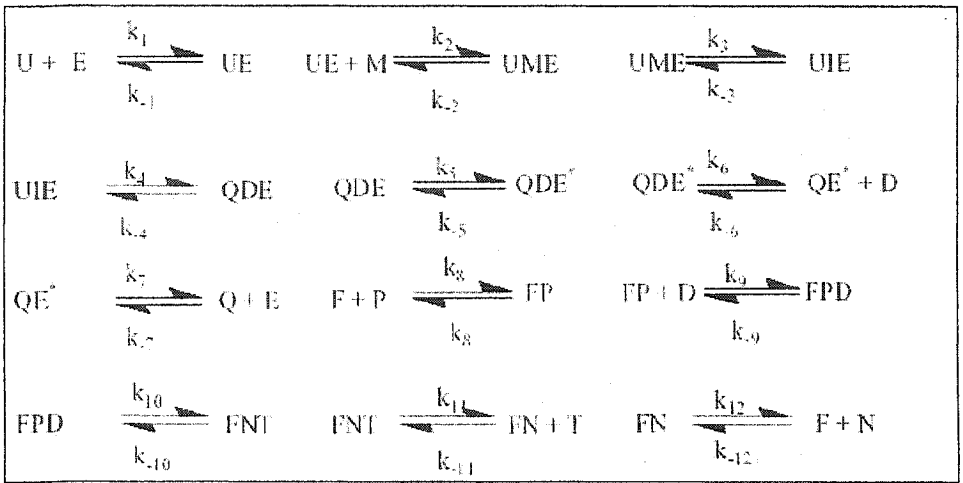

U = dUMP	E = TS active site	M = CH_2H_4F	Q = dTMP	I = Intermediate
D = H_2F	E^* = Activated TS	F = DHFR active site		P = NADPH
N= $NADP^+$	T = H_4F			

$k_1 = 2.3\ \mu M^{-1}s^{-1}$	$k_{-1} = 90\ s^{-1}$	$k_2 = 4\ \mu M^{-1}s^{-1}$	$k_{-2} = 20\ s^{-1}$	$k_3 = 45\ s^{-1}$	$k_{-3} = 2\ s^{-1}$
$k_4 = 130\ s^{-1}$	$k_{-4} = 0\ s^{-1}$	$k_5 = 17\ s^{-1}$	$k_{-5} = 0.1\ s^{-1}$	$k_6 = 200\ s^{-1}$	$k_{-6} = 2\ \mu M^{-1}s^{-1}$
$k_7 = 200\ s^{-1}$	$k_{-7} = 10.9\ \mu M^{-1}s^{-1}$	$k_8 = 9\ \mu M^{-1}s^{-1}$	$k_{-8} = 40\ s^{-1}$	$k_9 = 5.7\ \mu M^{-1}s^{-1}$	$k_{-9} = 9\ s^{-1}$
$k_{10} = 130\ s^{-1}$	$k_{-10} = 0.001\ s^{-1}$	$k_{11} = 4.5\ s^{-1}$	$k_{-11} = 10\ \mu M^{-1}s^{-1}$	$k_{12} = 95\ s^{-1}$	$k_{-12} = 2.6\ \mu M^{-1}s^{-1}$

Reproduced with permission of the copyright owner. Further reproduction prohibited without permission.

Substrate Channeling

Special attention was paid to the early TS-DHFR time points because a lag in H_4folate production and a large build-up of H_2folate would be evidence against substrate channeling. There is clear evidence for H_2folate channeling by *L. major* TS-DHFR [56, 71, 96]. As will be presented in Chapter 4, H_4folate is formed from the earliest time points with the *L. major* wild-type bifunctional TS-DHFR enzyme (no lag in product formation at DHFR) and only a modest amount of H_2folate accumulates, peaking at 14% of tritiated material [96]. Similar behavior is observed with *T. gondii* TS-DHFR [30]. Conversely, when *E. coli* monofunctional TS and DHFR are combined as a non-channeling control, H_2folate concentration rises more rapidly than H_4folate and there is almost no H_4folate present at the earliest time points, suggesting a lag in product formation at DHFR; H_2folate peaks at 44-60% of tritiated material [96]. In contrast to the other bifunctional enzymes studied, *C. hominis* generates a large accumulation of H_2folate: comprising up to 65% of radiolabeled material (Fig. 3.0 A), and there is a clear lag in production of H_4folate (Fig. 3.0 B). Although the minimal kinetic mechanism developed for *C. hominis* TS-DHFR predicts a shorter but more complete lag (Fig. 3.0 C), addition of a channeling step to the mechanism results in a significantly worse fit at early time points.

Substrate channeling was also assessed using a steady-state spectroscopic method developed by D. V. Santi's group to visualize the presence or absence of a lag in $NADP^+$ production via the DHFR catalyzed reduction of H_2folate formed at TS [65]. Trujillo *et al.* [97] report a lag in the production of $NADP^+$ in a coupled assay using monofunctional TS and DHFR, or a mixture of the *T. gondii* TS domain with the *T. gondii* DHFR

Reproduced with permission of the copyright owner. Further reproduction prohibited without permission.

domain. In the case of the *T. gondii* bifunctional TS-DHFR enzyme, no lag was observed suggesting that H_2folate is directly channeled from TS to DHFR. Spectroscopic signal change resulting from NADPH consumption is monitored at 340 nm. The equation for $NADP^+$ formation via the DHFR catalyzed oxidation of NADPH and reduction of H_2folate produced at TS is:

$[NADP^+] = v_1 t + (v_1 / v_2)(K_m e^{-v2t/Km} - 1)$

K_m is the K_m for H_2folate; v_1 is the rate of TS (μM/min) under coupled assay conditions; and v_2 is the DHFR rate (μM/min) using near-saturating substrate concentrations. When $NADP^+$ concentration is plotted versus time, the steady-state concentration of H_2folate corresponds to $v_1 K_m / v_2$ and the predicted lag time prior to steady-state H_2folate accumulation is K_m / v_2. In the case of *C. hominis*, conditions corresponding to a predicted lag of 30 s in the absence of substrate channeling (10.8 nM enzyme), produced such a lag (Fig. 3.6).

Domain-Domain Communication: Ligand Binding Effects

It was observed with *L. major* TS-DHFR that ligand binding at one active site affects activity at the active site of the other enzyme, evidence of communication between the TS and DHFR domains [56]. The effects of ligand binding in apicomplexa were evaluated with *C. hominis* TS-DHFR and with the *T. gondii* enzyme for the sake of comparison.

Effects of TS ligands on DHFR burst and single enzyme turnover reactions were assessed by stopped-flow fluorescence (Ex. 290 nm, Em. 450 nm). In the case of *L. major,* formation of the dUMP-CH_2H_4folate-enzyme ternary complex at TS accelerates the DHFR rate 20-fold [56]. With *C. hominis* and *T. gondii*, the DHFR burst rate was fast

Reproduced with permission of the copyright owner. Further reproduction prohibited without permission.

Fig. 3.6 Steady-state spectroscopic analysis to assess $NADP^+$ production by *C. hominis* TS-DHFR. A lag in $NADP^+$ production that matches calculated predictions for "no substrate channeling" is observed with 10.8 nM *C. hominis* TS-DHFR.

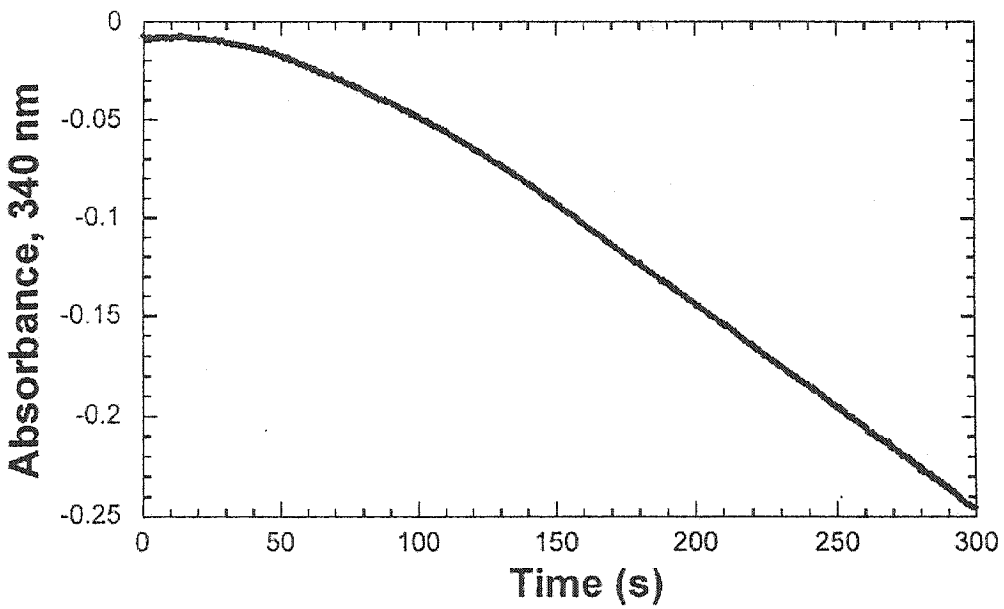

Reproduced with permission of the copyright owner. Further reproduction prohibited without permission.

even in the absence of TS ligands (7.5 μM TS-DHFR, 50 μM H_2folate), and no acceleration or amplitude changes were observed in the presence of 100 μM FdUMP or 100 μM FdUMP + 50 μM CH_2H_4folate. Instead there was a slight decrease in the DHFR rate, likely due to direct inhibition of the DHFR active site by CH_2H_4folate. It was confirmed spectroscopically that addition of FdUMP + CH_2H_4folate annulled TS activity, establishing formation of a non-productive ternary complex (unable to undergo catalysis). Seventy-four % of *C. hominis* and 79% of *T. gondii* DHFR activity was observed in the presence of the ternary complex; 70% of *T. gondii* DHFR activity was observed in the presence of 50 μM CH_2H_4folate alone.

The TS dimer is a half-sites reactivity enzyme (at any given time, only one half of the TS dimer is catalytically active) and conformational changes upon ligand binding lead to asymmetric binding sites with differential substrate affinities at each half of the dimer [43, 99, 100]. We sought to determine whether coordination of the two TS active sites to provide half-sites reactivity impacts DHFR activity. DHFR single enzyme turnover rates were determined under conditions where one or both TS active sites are predicted to be ligand-bound. Experiments were carried out with 50 μM TS-DHFR; 10 μM H_2folate; and two sets of TS specific ligands: FdUMP (500 μM) + CH_2H_4folate (50 μM) to provide covalent ligation of the TS active site and dUMP (25 μM or 500 μM) + PDDF (25 μM) to provide non-covalent ligation of the TS folate-binding site (PDDF lacks an N5-methyl moiety, prohibiting covalent bonding to dUMP). *C. hominis* and *T. gondii* DHFR rates were unchanged by half- or full-sites TS occupancy with covalent or non-covalent ligands.

Reproduced with permission of the copyright owner. Further reproduction prohibited without permission.

Effects of DHFR ligands on TS burst and single enzyme turnover reactions were assessed by stopped-flow fluorescence (Ex. 287 nm, Em. 340 nm) and rapid chemical quench, respectively, under conditions where ligand-binding effects were observed with *L. major*. With *L. major*, an additional conformational change at TS occurs in the presence of the DHFR ligand, NADPH, and addition of the DHFR folate inhibitor, methotrexate, results in a 4-fold slower TS single turnover rate [56]. Combination of *T. gondii* TS-DHFR (7.5 μM) and FdUMP (100 μM) resulted in a single exponential TS burst of 2.5 s^{-1} in the presence or absence of NADPH (500 μM) +/- methotrexate (8 μM). A single enzyme turnover experiment (41 μM *T. gondii* TS-DHFR; 500 μM dUMP; 14 μM CH_2H_4folate) revealed 80% of *T. gondii* TS single enzyme turnover activity in the presence of methotrexate (45 μM). The corresponding *C. hominis* experiments were performed using trimethoprim, a more specific DHFR inhibitor, under burst conditions; the TS profile was similar in the presence or absence of NADPH +/- trimethoprim (in this case, no burst). *C. hominis* exhibited 100% of TS single turnover activity in the presence of trimethoprim (45 μM TS-DHFR; 50 μM trimethoprim).

DISCUSSION

Our kinetic characterization of the recently crystallized *C. hominis* TS-DHFR enzyme yielded surprising results in all three areas of focus: determination of the enzyme mechanism, substrate channeling, and domain-domain communication. Interestingly, *C. hominis* TS-DHFR exhibited significant mechanistic differences from enzymes of both the kinetoplastid protozoa, *L. major* and the apicomplexan protozoa, *T. gondii*. In fact, all of the mechanistic features found to be shared across the two bifunctional TS-DHFR classes are also shared by monofunctional TS and DHFR, suggesting that these are

Reproduced with permission of the copyright owner. Further reproduction prohibited without permission.

fundamental characteristics that preceded the gene-fusion event. In all cases, DHFR catalytic activity is faster than TS, and chemistry is overall rate-limiting at TS (no burst in dTMP formation), whereas a step after chemistry, such as product formation, is rate-limiting at DHFR (a burst in NADPH consumption is observed).

Remarkably, the most unusual features of the *C. hominis* mechanism involve the TS domain, which is more highly conserved than DHFR. At 45 s^{-1}, *C. hominis* TS is 10 to 40-fold faster than other TS enzymes characterized. Although *C. hominis* does exhibit weaker affinity for dUMP than the other enzymes studied, the most important differences appear to involve the TS folate binding region. In delineating the *C. hominis* TS-DHFR kinetic reaction mechanism, it was necessary to include the slow conformational change observed following binding of the folate analog, PDDF. Additionally, while there is HPLC evidence for a *C. hominis* TS intermediate, no pre-steady-state burst in consumption of the cofactor, CH_2H_4folate, is observed. The HPLC traces indicate that, like with *T. gondii*, a TS intermediate forms early in the time course and is consumed. With *T. gondii* and *L. major,* however, a pre-steady-state burst in consumption of the cofactor, CH_2H_4folate, is observed. The burst is also thought to indicate a TS intermediate, possibly the iminium form of CH_2H_4folate, for which the rate of formation is faster than chemistry. Modeling indicates that the fast *C. hominis* TS activity would make a pre-steady-state burst in consumption of CH_2H_4folate very difficult to detect.

In *C. hominis* TS-DHFR, the essential TS catalytic residues from the well characterized *L. casei* enzyme are conserved [101]; however, differences in two additional conserved residues near the folate-binding domain could help explain *C. hominis*' unusual TS activity. In place of a glycine found in human, *P. carinii*, *L. major*,

Reproduced with permission of the copyright owner. Further reproduction prohibited without permission.

T. gondii, and *P. falciparum* TS, *C. hominis* has a serine (Ser 290). This serine provides an additional hydrogen bond to the glutamate tail of the folate substrate. In place of a phenylalanine found in all of the species listed above, *C. hominis* has an alanine (Ala 287) [7]. Unlike alanine, bulky phenylalanine impedes the charged glutamate tail. It was previously observed with folylpolyglutamates, which also increase folate substrate affinity for TS via the glutamate tail, that the TS mechanism is altered [98]. *C. hominis* TS does have a higher affinity for the folate analog PDDF than does *L. major* TS (with a faster on rate and similar off rate) [96], but *T. gondii* TS has an even higher affinity for PDDF, so affinity alone fails to explain *C. hominis*' unusual TS behavior. On the other hand, only with the *C. hominis* enzyme does addition of PDDF result in biphasic behavior, with a fast PDDF concentration-dependent phase followed by a slower PDDF concentration-independent phase thought to represent a conformational change following binding.

Perhaps the most important finding of this research is that *C. hominis* TS-DHFR is the first bifunctional TS-DHFR enzyme studied for which there is clear mechanistic evidence against H_2folate substrate channeling. With *L. major* TS-DHFR there are multiple lines of structural and mechanistic evidence to support the possibility of channeling of H_2folate from the TS active site, where it is produced, to the DHFR active site, where it is reduced to H_4folate [6, 56, 96]. With the newly crystallized apicomplexan proteins, however, there is no obvious structural explanation for substrate channeling, as solvent exposed basic residues do not follow a clear path. Furthermore, the TS and DHFR active sites are found on opposite faces of each apicomplexa TS-DHFR monomer, meaning that H_2folate would have to turn a corner to transit from TS to DHFR or, as

Reproduced with permission of the copyright owner. Further reproduction prohibited without permission.

suggested by Yuvaniyama *et al* [8] follow a longer but straighter path from the TS active site of one monomer to the DHFR active site of the opposite half of the dimer. The orientation of the TS and DHFR active sites in the apicomplexa proteins also make channeling via conformational change less likely [29].

Consistent with the structural predictions, *C. hominis* exhibits an even more significant accumulation of H_2folate and lag in H_4folate formation than was observed with the combination of *E. coli* monofunctional TS + DHFR, used previously as a non-channeling control [96]. *C. hominis* TS-DHFR also exhibits a lag in $NADP^+$ formation at DHFR following H_2folate formation at TS in a steady-state channeling assay. It is not clear why the accumulated H_2folate is not fully consumed over the course of 1 min, although one possibility may be that it is bound non-productively.

Just as the recent crystal structures provide evidence for two structural families (short and long linker), our data suggest two corresponding mechanistic families of TS-DHFR enzymes: those that do or do not exhibit domain-domain communication via ligand binding at TS affecting DHFR activity and vice-versa. TS-DHFR from the apicomplexa parasites *C. hominis* and *T. gondii* are similar in that they exhibit maximal DHFR activity even when TS is in an unliganded state (130 s^{-1} and 180 s^{-1}, respectively), with no further acceleration upon complex formation at TS. This differs from *L. major* in which DHFR rate is relatively slow at 6.4 s^{-1}, but is accelerated to 120 s^{-1} following ternary complex formation at TS [56]. Indeed, whereas there are multiple lines of evidence for domain-domain communication in *L. major* TS-DHFR, no such ligand effects were found with the apicomplexa proteins studied.

Reproduced with permission of the copyright owner. Further reproduction prohibited without permission.

The structural variations may account for these mechanistic distinctions between parasite classes. The *L. major* TS-DHFR structure is different from those of the apicomplexan proteins in that there is virtually no junctional region between TS and DHFR, but there is a 22 amino acid N-terminal DHFR tail that wraps the TS domain. Attempts to fully or partially remove the N-terminal tail did not yield active protein and similarly, attempts to delete the *L. major* DHFR domain did not yield active TS, suggesting that the N-terminal tail is crucial for protein folding and/or stability (Johnson, E.F. and Atreya, C. E., unpublished data). Whereas the short linker between *L. major* TS and DHFR limits the range of DHFR orientations relative to TS [9], we hypothesize that this N-terminal tail may serve as a sensor or brake, facilitating communication between domains and modulating activity.

By contrast, the N-terminal tail is essentially absent in the apicomplexan proteins. *P. falciparum* does have a short N-terminal extension, but it points upward away from TS. A recent study confirms that the 6 amino acid *P. falciparum* N-terminal extension is crucial to DHFR but not to TS activity [102]. What the apicomplexa proteins do possess is extensive linker regions, ranging in length from 58-89 amino acids. In a corset-like fashion, cross-over or donated helices make extensive contacts with the DHFR domain of the opposite TS-DHFR monomer. Like the *L. major* N-terminal tail, there is evidence that both the *P. falciparum* junctional region and DHFR domain are required for TS activity [8, 103]. The *C. hominis* cross-over helix makes extensive van der Waal's and hydrogen bonding interactions with the DHFR domain from the other half of the dimeric enzyme. It is possible that the cross-over helixes serve to hold the dimeric, bifunctional apicomplexa TS-DHFR proteins together in a stable, active conformation.

Reproduced with permission of the copyright owner. Further reproduction prohibited without permission.

Without evidence for domain-domain communication from ligand-binding experiments and, at least in the case of *C. hominis* TS-DHFR, evidence against substrate channeling, why might the apicomplexa proteins exist as bifunctional enzymes? One remaining potential advantage of bifunctionality is for coupled translational autoregulation. In translational regulation, mRNA binding to protein results in translational repression [35]. Indeed, Zhang and Rathod [36] report the existence of translational repression in *P. falciparum* TS-DHFR: mRNA coding for TS and the junctional region binds to the DHFR domain of the protein, blocking translation. The possibility of coupled translational autoregulation by *C. hominis* TS-DHFR will be a topic of future investigation.

The recent availability of crystal structures from *P. falciparum* and *C. hominis* TS-DHFR combined with this detailed mechanistic analysis of the *C. hominis* enzyme greatly enhances our understanding of bifunctional TS-DHFR. Points learned from this research will serve to guide further study. Whereas it is typically more difficult to achieve species specificity with inhibitors directed at the TS versus the DHFR active-site, unique mechanistic features of *C. hominis* TS suggest the possibility for a specific inhibitor directed at this active site. Previous efforts to find a non-active site inhibitor specific for a bifunctional enzyme were targeted at the putative channeling region of *L. major* TS-DHFR (Chapter 5, [104]). Mechanistic evidence against substrate channeling by *C. hominis* TS-DHFR, as well as structural differences, indicate that novel non-active site targets should be explored in this enzyme.

Reproduced with permission of the copyright owner. Further reproduction prohibited without permission.

Part B. Preliminary Mechanistic Analysis of P. falciparum TS-DHFR

Annually, another apicomplexan protozoa, *P. falciparum,* is responsible for approximately 500 million cases of malaria and 2 million fatalities worldwide [25]. Furthermore, the parasite has developed resistance to virtually all currently available antimalarial drugs [26, 27]. Solution of the crystal structure of *P. falciparum* TS-DHFR represents a major step toward the development of new anti-malarial drugs and novel non-active site drug targets [8, 49]. Disordered electron density among critical residues (amino acids 232-280 in the junctional region), combined with a notoriously challenging protein purification and issues of enzyme stability have made the *P. falciparum* enzyme a less accessible target for detailed mechanistic studies. Nonetheless, a preliminary mechanistic analysis of *P. falciparum* TS-DHFR was conducted using protein kindly provided by Dr. Worachart Sirawaraporn.

To monitor the *P. falciparum* TS-DHFR reaction, the bifunctional enzyme (45 μM) was pre-incubated with saturating concentrations of dUMP (500 μM) and NADPH (500 μM) and then mixed with a limiting amount of radiolabeled CH_2H_4folate (11 μM). The *P. falciparum* TS-DHFR rate is 1 s^{-1}, similar to that observed with *L. major* and *T. gondii* (2.6 s^{-1} and 5.5 s^{-1}, respectively) when one takes into account the effects of high glycerol (Fig. 3.7A). *P. falciparum* TS-DHFR requires storage at relatively low protein concentration in 20% glycerol for stability; addition of an equivalent amount of glycerol had no effect on the *T. gondii* DHFR single enzyme turnover reaction, but led to a 38% reduction in the TS-DHFR rate. In addition, like with *L. major* but unlike the faster apicomplexa TS-DHFR enzymes, no TS intermediate was observed by HPLC.

Reproduced with permission of the copyright owner. Further reproduction prohibited without permission.

To monitor the *P. falciparum* DHFR reaction, the bifunctional TS-DHFR enzyme (45 μM) was pre-incubated with a saturating concentration of NADPH (500 μM) and then mixed with a limiting amount of radiolabeled H_2folate (11 μM). The *P. falciparum* DHFR rate was found to be 78 s^{-1} (Fig 3.7 C). Like with the other apicomplexa TS-DHFR proteins but not *L. major*, DHFR appears to be in an "activated" state even in the absence of TS ligands.

A DHFR burst with a rate of 34 s^{-1} was visualized by stopped-flow fluorescence using (Ex 290 nm, Em. 450 nm; 7.5 μM TS-DHFR; 50 μM H_2folate, 500 μM NADPH) (Fig. 3.8). The slow DHFR burst rate is partially attributable to the high glycerol concentration: addition of an equivalent amount of glycerol to that in the *P. falciparum* reaction resulted in a 25% reduction in *T. gondii* burst rate. Like with *C. hominis*, but unlike *T. gondii* or *L. major*, no burst in CH_2H_4folate consumption was observed with *P. falciparum* TS-DHFR (340 nm; 25 μM TS-DHFR, 1mM dUMP, 500 μM CH_2H_4folate) (Fig. 3.9).

Unlike *C. hominis* TS-DHFR, there is at present no evidence against substrate channeling. With *P. falciparum* there is no lag in production of H_4folate, and H_2folate peaks at 12% of tritiated material (Fig. 3.7B), suggesting that the H_2folate produced at TS is channeled to DHFR without equilibration in bulk solution. Conditions required for *P. falciparum* TS-DHFR protein stability interfered with the steady-state channeling assay.

Reproduced with permission of the copyright owner. Further reproduction prohibited without permission.

Fig. 3.7 TS-DHFR and DHFR single turnover reaction time courses from *P. falciparum*. *P. falciparum* TS-DHFR: 45 μM enzyme reacted with 11 μM tritiated CH_2H_4folate. CH_2H_4folate consumption (■), as well as H_2folate and H_4folate production are reported (▲ and ● respectively); maximal H_2folate accumulation is 12% of tritiated material (*A*). *B,* Magnification of the early of *P. falciparum* TS-DHFR time course illustrating that there is no lag in product formation at DHFR: H_4folate (●) is formed from the earliest time points. *C,* DHFR single turnover reaction time course from *P. falciparum*: 45 μM TS-DHFR reacted with 11 μM tritiated H_2folate.

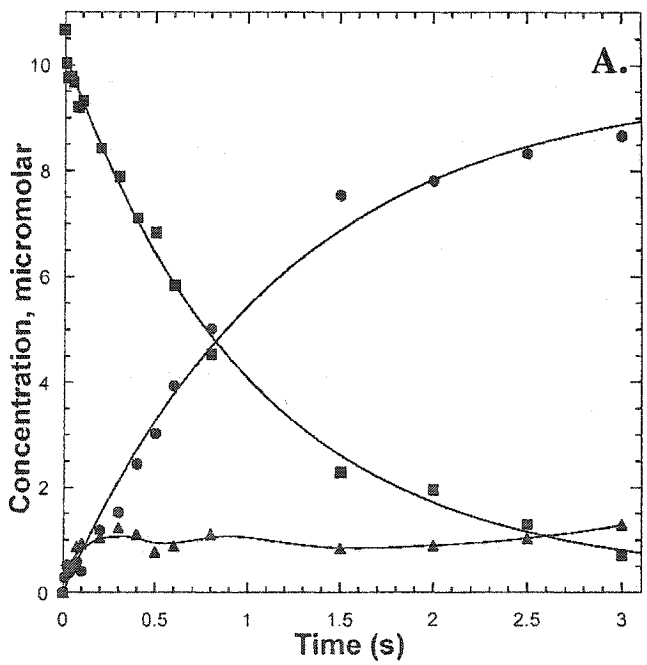

Reproduced with permission of the copyright owner. Further reproduction prohibited without permission.

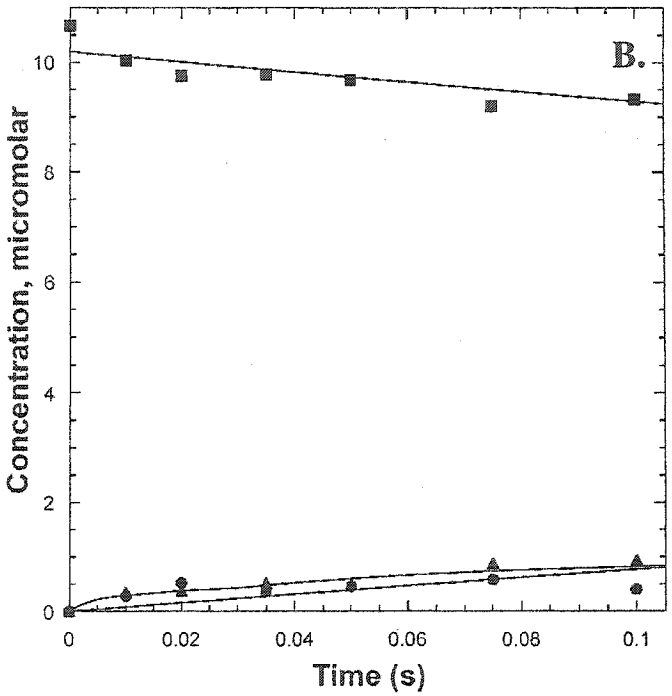

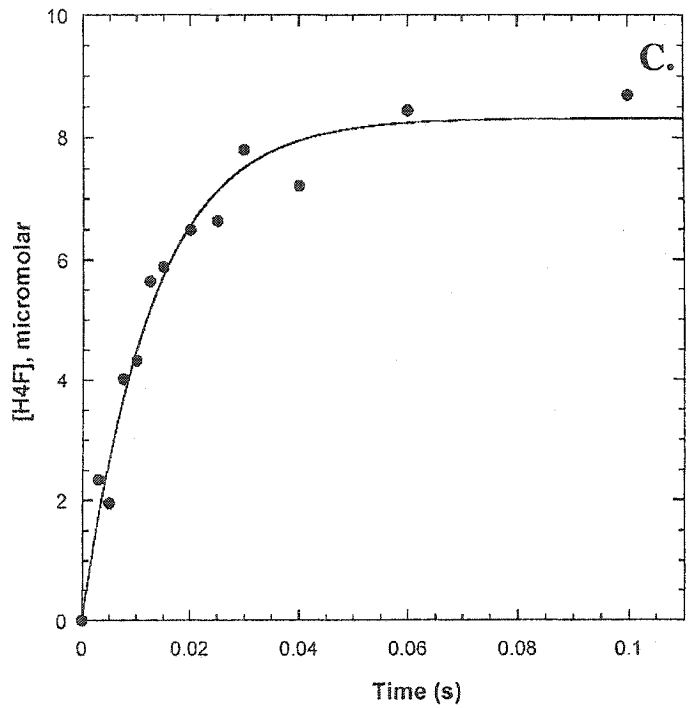

Reproduced with permission of the copyright owner. Further reproduction prohibited without permission.

Fig. 3.8 *P. falciparum* DHFR pre-steady state burst as measured by coenzyme fluorescence energy transfer. Averaged stopped-flow fluorescence traces (Ex 290 nm; Em 450 nm) showing the time dependent formation of $NADP^+$ after mixing a solution of TS-DHFR (7.5 μM) and H_2folate (50 μM) with NADPH (500 μM) *P. falciparum* TS-DHFR, rates for the fast and slow phases are 22 s^{-1} and 2.6 s^{-1}. Slow rates are partially attributable to effects of high glycerol concentrations.

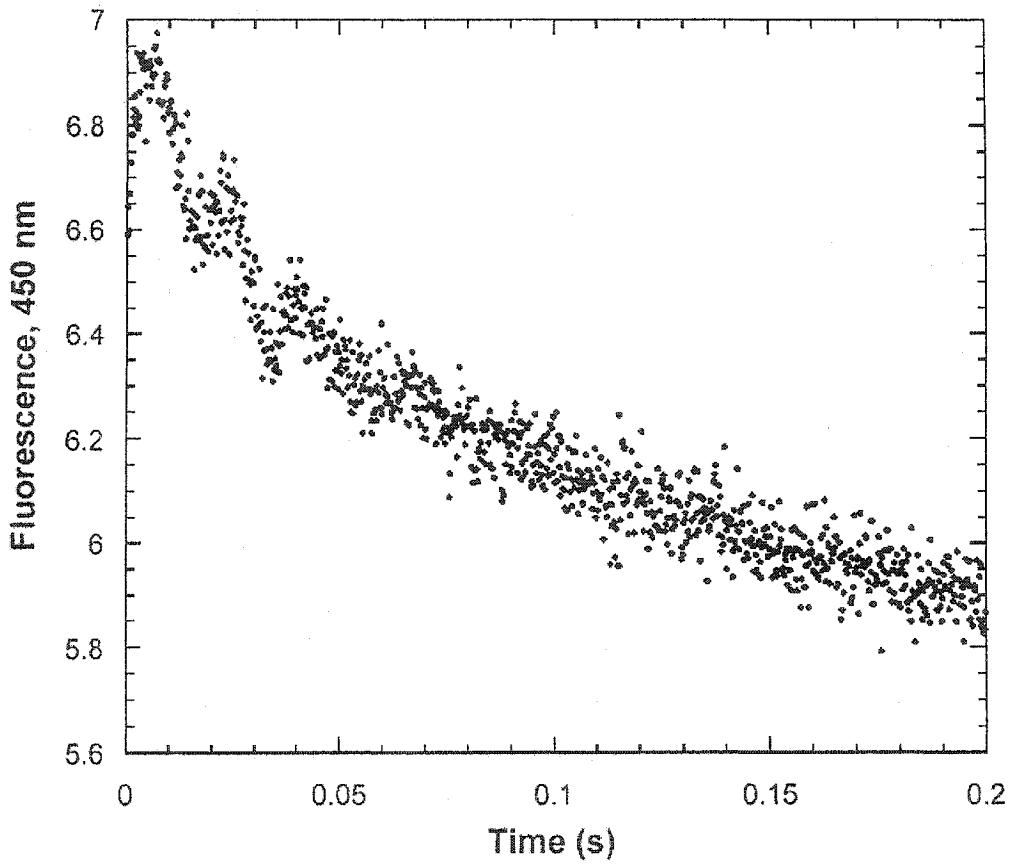

Reproduced with permission of the copyright owner. Further reproduction prohibited without permission.

Fig. 3.9 *P. falciparum* TS pre-steady-state burst experiment

Stopped-flow absorbance at 340 nm monitored when *P. falciparum* TS-DHFR (25 μM) is preincubated with a large excess of dUMP (1mM) and then mixed with CH_2H_4folate (500 μM).

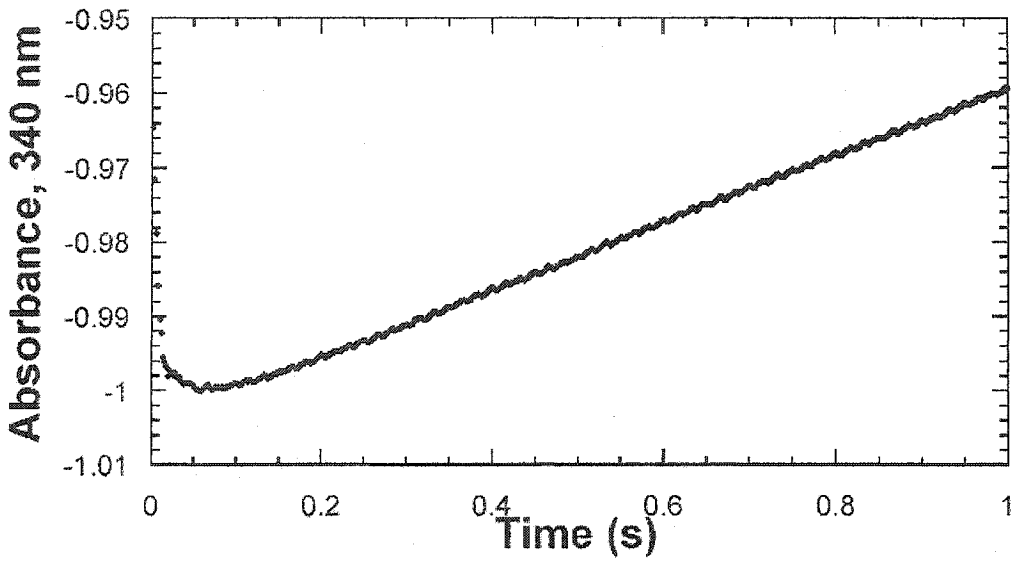

Reproduced with permission of the copyright owner. Further reproduction prohibited without permission.

Chapter Four

Probing Electrostatic Channeling and Domain-Domain Communication in Bifunctional TS-DHFR Using Site-Directed Mutagenesis

Reproduced with permission of the copyright owner. Further reproduction prohibited without permission.

Part A. Use of Site-Directed Mutagenesis to Probe Electrostatic Channeling in L. major TS-DHFR

INTRODUCTION

When the crystal structure of *L. major* TS-DHFR was solved, a 40 Å "electrostatic highway" across the surface of the protein was observed, and was proposed to be a conduit for electrostatic channeling [6, 29]. Electrostatic channeling is a mechanism which would enable negatively charged H_2folate produced at the TS active-site to be handed-off along a series of solvent-exposed lysine and arginine residues to the DHFR active site, where it is converted to H_4folate, without equilibration in bulk solution [6].

In the TS domain, contributors to the positively charged potential are Lys 282, Arg 283, and Arg 287, conserved in all TS species. DHFR is much less conserved than TS, and in the DHFR domain of the *L. major* bifunctional enzyme there is a 12 amino acid loop not present in *E. coli;* 6 of these residues are positively charged. The positively charged residues: Lys 66, 67, 72 and 73, and Arg 64 and 74, are solvent exposed and also take part in the putative channel (Fig. 4.0). TS is connected to DHFR by a very short tether; it is predicted that torsional rotation of Arg 287 would position its side chain 10-12 Å from that of Lys 73 in the DHFR domain [6].

Reproduced with permission of the copyright owner. Further reproduction prohibited without permission.

Fig. 4.0 Putative channel residues in *L. major* TS-DHFR. Structure of TS-DHFR from *L. major* with TS shown in red, DHFR in blue, TS and DHFR ligands in green, and solvent exposed lysines and arginines in magenta.

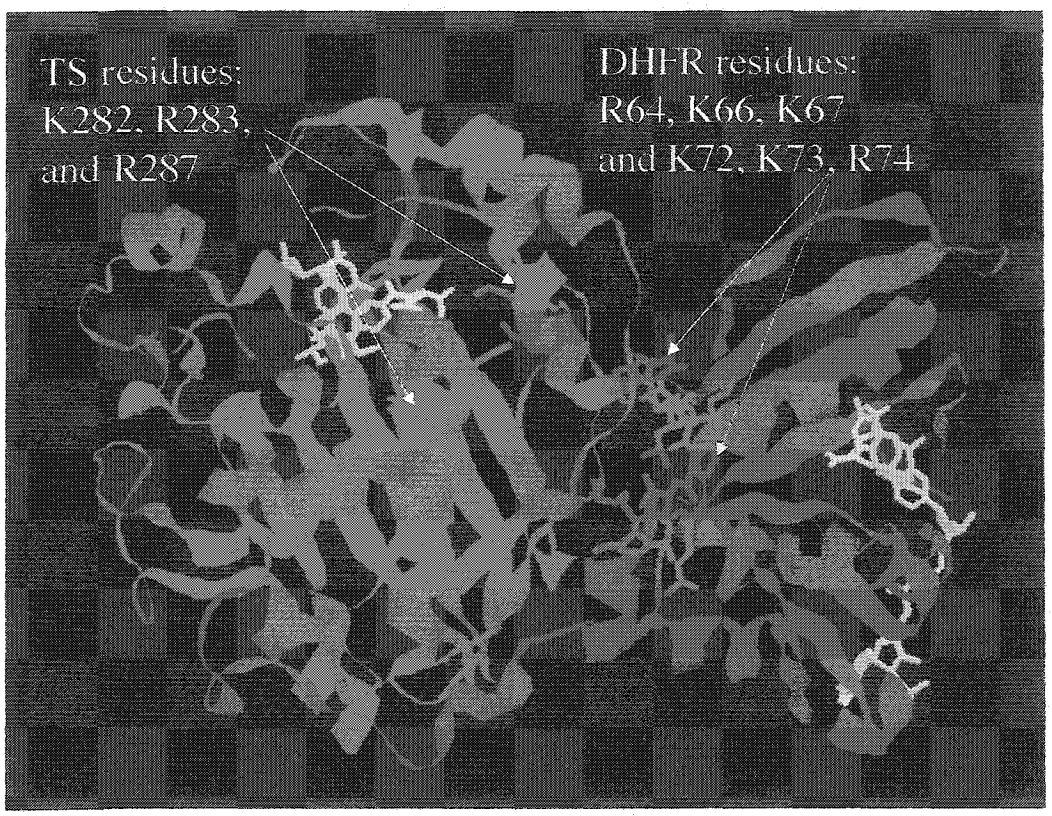

Reproduced with permission of the copyright owner. Further reproduction prohibited without permission.

In Part A of this chapter we probe the electrostatic channel hypothesis by mutation of solvent exposed basic residues in the shallow groove region of *L. major* TS-DHFR predicted to participate in channeling. These TS-DHFR channel mutants are assessed for impaired channeling using two criteria: a lag in product formation at DHFR and increased H_2folate accumulation. An ancillary goal is to use TS pre-steady-state burst experiments to ascertain whether these same residues might mediate domain-domain communication, or conformational changes induced upon ligand binding at one active site that affect activity at the active site of the other enzyme, and one interesting mutant is further investigated.

RESULTS

Creation of Channel Mutants[4]

We sought to test the electrostatic channeling hypothesis by mutating lysines and arginines thought to make up the channel to either glutamic acid (charge reversal); or alanine or glutamine (charge neutralization). The residues mutated were Lys 282, Arg 283, and Arg 287 in the TS domain; and Lys 66, 67, 72 and 73, and Arg 64 and 74 in the DHFR domain. A total of 12 channel mutants were successfully created with up to 6 residues changed at once; 2 mutants contained changes in both the TS and DHFR domains (Table 4.0). Consistently, mutation of K73 or R74 led to very low yields of active enzyme and large amounts of insoluble enzyme, suggesting that these DHFR residues may be important for protein folding/domain stability. Insufficient active enzyme for transient kinetics analysis was recovered from attempts to make the following

[4] Eric F. Johnson, then in the K.S. Anderson lab, participated in creation of the channel mutants.

Reproduced with permission of the copyright owner. Further reproduction prohibited without permission.

Table 4.0: Relative DHFR and TS-DHFR activity; lag in product formation at DHFR; and H_2folate accumulation by *L. major* TS-DHFR charge reversal and charge neutralization mutants.

Mutant	**DHFR Activity**	**TS-DHFR Activity**	**Lag to DHFR**	**Increased H_2folate**
Charge Reversal	%	%		
R283E	Wild-type	40	No	No
R287E	Wild-type	45	No	No
K282E, R283E	Wild-type	0	No (TS dead)	No (TS dead)
K66E, K67E	Wild-type	Wild-type	No	No
K72E	Wild-type	Wild-type	No	No
K73E	Wild-type	Wild-type	No	No
K72E, K73E	Wild-type	Wild-type	No	No
K72E, K73E, R74Q	Wild-type	Wild-type	No	No
Charge Neutralization				
R64Q	124	144	No	No
R74Q	Wild-type	114	No	No
R64Q, K66A, K67A	143	143	No	No
R64Q, K66A, K67A, R287Q	Wild-type	45	No	No
R64Q, K66A, K67A, K72A, K73A, R287Q	65	22.5	No	No

DHFR and TS-DHFR activity is presented as the single-turnover rate of the mutant enzyme divided by that of wild-type: a difference of <10% is considered to be like wild-type. Criteria for increased H_2folate accumulation was >5% above that observed with wild-type *L. major*.

Reproduced with permission of the copyright owner. Further reproduction prohibited without permission.

3 mutants: R74E; K66E, K67E, K72E, K73E, R64Q, R74Q; and R64Q, K66A, K67A, K72E, K73E. Similarly, attempts to completely remove the 12 amino acid basic loop present in *L. major* but not *E. coli* DHFR (residues 62-73 in *L. major*) did not yield soluble enzyme. By doing large growths (typically 22 L), however, we were still able to make and test 3 combination mutants that included mutation of K73 (Table 4.0).

Steady-State Spectroscopic Analysis to Assess $NADP^+$ Production

Meek *et al.* [65] report a lag in the production of $NADP^+$ via the DHFR catalyzed reduction of H_2folate formed by TS in a coupled assay using *L. casei* monofunctional TS and DHFR. In the case of the *L. tropica* bifunctional TS-DHFR enzyme, no lag was observed suggesting that H_2folate is directly channeled from TS to DHFR. The equation for $NADP^+$ formation via the DHFR catalyzed oxidation of NADPH and reduction of H_2folate produced at TS is: $[NADP^+] = v_1 t + (v_1 / v_2)(K_m e^{-v2t/Km} - 1)$

K_m is the K_m for H_2folate; v_1 is the rate of TS (μM/min) under coupled assay conditions; and v_2 is the DHFR rate (μM/min) using near-saturating substrate concentrations. When $NADP^+$ concentration is plotted versus time, the steady-state concentration of H_2folate corresponds to $v_1 K_m / v_2$ and the predicted lag time prior to steady-state H_2folate accumulation is K_m / v_2.

Spectroscopic signal change from NADPH consumption, monitored at 340 nm, depends on H_2folate formation at TS and thus is proportional to TS activity; whereas, lag time is inversely proportional to DHFR activity. To amplify signal change and lag time, TS activity must be maximized and DHFR activity minimized. With monofunctional enzymes this can be accomplished by adjusting the relative ratios of TS:DHFR. The

Reproduced with permission of the copyright owner. Further reproduction prohibited without permission.

bifunctional enzyme poses a particular challenge however, since the ratio of TS:DHFR active sites is fixed at 1:1 (or 0.5:1 if TS half-sites activity is taken into account) and the ratio of specific activities is 1:5.7 (TS:DHFR) for *L. major*.

With a K_m of 0.6 μM for H_2folate and the bifunctional enzyme, the steady state accumulation of H_2folate is fixed at 0.11 μM, near reported the 0.1 μM detection limit [65], and corresponding to an absorbance change of 6.6×10^{-4} AU (ε_{340} for H_2folate and TS-DHFR= 6000 $mM^{-1}cm^{-1}$). Using a standard (1 cm pathlength) quartz cuvette, we observed unacceptable signal to noise in both absorbance (340 nm) and fluorescence (Ex 340 nm; Em 450 nm) spectra, so a 10 cm pathlength quartz observation cell was employed with a Perkin Elmer Lambda 2 UV/Vis Spectrophotometer. Here 10 nM *L. major* TS-DHFR represents the lower limit of ability to clearly detect signal change from NADPH consumption following H_2folate production at TS. Ten nM TS-DHFR corresponds to a lag time of 18 s, also near the lower limit of detection when start and mixing times are accounted for.

Using these conditions, we observed a lag with *E. coli* monofuctional TS+ DHFR but not with wild-type *L. major* TS-DHFR although one was predicted, supporting the existence of channeling by the bifunctional enzyme (Fig. 4.1 A-B). The following *L. major* TS-DHFR mutants were tested under similar conditions: R283E; R287E; R64Q; R74Q; and R64Q, K66A, K67A, R287Q. No convincing evidence of a lag in $NADP^+$ production was observed with any of these putative channel mutants (Fig 4.1 C-D).

Reproduced with permission of the copyright owner. Further reproduction prohibited without permission.

Fig. 4.1 Steady-state spectroscopic analysis to assess $NADP^+$ production by *E. coli* TS + DHFR, *L. major* TS-DHFR and the *L. major* R64Q, K66A, K67A and R283E mutants. *A*, A lag in $NADP^+$ production is observed in the coupled assay with *E. coli* TS + DHFR at concentrations matching the TS and DHFR activities of 10 nM *L. major* TS-DHFR. No lag was observed with 10 nM *L. major* TS-DHFR, however, supporting the existence of substrate channeling by the bifunctional enzyme (*B*). A lag was also absent in the case of the *L. major* mutants, R64Q, K66A, K67A, at 10 nM (*C*) and R283E, tested at 20 nM since TS-DHFR activity is roughly half that of the wild-type enzyme (*D*).

Reproduced with permission of the copyright owner. Further reproduction prohibited without permission.

Fig. 4.1

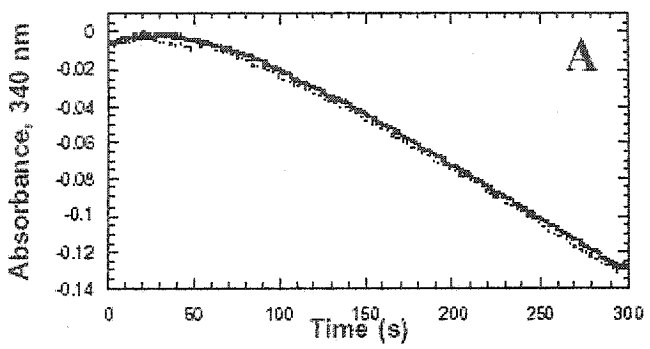

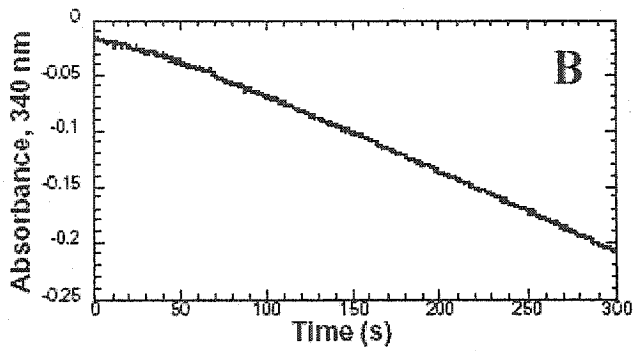

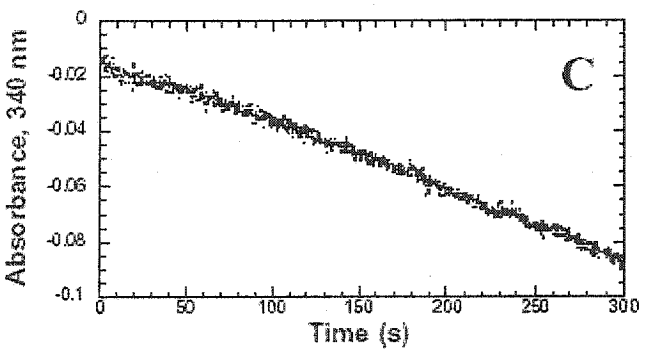

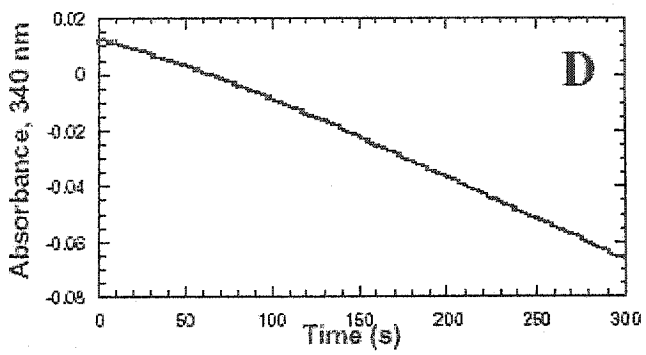

Reproduced with permission of the copyright owner. Further reproduction prohibited without permission.

Single Enzyme Turnover Experiments to Look for a Lag in H_4folate Production and Increased H_2folate Accumulation

Whereas steady-state kinetic analysis is an indirect method from which one can infer information about the rate-limiting step of an enzymatic reaction, transient kinetics allows one to directly measure individual steps in a kinetic pathway as well as to define the reaction kinetics of intermediate formation. Transient kinetics has several advantages for investigation of substrate channeling since, in principle, this technique enables one to directly monitor chemical catalysis at each active site as well as the transit of the putative intermediate from one active site to another [63, 105]. In the case of bifunctional TS-DHFR, transient kinetic analysis was used to look for a lag in H_4folate production and increased build-up of H_2folate as evidence of impaired channeling.

Single enzyme turnover experiments, which measure the rate of the chemical conversion of substrate to product at the active site under conditions where enzyme concentration is sufficiently high that substrate binding is not rate-limiting, were performed using a rapid chemical quench apparatus. In the case of combination of the *E. coli* monofunctional TS and DHFR, H_2folate concentration rises more rapidly than H_4folate and there is almost no H_4folate present at the earliest time points, suggesting a lag in product formation at DHFR (Fig. 4.2 A-B). Early in the time course, H_2folate makes up 44-60% of the tritiated material when equal concentrations of monofunctional *E. coli* TS and DHFR are combined. Conversely, H_4folate is formed from the earliest time points with the wild-type bifunctional TS-DHFR enzyme from *L. major* (no lag) and only a modest amount of H_2folate accumulates, peaking at 14% of tritiated material (Fig.

Reproduced with permission of the copyright owner. Further reproduction prohibited without permission.

4.2 C-D). Note that the *E. coli* enzymes are faster than *L. major* TS and DHFR, so overall product formation over the course of 0.1 s is greater.

The putative channel mutants were each evaluated for changes in the rate of the TS-DHFR and DHFR reactions. With each mutant tested, full time courses for both wild-type *L. major* and the mutant were completed, along with t=0 and t=60 s controls. The TS reaction was not evaluated independently, since the rate of chemistry for TS is significantly slower than that of DHFR in *L. Major* (2 s^{-1} versus 20 s^{-1}), the rate of TS limits and is equivalent to that of TS-DHFR. To monitor the TS-DHFR reaction, the bifunctional TS-DHFR enzyme (50 μM) was preincubated with saturating concentrations of dUMP and NADPH (500 μM each) and then mixed with a limiting amount of radiolabeled CH_2H_4folate (12.5 μM). To monitor the DHFR reaction, the bifunctional TS-DHFR enzyme (50 μM) was preincubated with a saturating concentration of NADPH (500 μM) and then mixed with a limiting amount of radiolabeled H_2folate (12.5 μM).

The data in Table 4.0 are presented as the ratios of the rate constants obtained for the mutant enzymes divided by that of wild-type; a difference of less than 10% is considered to be like wild-type. The TS mutants R283E and R287E were both found to have approximately half of wild-type TS-DHFR activity, with no impairment of DHFR alone; K282E, R283E was found to be TS dead, again with no impairment of DHFR. DHFR mutants including R64Q tended to have a slightly faster TS-DHFR rate and a significantly faster DHFR rate. No differences in behavior were observed between charge reversal and charge neutralization mutants.

Representative TS-DHFR and DHFR time courses from the R64Q, K66A, K67A, R287Q mutant are presented in Fig. 4.3. The R64Q, K66A, K67A, R287Q mutant is

Reproduced with permission of the copyright owner. Further reproduction prohibited without permission.

Fig. 4.2 TS-DHFR single turnover reaction time courses from *E. coli* and *L. major*. *A-B,* TS and DHFR reactions with monofunctional enzymes: 40 μM *E. coli* TS + 40 μM *E. coli* DHFR reacted with 12.5 μM tritiated CH_2H_4folate. CH_2H_4folate consumption (■), as well as H_2folate and H_4folate production are reported (▲ and ●, respectively): note maximal H_2folate accumulation of 45% of tritiated material (*A*). *B,* Magnification of the early time course illustrating that, in the case of *E. coli* TS+DHFR, there is a lag in product formation at DHFR: H_2folate (▲) accumulates before significant conversion to H_4folate (●). *C-D* Compare to the *L. major* TS-DHFR reaction, where when 50 μM bifunctional enzyme is reacted with 12.5 μM tritiated CH_2H_4folate, maximum accumulation of H_2folate is 14% of tritiated product (▼) (*C*) and H_4folate (●) is formed from the earliest time points (*D*).

Reproduced with permission of the copyright owner. Further reproduction prohibited without permission.

Fig. 4.2

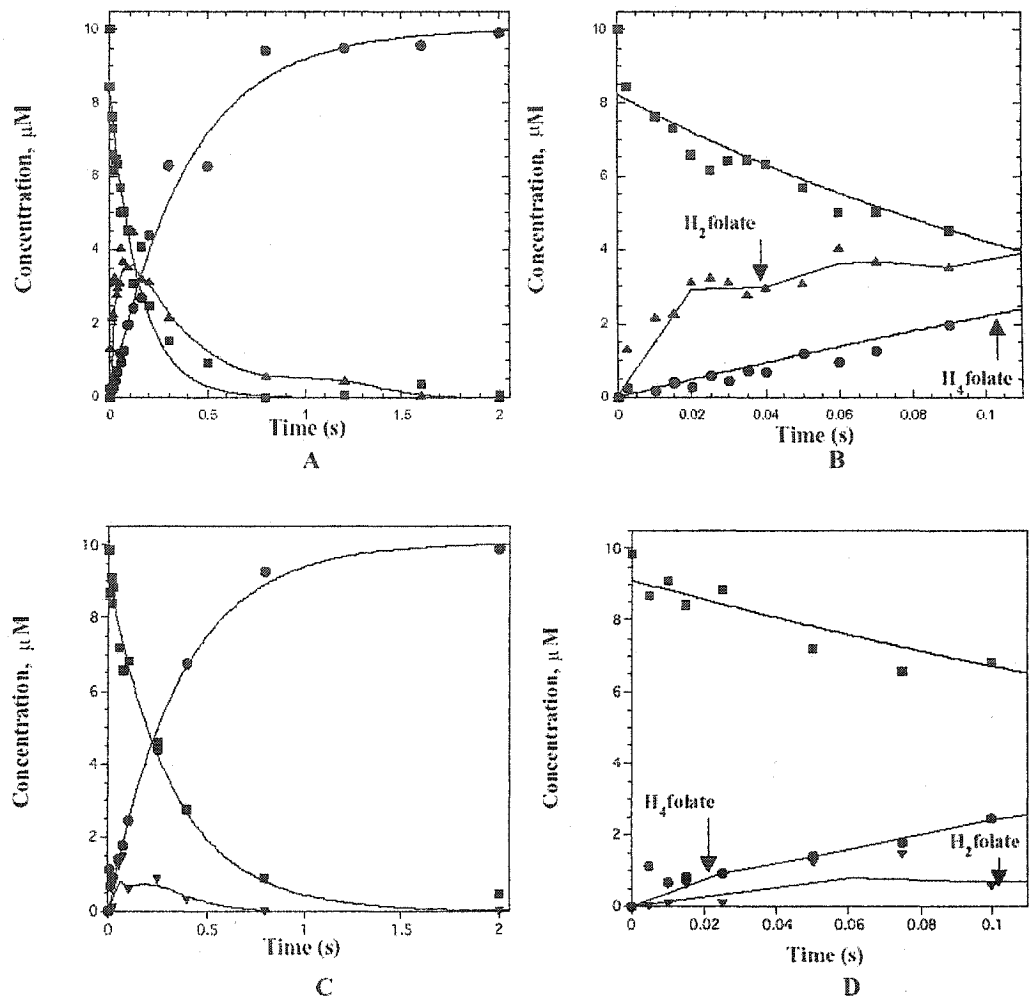

Reproduced with permission of the copyright owner. Further reproduction prohibited without permission.

Fig. 4.3 Representative TS-DHFR and DHFR reactions: the R64Q, K66A, K67A, R287Q mutant. 50 μM wild-type or mutant enzyme was reacted with 12.5 μM tritiated substrate. *A,* TS-DHFR reaction: the mutant *L. major* TS-DHFR enzyme exhibits 45% of wild-type activity, as measured by rate of formation of H_4folate (wild-type: solid lines, closed circles; mutant: dashed lines, open circles). A comparable accumulation of H_2folate is observed with wild-type and mutant enzyme (wild-type: solid lines, closed triangles; mutant: dashed lines, open triangles). *B,* Magnification of the early R64Q, K66A, K67A, R287Q mutant time course: at the earliest time points both products are below detectible limits, but H_4folate (○) is visualized as soon as product is detected (no lag). (CH_2H_4folate (□); H_2folate (▽)). *C,* The mutant enzyme exhibits 100% of wild-type DHFR activity, as measured by rate of formation of H_4folate (● - wild-type; ○ - mutant).

Reproduced with permission of the copyright owner. Further reproduction prohibited without permission.

Fig. 4.3

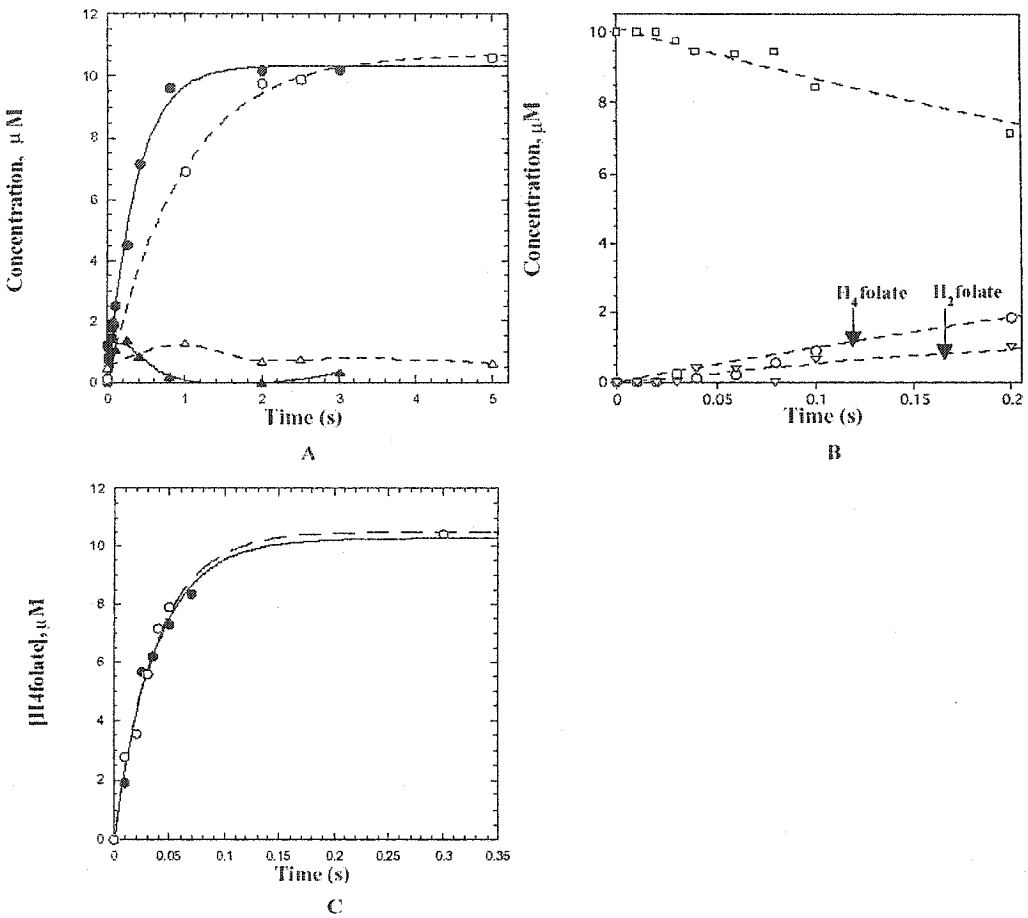

Reproduced with permission of the copyright owner. Further reproduction prohibited without permission.

slower overall, so at the earliest time points both products (di- and tetrahydrofolate) are below detectable limits, but H_4folate is visualized as soon as product is detected (no lag) (Fig. 4.3 B). While peaking later in the slower, mutant enzyme, the amplitude of maximal H_2folate accumulation is the same for the mutant and wild-type TS-DHFR enzymes. Surprisingly, no lag in H_4folate production or buildup of H_2folate beyond that observed with wild-type *L. major* was seen with any of the mutants (Table 4.0).

Pre-steady-state Burst Experiments to Examine Effects of Mutations on TS Catalysis

Stopped-flow absorbance and rapid chemical quench experiments were performed under pre-steady-state burst conditions (substrate in 3-5 fold excess over enzyme) to determine whether the channel residues might participate in conformational change, specifically the domain movement involved in TS catalysis. It is known that chemistry is overall rate-limiting at TS, as demonstrated in Fig. 4.4 A: under pre-steady-state burst conditions, where *L. major* TS-DHFR (25 μM) is pre-incubated with excess [^{14}C]dUMP (90 μM) prior to mixing with a large excess of CH_2H_4folate (250 μM), the TS reaction occurs at a linear steady-state rate with no burst in [^{14}C]dUMP consumption or [^{14}C]dTMP formation. The absence of a burst confirms that chemistry or a preceding step is rate-limiting in the TS reaction. A pre-steady-state burst is observed for consumption of the cofactor, CH_2H_4folate, however, suggesting formation of a TS intermediate, likely the iminium form of CH_2H_4folate, with a rate of formation that exceeds the rate of chemistry (Fig. 4.4 B).

Reproduced with permission of the copyright owner. Further reproduction prohibited without permission.

Fig. 4.4 TS pre-steady-state burst experiments. *A*, Rapid chemical quench TS burst experiment where *L. major* TS-DHFR (25 μM) is pre-incubated with excess [^{14}C]dUMP (90 μM) prior to mixing with a large excess of CH_2H_4folate (250 μM). *B-C*, Stopped-flow absorbance at 340 nm was monitored when *L. major* TS-DHFR (25 μM) was preincubated with a large excess of dUMP (1 mM) and then mixed with CH_2H_4folate (500 μM). *B*, Wild-type TS-DHFR. *C*, The R283E TS-DHFR mutant enzyme.

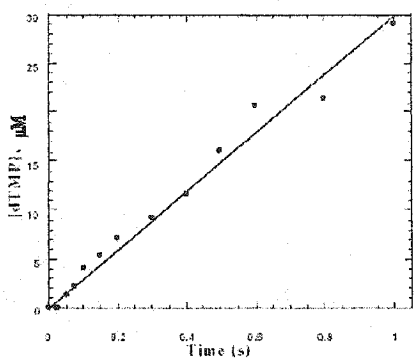

A

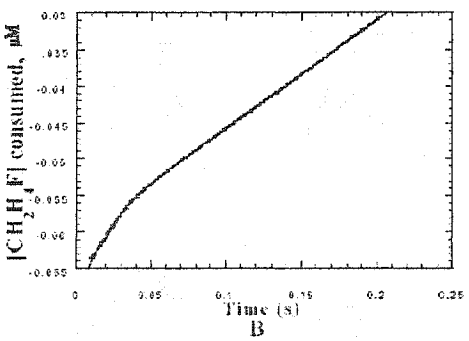

B

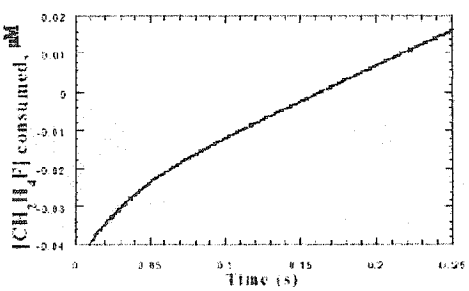

C

Reproduced with permission of the copyright owner. Further reproduction prohibited without permission.

Several of the channel mutants were tested for a burst in CH_2H_4folate consumption to examine the effect of mutation on TS catalysis. R64Q; R283E; and R287E were tested by rapid chemical quench. R64Q; R64Q, K66A, K67A; R74Q; R283E; and R287E were tested using stopped-flow absorbance. In the case of each of the mutants tested using either technique, a biphasic TS burst with a fast and a slow phase was observed, suggesting that the mutated residues are not critical to TS catalysis. Burst amplitudes were similar for each of the mutants tested, but R283E exhibited a pre-steady state burst rate that was roughly half of that observed with the wild-type enzyme (33 μMs^{-1} versus 63 μMs^{-1}) (Fig. 4.4 C).

Further Characterization of the TS Dead Mutant: K282E, R283E

We sought to determine the molecular mechanism by which the K282E, R283E mutant, with two non-active site mutations near the folate binding site in TS, is devoid of TS activity. The mutation homologous to K282E in *E. coli*, K48E, was also found to be TS dead but no analysis has been reported [38]. As detailed in Chapter 2, it was determined by fluorimetry that the concentration of TS active sites capable of binding PDDF with the TS dead mutant is equivalent to the protein concentration. We examined whether the lack of activity is due to: 1. decreased binding affinity for folates, 2. impaired nucleotide binding or inability to form the FdUMP-CH_2H_4folate-enzyme ternary complex prior to chemistry, or 3. global structural instability.

1. Binding affinity for PDDF and CH_2H_4folate. Stopped-flow fluorescence was used to measure the binding affinity of K282E, R283E for the folate-analog, PDDF, relative to that of wild-type. The k_{on} was obtained by titrating 100 nM wild-type or

Reproduced with permission of the copyright owner. Further reproduction prohibited without permission.

mutant TS-DHFR with increasing amounts of PDDF and plotting k_{obs} (s^{-1}) versus concentration of PDDF added: $k_{obs} = k_{on}[PDDF] + k_{off}$ (Fig. 4.5). An independent and more precise way to measure the k_{off} for PDDF is to measure the rate when PDDF is competed with an excess of a ligand that binds at the same site. This was accomplished by competing 5 μM PDDF with 100 μM CH_2H_4folate in the presence of 200 nM wild-type or TS-dead *L. major* TS-DHFR. For the wild-type enzyme, k_{off} was found to be 2.6 s^{-1} and k_{on} was 21.3 $s^{-1}\mu M^{-1}$; $K_d = k_{off}/k_{on} = 122$ nM. For the TS-dead mutant, k_{off} was found to be 2.05 s^{-1} and k_{on} was 16.52 $s^{-1}\mu M^{-1}$; so the K_d for PDDF was 124 nM (Fig. 4.5). The wild-type and TS-dead enzymes also had a similar k_{off} for CH_2H_4folate (200 nM enzyme + 5 mM CH_2H_4folate, competed with 50 μM PDDF): for wild-type TS-DHFR, the k_{off} for CH_2H_4folate was found to be 5.83 s^{-1}; and it was 4.1 s^{-1} for the TS-dead mutant.

2. FdUMP Binding and FdUMP-CH_2H_4folate-Enzyme Ternary Complex Formation. Size exclusion columns were used to investigate binding of ^{14}C labeled FdUMP to the enzyme since no fluorescence signal was detected upon addition of dUMP or the analog, FdUMP. FdUMP nucleotide binding was found to be similar for the wild-type and TS-dead enzymes. When radiolabeled FdUMP (20 μM) was added to either wild-type or TS dead TS-DHFR (50 μM), a small portion of total counts were recovered in the flow-through, representing enzyme-bound FdUMP. It is thought that the low percent bound is a reflection of the high off rate for FdUMP (Fig. 4.6). When excess cold dUMP (100 μM) was added at the same time as the ^{14}C labeled FdUMP and enzyme, significantly fewer counts were found in the flow-through, indicating that the FdUMP is able to be competed off by dUMP.

Reproduced with permission of the copyright owner. Further reproduction prohibited without permission.

Fig. 4.5 Stopped-flow fluorescence experiment to measure the binding affinity of the K283E, R283E mutant for PDDF. *A,* Representative stopped-flow trace of fluorescence at 380 nm versus time, observed upon mixing K282E, R283E TS-DHFR with PDDF (2.5 μM). *B,* Plot of concentration dependent rate (k_{obs}) versus PDDF concentration.

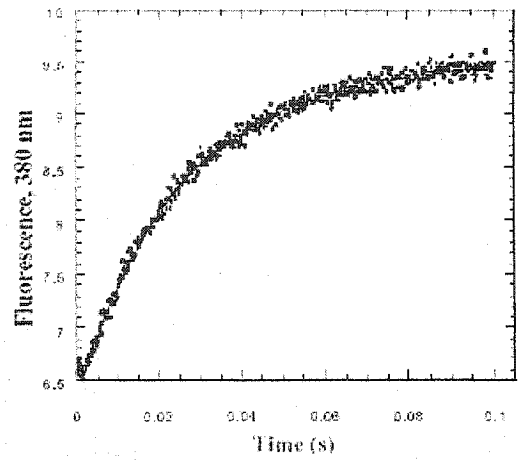

A

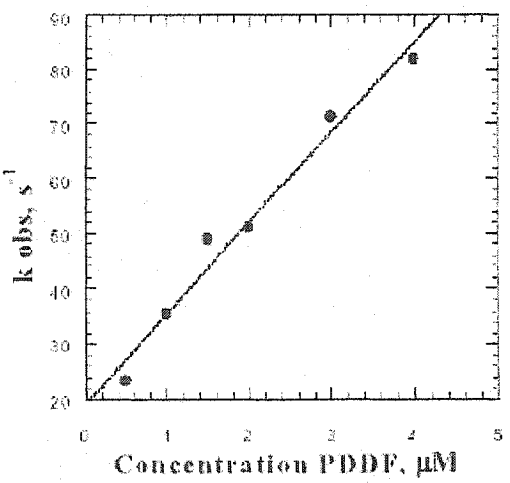

B

Reproduced with permission of the copyright owner. Further reproduction prohibited without permission.

Fig. 4.6 Spin column assays to assess FdUMP binding and covalent (FdUMP-CH_2H_4folate-enzyme) complex formation by the TS-dead mutant. Percent ^{14}C-Labeled FdUMP (*FdUMP) bound to wild-type (black) or mutant (gray) TS-DHFR is reported for various conditions. 1) When *FdUMP (20 μM) was added to wild-type or TS-dead enzyme (50 μM), a small proportion of total ^{14}C counts were recovered in the flow-through, representing enzyme-bound *FdUMP (12% and 7% of counts in with the wild-type and mutant enzymes, respectively). 2) *FdUMP may be competed off either enzyme with excess cold dUMP (100 μM). 3) Significantly more *FdUMP remains bound to enzyme in the presence of excess CH_2H_4folate (100 μM), although the mutant does not bind as well as wild-type (~15% versus ~60% of *FdUMP bound). Error bars represent differences observed when the experiment was duplicated. 4) Comparatively less *FdUMP can be competed off wild-type enzyme by cold dUMP in the presence of CH_2H_4folate, suggesting that a covalent complex is forming, as predicted. Again, a difference is observed between the wild-type and mutant enzymes: 80% of *FdUMP remains bound to the wild-type enzyme in the presence of excess CH_2H_4folate and dUMP, whereas only 33% remains bound to the K282E, R283E mutant.

Reproduced with permission of the copyright owner. Further reproduction prohibited without permission.

Fig. 4.6

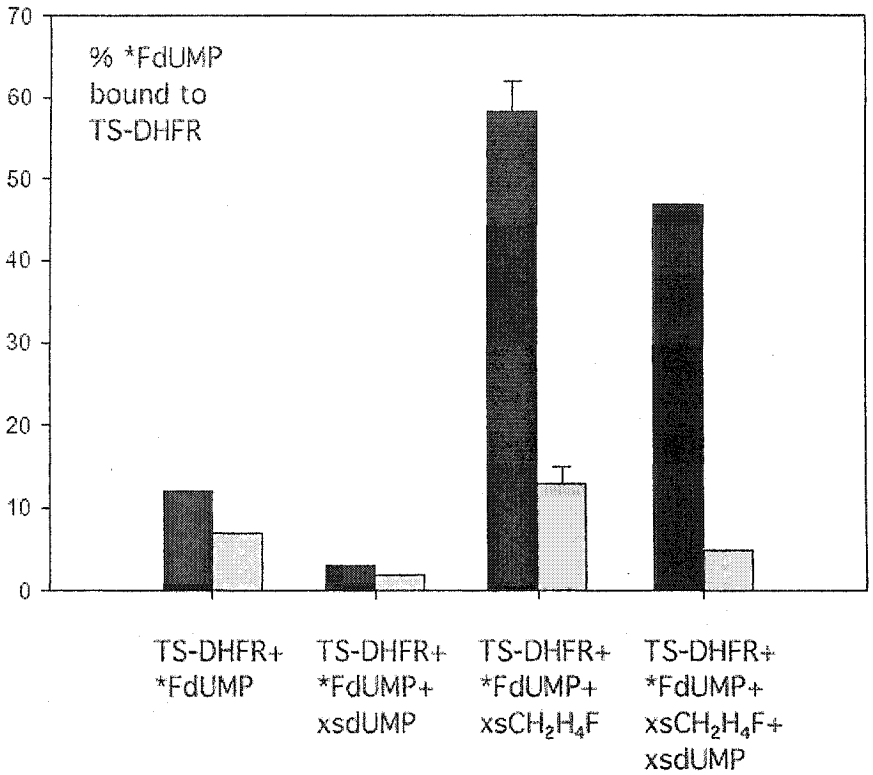

Reproduced with permission of the copyright owner. Further reproduction prohibited without permission.

It is known that, prior to chemistry, a dUMP-CH_2H_4folate-enzyme ternary complex is formed. With the wild-type TS enzyme, FdUMP can be used to trap this ternary complex as a covalent intermediate [41, 56]. To assess the ability of the mutant enzyme to form the covalent complex, 50 μM enzyme was preincubated with excess unlabeled CH_2H_4folate (100 μM) and radiolabeled FdUMP (20 μM). In this case, approximately 60% of the total FdUMP was bound to wild-type enzyme, whereas less than 20% was bound to the TS-dead mutant (Figure 4.6). When excess unlabeled FdUMP (100 μM) was added to the pre-incubation mix, approximately 50% of the total FdUMP added still remained bound to the wild-type enzyme, but only 5% remained bound to the mutant (Fig. 4.6). These results imply that the K282E, R283E TS-dead mutant is unable to properly form the covalent dUMP-CH_2H_4folate-enzyme complex requisite for chemistry to take place.

3. Restoration of Activity to Assess Global Stability. From studies in *E. coli*, it is known that TS, which exists as a dimer in most species, exhibits half-the-sites activity, meaning that at any given time, only one-half of the TS dimer is kinetically competent [38, 39]. In *E. coli* TS it was shown that the amino acid Arg 126 participates in the catalytic site of the opposite half of the dimer, and that a TS-dimer in which both R126 residues have been mutated to glutamic acid is TS dead. When a TS-mutant that is dead due to a mutation outside of the active site is combined with the R126E mutant to form a heterodimer, however, full TS activity is restored. In the heterodimer, one-half of the dimer now effectively has two mutations (as R126 contributes to the opposite half), but

Reproduced with permission of the copyright owner. Further reproduction prohibited without permission.

the TS subunit containing R126E is catalytically active, as a normal R126 has been contributed by the non-active site mutant.

In *E. coli*, one TS dead mutant whose activity can be restored by heterodimerization is K48E, homologous to K282E in *L. major* [38]. We hypothesized that, if K282 and R283 were crucial to global stability of the protein, then dissociating the TS dimer and reassociating the K282E, R283E mutant with an active site mutant may not lead to restoration of TS activity. To test whether activity could be restored to K282E, R283E, the equivalent mutation to *E. coli* R126E was made in *L. major* TS-DHFR: R380E. The R380E homodimer was shown to be TS dead by a spectroscopic enzyme activity assay and by rapid chemical quench. When 0.41 μM R380E was incubated with 4.1 μM K282E, R283E in the presence of urea to facilitate subunit exchange (1 M urea, 25 mM potassium phosphate, pH to 7.5), activity was restored.

DISCUSSION

As a direct test of the electrostatic channeling hypothesis in *L. major* TS-DHFR, 12 putative channel mutants were created: up to 6 amino acids were mutated at once, and 2 mutants contained changes in both the TS and DHFR domains. Both charge neutralization and charge reversal mutants were made. The mutants were evaluated for impaired channeling using two critera: a lag in product formation at DHFR and increased H_2folate accumulation.

The mutants were first analyzed in a steady-state spectroscopic experiment for a lag in production of $NADP^+$ via the DHFR catalyzed reduction of H_2folate produced at TS. Meek *et al.* [65] observed a lag in the case of a monofunctional TS and DHFR

Reproduced with permission of the copyright owner. Further reproduction prohibited without permission.

coupled assay but not with the bifunctional TS-DHFR enzyme suggesting that, in the case of the bifunctional enzyme, H_2folate produced at TS is channeled across the surface of the enzyme from TS to DHFR without equilibration into bulk solvent. We observed similar behavior using wild-type monofunctional and bifunctional enzymes; however, no clear lag was observed with any of the putative electrostatic channel mutants suggesting that at this level of analysis, these mutations were not interfering with channeling behavior.

Since we were close to the limits of detection, however, we were not confident of our ability to detect subtle channeling impairment resulting from mutagenesis using this assay. Single enzyme turnover experiments, which allow for direct monitoring of the active sites, were designed and radiolabeled substrates were used to enhance sensitivity and ability to quantify H_2folate accumulation. The mutants were analyzed under single enzyme turnover conditions by rapid chemical quench for a lag in H_4folate production and an increased accumulation of H_2folate, evidence that, as a result of disruption of the electrostatic channel, H_2folate is now leaving the surface of the enzyme at TS and rebinding the DHFR site after equilibration with bulk solution. A lag in production of H_4folate and a large accumulation of H_2folate was observed when *E. coli* monofunctional TS and DHFR were combined at a ratio of 1:1. No lag in H_4folate production was observed in the case of the *L. major* bifunctional TS-DHFR enzyme and only a small amount of H_2folate accumulated, 3-fold less than with *E. coli* TS + DHFR.

It is unclear whether the H_2folate observed with the bifunctional enzyme is formed as a result of full TS catalysis or if it is a breakdown product of the TS iminium ion intermediate. If the product of TS catalysis, it suggests that a small percentage of

Reproduced with permission of the copyright owner. Further reproduction prohibited without permission.

H_2folate dissociates from the wild-type TS-DHFR enzyme and rebinds at DHFR. A much larger accumulation, comparable to that observed with *E. coli* TS +DHFR, is predicted in the absence of channeling [56]. Therefore, what we would like to stress is the 3-fold difference in H_2folate accumulation between *E. coli* TS + DHFR and *L. major* TS-DHFR. If the putative electrostatic channeling mutants were even partially channeling impaired, this 3-fold difference provides ample latitude to detect subtle changes. The difference in behavior between monofunctional TS + DHFR and bifunctional TS-DHFR is, however, unchanged by mutation of the putative electrostatic channeling residues; none of the putative channel mutants exhibited a lag in H_4folate production or increased H_2folate accumulation. Results from single enzyme turnover experiments confirm findings of the steady-state assay; no evidence of impaired channeling was observed with any of the putative electrostatic channeling mutants and monoglutamyl folate substrates.

We also performed TS experiments under pre-steady-state burst conditions to determine whether the solvent exposed basic residues are involved in conformational changes associated with TS catalysis, specifically formation of the TS iminium ion intermediate. In the case of the wild-type enzyme and each of the charge reversal or charge neutralization mutants tested, we observed a burst in consumption of the cofactor, CH_2H_4folate at TS [30]. Since chemistry is overall rate-limiting at TS (no burst in dUMP consumption or dTMP formation), the observation of a burst in CH_2H_4folate consumption signifies the presence of a TS intermediate, most likely the iminium form of CH_2H_4folate. Our results suggest that the putative channel residues are not critical to iminium ion formation. Paralleling our single-enzyme turnover findings, the R283E mutant exhibited

Reproduced with permission of the copyright owner. Further reproduction prohibited without permission.

a burst rate that was roughly half of that observed with the wild-type enzyme, indicating impairment of an early step in the kinetic mechanism.

Additional findings were that mutation of K73 or R74 resulted in largely insoluble protein, suggesting that these residues may play a role in protein folding, and that the R64Q mutation resulted in faster rates for both TS and DHFR. It is possible that R64 is involved in domain-domain communication and that its normal role is to limit the rate of the TS reaction, but this has yet to be investigated.

The K282E, R283E mutant was found to be TS dead. In *E. coli*, mutation of the residue homologous to K282E alone resulted in a TS dead enzyme, but no mechanism of inactivation was reported [38]. It was predicted that the K282E, R283E mutation would prohibit folate binding at the TS site based on the crystal structure of *L. major* TS-DHFR (Fig. 4.7), and because corresponding residues in *Lactobacillus casei* are known to participate in polyglutamyl folate binding [6]. Surprisingly, binding of CH_2H_4folate or the folate analog, PDDF, was not impaired in the TS-dead mutant. Instead, our studies suggest that K282 and/or R283 are required for ternary complex formation (FdUMP-CH_2H_4folate-enzyme) prior to chemistry. Since R283E alone results in 40% TS activity but a normal TS burst, indicating formation of the iminium ion intermediate, it follows that K282 is likely the more critical residue for ternary complex formation. It also appears that there is no global structural disturbance as the TS-dead mutant is able to restore activity to the active site mutant, R380E, when heterodimers are formed. Finally, we hope to investigate the structural consequences of this mutation by solving the crystal structure in the presence and absence of ligands.

Reproduced with permission of the copyright owner. Further reproduction prohibited without permission.

Fig. 4.7 Model of the TS-dead (K282E, R283E) *L. major* TS-DHFR mutant. TS is in red; DHFR in blue; PDDF in green; and dUMP in yellow. Proximity of the TS mutations to the folate analog, PDDF, at the TS active site is greater than to the dUMP binding site (4.27 Å versus 12.25 Å), leading to the prediction that the K282E, R283E mutant was TS dead due to impaired folate binding.

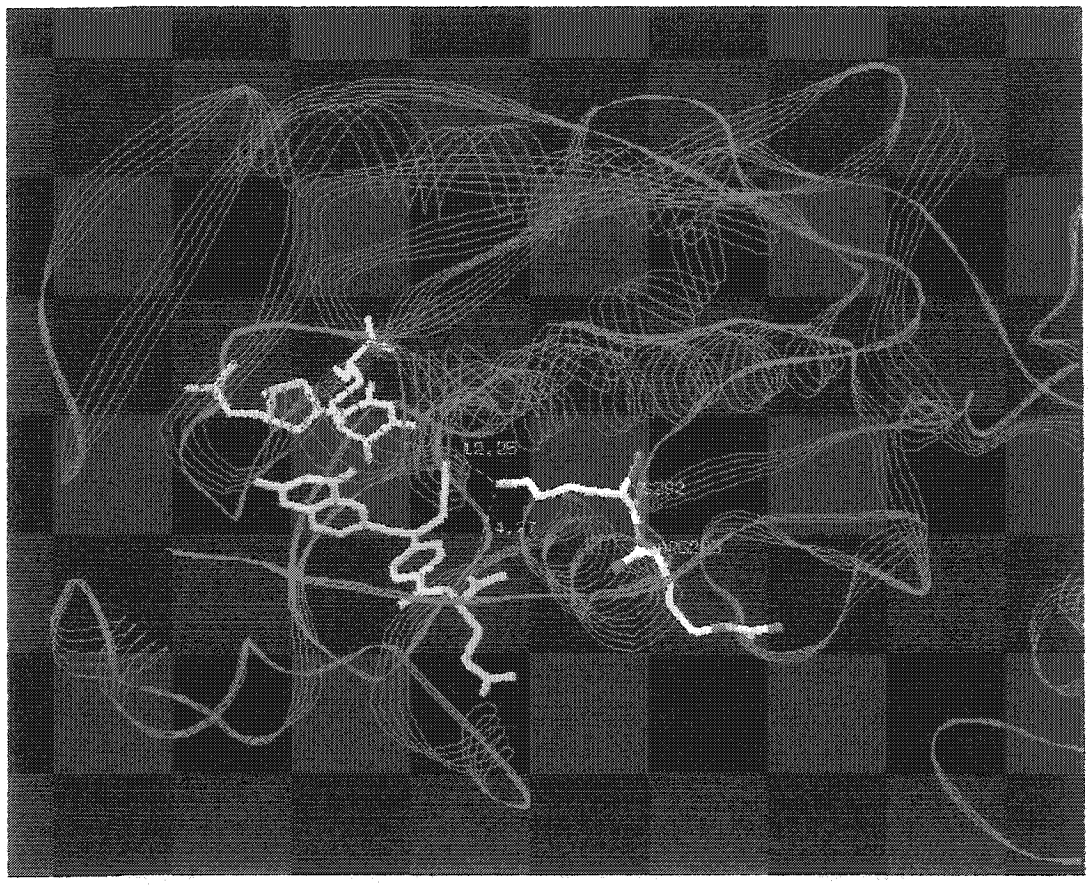

Reproduced with permission of the copyright owner. Further reproduction prohibited without permission.

The site-directed mutagenesis data presented in this study does not support the hypothesis that substrate channeling in the bifunctional TS-DHFR enzyme from *L. major* occurs via electrostatic interactions between the negatively charged H_2folate and a series of lysine and arginine residues on the surface of the protein. It now seems probable that channeling instead occurs in conjunction with domain-domain communication, or conformational changes induced by ligand binding at one active site that affect activity at the active site of the other enzyme. In the next chapter we present research that begins to address the coupling of channeling and communication through investigation of a small molecule inhibitor that binds in the channel region [104]. In Part B of this chapter we apply site-directed mutagenesis to probe the mechanistic and structural determinants of TS-DHFR domain-domain communication in apicomplexan parasites with the ultimate goal of developing non-active site therapies for protozoal infection.

Reproduced with permission of the copyright owner. Further reproduction prohibited without permission.

Part B. Use of Site-Directed Mutagenesis to Probe Domain-domain Communication in Apicomplexan TS-DHFR

1. Analysis of a *T. gondii* C-terminal Deletion Mutant (V610Am).

A *T. gondii* C-terminal deletion mutant, V610Am[5], was created to elucidate the role of the C-terminal amino acid, known to mediate conformational change at TS, in communication between domains of the bifunctional TS-DHFR enzyme, and also as a means of trapping the putative iminium ion intermediate. In TS catalysis dUMP binds first, then CH_2H_4folate; this is followed by movement of the C-terminus to form a "closed" active site, required for catalysis to proceed [41-43, Fig. 1.3]. We have created the first bifunctional TS-DHFR C-terminal deletion mutant, *T. gondii* V610Am, to determine whether maintaining TS in an obligate "open" conformation has an effect on DHFR activity.

The *T. gondii* V610Am mutant was also created with hopes of trapping the putative TS iminum ion intermediate in order to determine whether the TS intermediate of our mechanistic studies represents a breakdown product of the iminium species. From mechanistic studies, chemistry is known to be overall rate-limiting at TS, but we observe a burst in CH_2H_4folate consumption by *L. major* and *T. gondii* TS-DHFR, which we attributed to a TS intermediate with a rate of formation that is faster than chemistry. A TS intermediate was also detected by HPLC with *T. gondii* and *C. hominis* TS-DHFR [30]. The crystal structure of a *Lactobacillus casei* TS C-terminal valine deletion mutant

Reproduced with permission of the copyright owner. Further reproduction prohibited without permission.

suggested the presence of hydroxymethylene tetrahydrofolate, a hydrolytic product of a putative TS iminium ion intermediate [48]. It was observed that deletion of the C-terminal valine resulted in an enzyme that while unable to catalyze dTMP formation, still bound dUMP and CH_2H_4folate. These findings led us to hypothesize that, without the C-terminal residue, the iminium species forms, but then breaks down since catalysis can no longer proceed; and perhaps the TS intermediate observed with the faster apicomplexan enzymes represents small amounts of this breakdown product.

Surprisingly, V610Am, while very slow, was not TS dead, it exhibited 0.6% and 0.2% of wild-type steady-state and single enzyme turnover activity, respectively (Fig. 4.8 A), and nearly full steady-state DHFR activity. There was no evidence by gel analysis of contaminating monofunctional TS and a methotrexate column was used in purification, selecting for DHFR. In the TS-DHFR reaction a small buildup of H_2folate was observed (6.6% maximum; species identity confirmed by a non-radiolabeled H_2folate standard). No intermediate was detected and radiolabel counts were preserved, indicating that the radiolabel was not trapped in a covalent complex with enzyme. A recent report also finds activity with the *L. casei* C-terminal deletion mutant [106]. The absence of the TS intermediate may be explained by the fact that crystallization conditions could not be fully replicated in our assays, as they result in protein precipitation.

It is known that, prior to chemistry, a dUMP-CH_2H_4folate-enzyme ternary complex is formed. With the wild-type TS enzyme, FdUMP can be used to trap this ternary complex as a covalent intermediate [41, 56]. To assess the ability of the V610Am mutant enzyme to form the covalent complex, 50 μM enzyme was preincubated with

[5] Am is the Amber stop codon, TAG

Reproduced with permission of the copyright owner. Further reproduction prohibited without permission.

excess unlabeled CH_2H_4folate (167 μM) and radiolabeled FdUMP (20 μM). ^{14}C-Labeled FdUMP alone does not pass through the size exclusion column, but in the presence of TS-DHFR enzyme, a much greater percentage of [^{14}C] FdUMP comes through the column when CH_2H_4folate is also added (levels similar to the wild-type *T. gondii* control). Moreover, in the presence of CH_2H_4folate, this [^{14}C] FdUMP cannot be competed off the enzyme with excess unlabeled dUMP (100 μM), suggesting that a covalent ternary complex has formed.

A burst in CH_2H_4folate consumption is not observed under conditions where a burst is observed with wild-type *T.gondii* TS-DHFR, indicating that the C-terminus is necessary for this activity (Fig. 4.8 B). A V610Am DHFR burst with a rate of 110 s^{-1} was observed in the presence or absence of TS ligands (Fig. 4.8 C), suggesting that the mutation does not affect communication between the TS and DHFR domains.

Reproduced with permission of the copyright owner. Further reproduction prohibited without permission.

Fig. 4.8 *T. gondii* V610Am TS-DHFR single turnover reaction time course (*A*), and TS and DHFR pre-steady-state burst experiments (*B-C*). *A*, 45 μM enzyme reacted with 13.5 μM tritiated CH_2H_4folate (■); a long time course reveals TS-DHFR activity (▲ -H_2folate; ● -H_4folate). *B*, Stopped-flow absorbance at 340 nm monitored when V610Am TS-DHFR (25 μM) is preincubated with a large excess of dUMP (1 mM) and then mixed with CH_2H_4folate (500 μM). *C*, Averaged stopped-flow fluorescence traces (Ex 290 nm; Em 450 nm) showing the time dependent formation of $NADP^+$ after mixing a solution of 7.5 μM V610Am TS-DHFR; 50 μM H_2folate; 500 μM NADPH. Rates for the fast and slow phases are 107 s^{-1} and 9 s^{-1}.

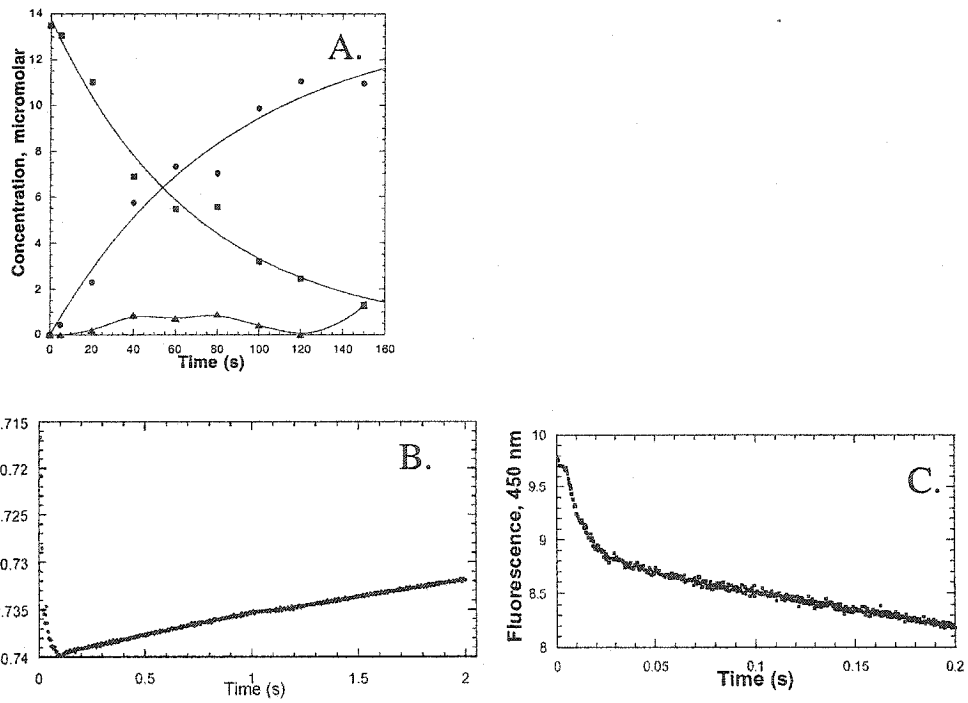

Reproduced with permission of the copyright owner. Further reproduction prohibited without permission.

2. Preliminary Mutational Analysis of *C. hominis* Cross-over Helix-DHFR Domain Hydrogen-bonding Interactions.

A principal mechanistic difference between *L. major* TS-DHFR and the apicomplexan enzymes studied is that *L. major* exhibits domain-domain communication, whereas ligand binding at one active site of the apicomplexan TS-DHFR bifunctional enzyme has no effect on activity of the other enzyme. A major structural difference between *L. major* TS-DHFR and the apicomplexan enzymes is that the former has a short linker (2 amino acids), whereas the latter have long linkers (58-93 amino acids) between the TS and DHFR domains. The long-linker is thought to be the principal determinant of the relative orientations of TS and DHFR domains in the apicomplexan enzymes [9]. The linker region of *C. hominis* TS-DHFR contains an 11-residue α helix that makes extensive van der Waals and hydrogen bonding interactions with the DHFR domain from the other half of the dimeric enzyme (Fig 4.9). This helix, termed the donated or cross-over helix, packs against the DHFR active site, making close contacts with catalytic residues. It has therefore been proposed that 1) this helix may be holding the structure in a stable, active conformation, precluding the communication effects observed between the *L. major* TS and DHFR domains and/or 2) the cross-over helix may itself act as a signaling mechanism between the two halves of the TS-DHFR dimer [9].

We sought to address the role of the α helix-DHFR domain interaction by mutagenesis of residues in the α helix that participate in salt-bridges with the DHFR domain of the other half of the dimer. Two mutations were generated: E205L and R210M. Glu 205 participates in a salt-bridge with Lys 38 at least part of the time (3.5Å) (Fig 4.9 B); Arg 210 in the cross-over helix participates in hydrogen bonds to 3 residues

Reproduced with permission of the copyright owner. Further reproduction prohibited without permission.

in the DHFR domain of the opposite half of the dimer (Fig 4.9 C): Glu 31, Cys 164 (backbone oxygen) and Glu 276 (Fig 4.9 D). Replacement amino acids were chosen on the basis of their inability to form hydrogen bonds, while still preserving the overall structure and helical nature of the linker region [107]. The kinetic properties of the mutants were evaluated to assess the importance of individual residues as hydrogen-bond formers to the functional and kinetic properties of the protein.

The specific activities of wild-type *C. hominis* TS and DHFR were found to be 2.4 s^{-1} and 2.3 s^{-1}, respectively, in a steady-state absorbance assay (340 nm). Both mutants were found to have TS specific activities similar to wild-type; E205L also exhibited similar DHFR activity, but R210M exhibited ~60% of wild-type DHFR specific activity. In single enzyme turnover experiments, both enzymes demonstrated equivalent TS-DHFR and DHFR rates as compared to wild-type. In the TS-DHFR reaction, evaluated by rapid chemical quench, rates of H_2folate and intermediate formation were also comparable, with maximum accumulation at 65% of the radioactive signal with the wild-type enzyme; 55% and 60% with the E205L and R210M mutants, respectively.

In a DHFR burst experiment, monitored by stopped flow fluorescence (Ex. 290 nm; Em 450 nm), both mutants produced a burst, with a similar burst rate and amplitude to that observed with the wild-type enzyme. Consistent with findings of the steady-state absorbance assay, the R210M steady-state rate found in the DHFR burst experiment was 58% of the wild-type rate.

The fact that the point mutations produced little effect on the kinetic properties of *C. hominis* TS-DHFR likely reflects the fact that the cross-over helix makes multiple interactions with the DHFR domain of the opposite half of the dimer. In the future, we

Reproduced with permission of the copyright owner. Further reproduction prohibited without permission.

will test the effects of making multiple point mutations or removing portions of the cross-over helix on enzyme kinetics, communication between the TS and DHFR domains, and between the two halves of the homodimeric enzyme. The mutants were however, found to be resistant to inhibition by small molecules predicted to bind in a pocket near the cross-over helix; these data are presented and discussed in Part B of Chapter 5.

Reproduced with permission of the copyright owner. Further reproduction prohibited without permission.

Fig. 4.9 *C. hominis* cross-over helix-DHFR domain salt-bridge interactions. The *C. hominis* cross-over helix, *A*. Hydrogen bonding interactions between Glu 205 and Lys 38, *B*, and between Arg 210 and Glu 31, *C*. Close-up of the hydrogen bonding interactions between Arg 210 and Glu 31 (violet), Cys 164 (blue), and Glu 276 (red), *D*. None of these bonds are present in the R210M mutant.

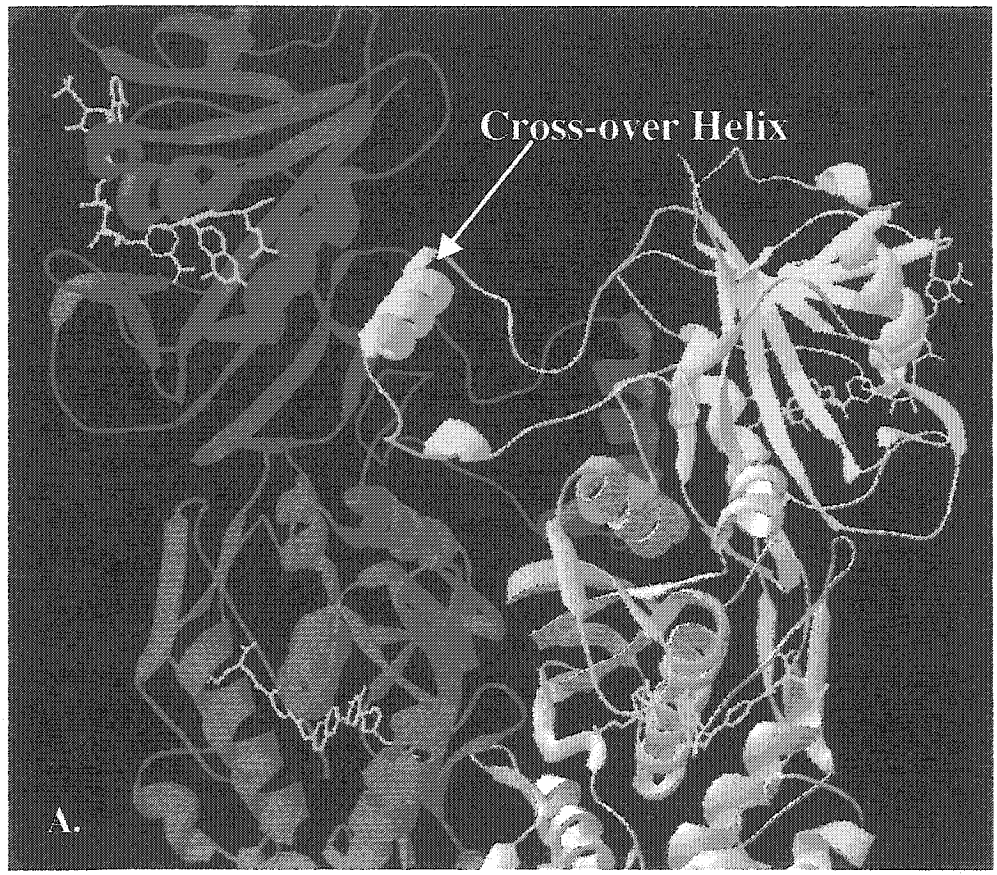

Reproduced with permission of the copyright owner. Further reproduction prohibited without permission.

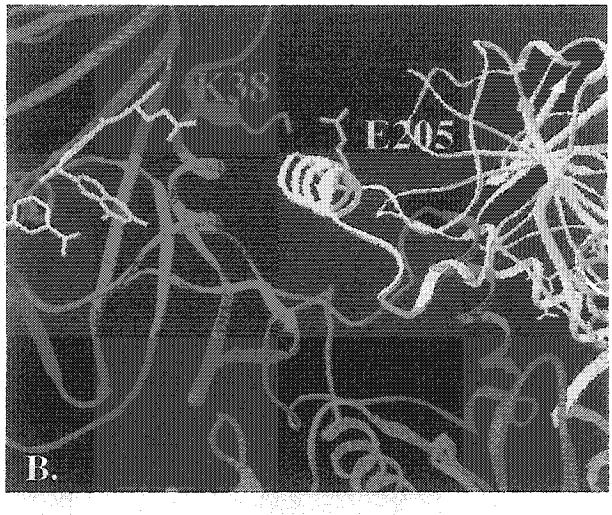

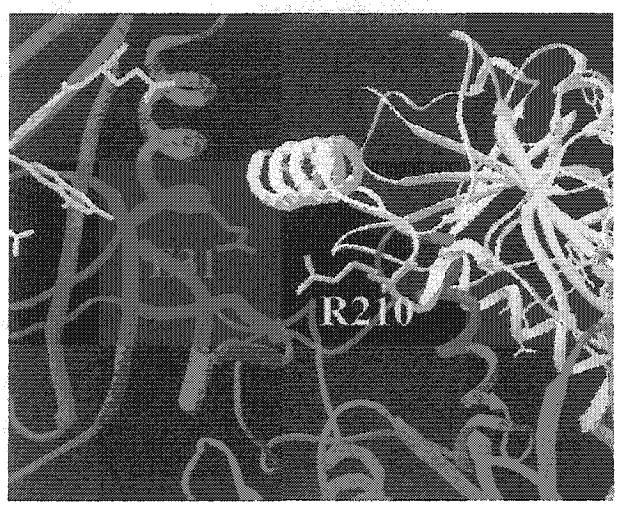

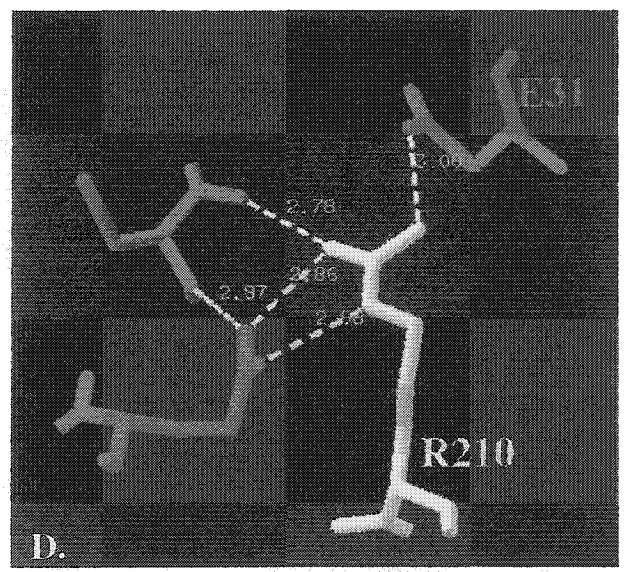

Reproduced with permission of the copyright owner. Further reproduction prohibited without permission.

Chapter Five

Use of Molecular Docking to Identify Non-Active Site Inhibitors of TS-DHFR

Reproduced with permission of the copyright owner. Further reproduction prohibited without permission.

Part A. Molecular Docking into the Putative Channel Region of L. major TS-DHFR

INTRODUCTION

In an effort to discover an inhibitor that would bind in the unique shallow groove region of the *L. major* bifunctional TS-DHFR enzyme, we turned to molecular docking screens of the Available Chemicals Directory (ACD) database. Such a strategy has been previously used to discover novel inhibitors of monofunctional TS, where a competitive inhibitor found by screening with the program NWU DOCK [79, 108, 109] was used as a novel scaffold compound for in-parallel, solid-phase synthetic elaboration, generating an analog with a K_i of 1.3 μM [110]. In addition, a preliminary DOCK screen produced a 900 μM non-competitive TS active-site inhibitor; a subsequent similarity search yielded derivatives with K_i values of less than 10 μM [111]. More broadly, both monofunctional TS and DHFR enzymes have been the foci of intense structure-based design efforts and are considered model enzymes for such projects [112-114, 140].

An unusual aspect of this project was the targeting of sites in the bifunctional TS-DHFR enzyme located in regions remote from the active sites. Enzyme active sites have traditionally served as the basis of structure-based drug discovery because they represent well defined and highly functionalized targets. By contrast, the shallow groove connecting the TS and DHFR active sites in bifunctional enzymes presents a particular challenge to structure-based efforts, including molecular docking. Successful targeting of the shallow groove region connecting the two active sites and forming the putative

Reproduced with permission of the copyright owner. Further reproduction prohibited without permission.

channel could produce novel and more specific therapies for protozoal diseases including toxoplasmosis and drug-resistant malaria.

Several docking searches were performed against subregions of a surface area of ~20 x 25 Å thought to define the central region of the electrostatic channel in *L. major* TS-DHFR (Fig. 5.0 A). This area includes the basic residues Lys 66, 67, 72, 73, 282 and Arg 64, 283, and 287, originally believed to be involved in shuttling the intermediate substrate, H_2folate, between the two catalytic sites [6]. Four subregions of the putative channel were screened against the 152,571 compounds in the 1995.2 version of the ACD of commercially available chemicals. From these screens, 14 compounds were purchased for testing as inhibitors of TS-DHFR (Table 5.0).

We report here that eosin B, predicted by DOCK to bind in the shallow groove region of the putative channel, including Arg 283 in the TS domain and Glu 151 in the DHFR domain (Fig. 5.0 B), inhibits the bifunctional enzyme. Eosin B (4',5'-dibromo-2',7'-dinitrofluorescein) is a halogenated xanthene dye (see Fig. 5.0 A and Table 5.0) whose spectrophotometric properties have been exploited to measure the protein concentration at low pH (1-3) [115]. Whereas related halogenated fluorescein derivatives are thought to be nonspecific inhibitors of several enzymes, acting through an aggregation-based mechanism, extensive kinetic characterization suggests that eosin B is inhibiting the bifunctional enzyme specifically [116].

The effects of eosin B on *L. major*, *T. gondii*, and *P. falciparum* parasite replication in cell culture were then evaluated. Eosin B was found to have significant activity against the apicomplexan protozoa, *T. gondii* and *P. falciparum*. This research also led to the surprising discovery of a folate transporter in *T. gondii* parasites.

Reproduced with permission of the copyright owner. Further reproduction prohibited without permission.

Fig. 5.0. Binding site of eosin B as predicted by DOCK. Target areas for DOCK searches in the putative electrostatic channel region of *L. major* TS-DHFR with eosin B bound (*A*). The shallow groove with the eosin B ligand shown in its best-docked orientation with carbon atoms in green (structure inset). The DHFR- and TS-binding sites are labeled, and the crystallographic ligands are displayed with carbon colored cyan. Stereo pair of the orientation of eosin B in the *L. major* TS-DHFR crystal structure as predicted by DOCK (*B*). Close polar contacts are indicated with dotted lines and the distance shown in Angstroms. Key residues are labeled: Arg 283, Glu 151, and the backbone carbonyl of Val 278 make close polar contacts with the ligand. Trp 286, Tyr 508, and Val 278 form a hydrophobic pocket for the phenyl moiety of eosin B.

Reproduced with permission of the copyright owner. Further reproduction prohibited without permission.

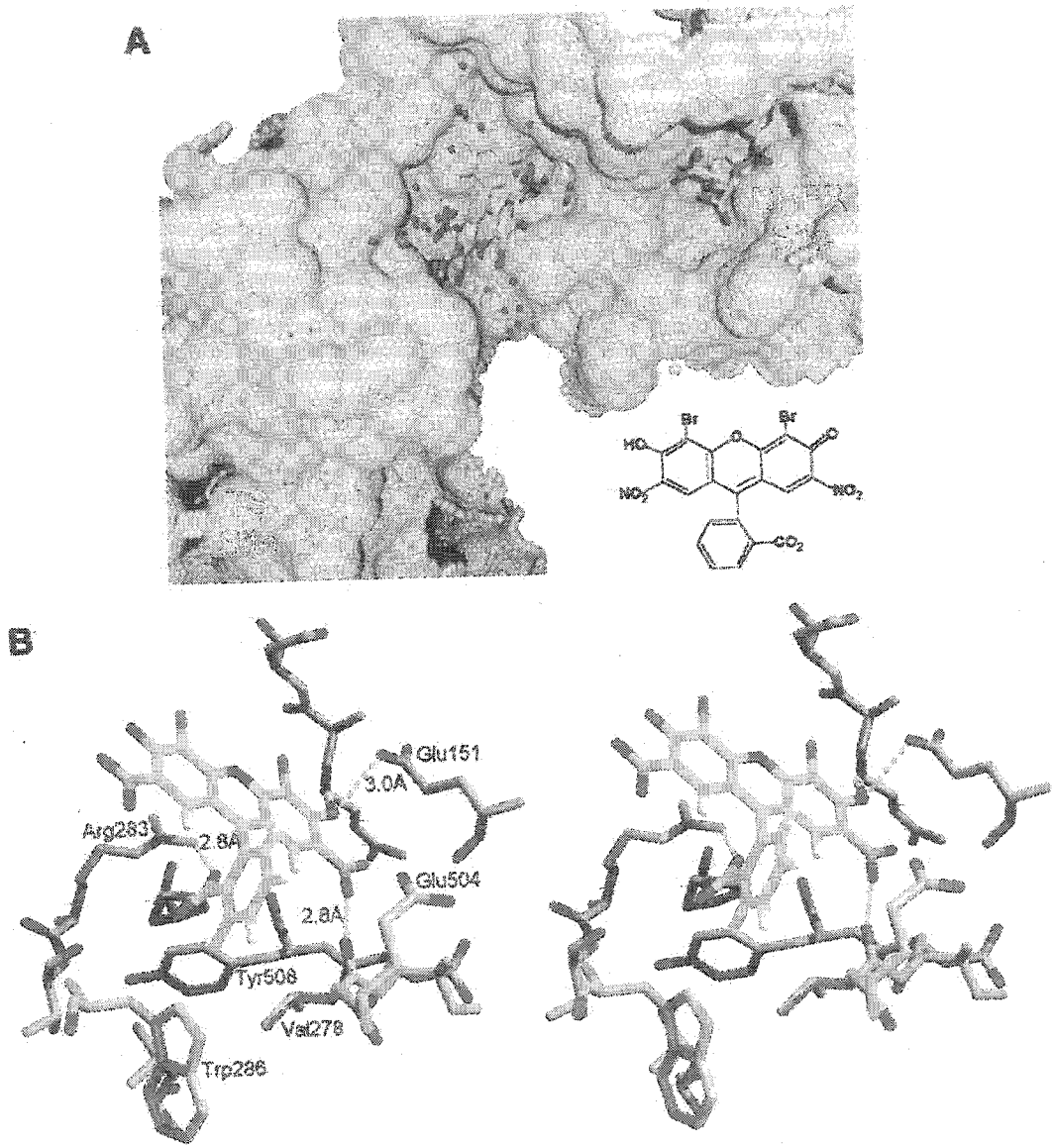

Reproduced with permission of the copyright owner. Further reproduction prohibited without permission.

Table 5.0. Dock hits tested

The 14 DOCK hits tested, along with the ACD code, two-dimensional structure, and DOCK energy score of each. All inhibitors were tested by rapid chemical quench at a concentration of 1 mM; 50 μM *L. major* TS-DHFR using the same set of reaction conditions as detailed for eosin B. An "*" indicates that upon initial characterization, inhibition was observed at a drug concentration of 1 mM, as compared with a DMSO control. One compound, 2,5,7-trinitro-9-oxo-9H-fluorene-4-carboxylic acid, elicited complex kinetic behavior, appearing to inhibit in a time-dependent and NADPH-dependent manner.

Reproduced with permission of the copyright owner. Further reproduction prohibited without permission.

Table 5.0

Compound Name/ Chemical Formula/ ACD Code	Structure	DOCK Score (kcal/mol)
Methyl 2-[(3,3-dimethyl-2-oxobutyl)thio]-6-methyl-5,5-dioxo-5,6-dihydro-5-lambda-6-benzo[C]pyrimido[4,5-E][1,2]thiazine-8-carboxylate $C_{19}H_{21}N_3O_5S_2$ MFCD00098670	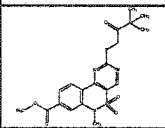	-17.1
2,5,7-trinitro-9-oxo-9H-fluorene-4-carboxylic acid $C_{14}H_5N_3O_9$ MFCD00180008	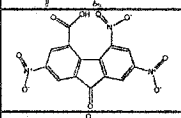	-14.7 (*)
N-(4-Nitrophenylsulfonyl)-L-phenylalanine $C_{15}H_{14}N_2O_6S$ MFCD00191470	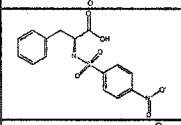	-15.7
METHYL 7-FLUORO-2-(METHOXYMETHYL)-5-OXO-5H-CHROMENO[2,3-B]PYRIDINE-3-CARBOXYLATE $C_{16}H_{12}FNO_5$ MFCD00139064	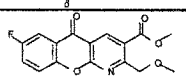	-16.1
5-ISATINSULFONIC ACID, SODIUM SALT HYDRATE $C_8H_4NO_5S \cdot Na \cdot H_2O$ MFCD00192236	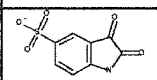	-13.1
2,2-dimethyl-4-oxo-7-[(phenylsulfonyl)oxy]-3,4-dihydro-2H-chromen-5-yl-benzene-1-sulfonate $C_{23}H_{20}O_8S_2$ MFCD00205533	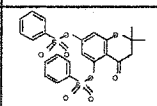	-18.7
4-hydroxy-3,5-dinitrobenzoic acid $C_7H_4N_2O_7$ MFCD00017000	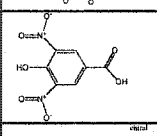	-13.7
N-O-NPS-glutamine $C_{11}H_{13}N_3O_5S$ MFCD00038157	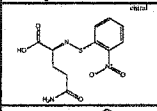	-15.3
3-amino-3-(2-nitrophenyl)propionic acid $C_9H_{10}N_2O_4$ MFCD00090356	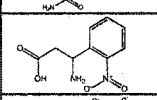	-17.3
2-([4-[(4-bromophenyl)thio]-3-nitrobenzyl]amino)propanoic acid $C_{16}H_{15}BrN_2O_4S$ MFCD00205447	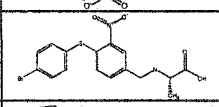	-17.4
N3-{4-chloro-2-[(2-phenylhydrazino)carbonyl]phenyl}-2 phenoxynicotinamide $C_{25}H_{19}ClN_4O_3$ MFCD00206034	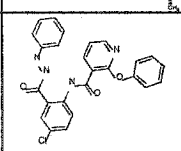	-24.8
2-(methoxycarbonyl)benzo[b]thiophen-3-yl-2-phenoxynicotinate $C_{22}H_{15}NO_5S$ MFCD00116956	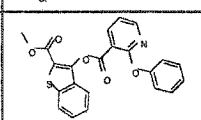	-19.6
5-benzyloxy-DL-tryptophan $C_{18}H_{18}N_2O_3$ MFCD00037968	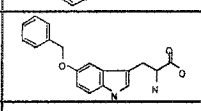	-12.2
Eosin B $C_{20}H_6Br_2N_2O_9 \cdot 2Na$ MFCD00005041	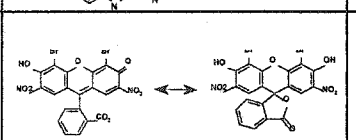	-14.2 *

Reproduced with permission of the copyright owner. Further reproduction prohibited without permission.

RESULTS

Molecular Docking Against *L. major* TS-DHFR[6]

The program NWU-DOCK DOCK [79, 108, 109], a derivative of DOCK 3.5 [81, 87] was used to screen 152,571 compounds of the ACD 1995.2 database for molecules complementary to the shallow groove, putative channeling region of protozoal TS-DHFR. To prepare the site for docking, all water and ion molecules were removed. Protonation of receptor residues and water molecules was done with Sybyl (Tripos, St. Louis, MO). Positions of some protons were then rotated manually to more appropriate orientations using MidasPlus [88]. The sphere set used contained 57 spheres and was obtained from reclustering spheres obtained from the sphgen program, part of the DOCK 3.5 package [82]. Force field and electrostatic grids were calculated with CHEMGRID [81] and DelPhi [85], respectively. DISTMAP was used to calculate the excluded volume grid [117].

On average, 3000 orientations and up to 2000 conformations were calculated in the site for each data base molecule. Molecules were scored and ranked based on their van der Waals and electrostatic complementarity to the putative channeling region, and corrected for polar and non-polar desolvation effects [108]. The docking calculation took 23 h on an Intel Pentium III 450 MHz CPU. Four hundred high scoring compounds were visually evaluated in the site in their docked conformations. Based on observed complementarity, and with an eye for testing different scaffolds, 14 compounds were ultimately ordered and tested for inhibition of TS-DHFR (Table 5.0). Of these, one (eosin B) showed significant enzyme inhibition when tested at micromolar concentrations.

---

[6] Molecular docking was performed by John J. Irwin and Brian K. Shoichet, now at UCSF. Figure 5.0 was created by John Irwin.

Reproduced with permission of the copyright owner. Further reproduction prohibited without permission.

Steady-state Quench Experiments to Determine IC_{50} of Inhibitor

A preliminary steady-state screening of DOCK hits indicated that eosin B inhibits the bifunctional TS-DHFR reaction, in which CH_2H_4folate is converted to H_4folate. Steady-state time courses for the reaction of 0.1 μM *L. major* TS-DHFR with 200 μM CH_2H_4folate in the presence of 0, 62, 125, or 250 μM eosin B revealed an IC_{50} of 100 μM (Fig. 5.1A). To evaluate whether the inhibitory activity of eosin B would translate to other bifunctional TS-DHFR enzymes, activity against the apicomplexa parasites, *T. gondii*, *P. falciparum*, and *C. hominis* was examined. Steady-state time courses for the reaction of 1.5 μM *T. gondii* TS-DHFR with 500 μM CH_2H_4folate in the presence of varying concentrations of eosin B yielded an IC_{50} of 180 μM (Fig. 5.1B). Steady-state time-courses for the reaction of 0.1 μM *P. falciparum* or *C. hominis* TS-DHFR with 200 μM CH_2H_4folate in the presence of 0 μM, 125 μM, 250 μM, or 375 μM, 500 μM, 1 mM, or 2 mM eosin B revealed IC_{50} values of 380 μM and 620 μM, respectively (Fig. 5.1D and F; Table 5.1).

In each case, steady-state inhibition by eosin B is saturable; at high eosin B concentrations complete inhibition is achieved. In steady-state experiments where either 0.1 or 1 μM *L. major* TS-DHFR was reacted with 100 μM CH_2H_4folate in the presence or absence of 125 μM eosin B, ~50% inhibition was observed at both enzyme concentrations (data not shown). These findings indicate that the enzyme inhibition is not dependent on enzyme concentration.

Reproduced with permission of the copyright owner. Further reproduction prohibited without permission.

Fig. 5.1. Eosin B dose response. *A*, steady-state time courses were completed in the presence of 0.1 μM *L. major* TS-DHFR, 200 μM CH_2H_4folate, and 0 μM (DMSO control), 62.5 μM, 125 μM, or 250 μM eosin B. An IC_{50} value of 100 μM was obtained by plotting the rates of the steady-state reactions versus eosin B concentration. *B*, steady-state time courses with 1.5 μM *T. gondii* TS-DHFR, 500 μM CH_2H_4folate, and varying concentrations of eosin B yielded an IC_{50} of 180 μM. *C*, in cell culture assays, an eosin B concentration of 180 μM also reduced *T. gondii* replication inside host cells by 50%, as expressed by counts/min of radiolabel incorporated into parasites. *D*, steady-state time courses for the reaction of 0.1 μM *P. falciparum* TS-DHFR, 200 μM CH_2H_4folate, and varying concentrations of eosin B yielded an IC_{50} of 380 μM. *E*, in cell culture assays measuring incorporation of [^{3}H] hypoxanthine, eosin B inhibited *P. falciparum* growth with an IC_{50} of 200 nM. *F*, steady-state time courses for the reaction of 0.1 μM *C. hominis* TS-DHFR, 200 μM CH_2H_4folate, and varying concentrations of eosin B yielded an IC_{50} of 620 μM.

Table 5.1. Summary of IC_{50} data presented in Fig. 5.1

	IC_{50}	
Parasite	**Steady-State**	**Cell Culture**
L. major	100 μM	5 mM
T. gondii	180 μM	180 μM
P. falciparum	380 μM	200 nM
C. hominis	620 μM	ND

Reproduced with permission of the copyright owner. Further reproduction prohibited without permission.

Fig. 5.1

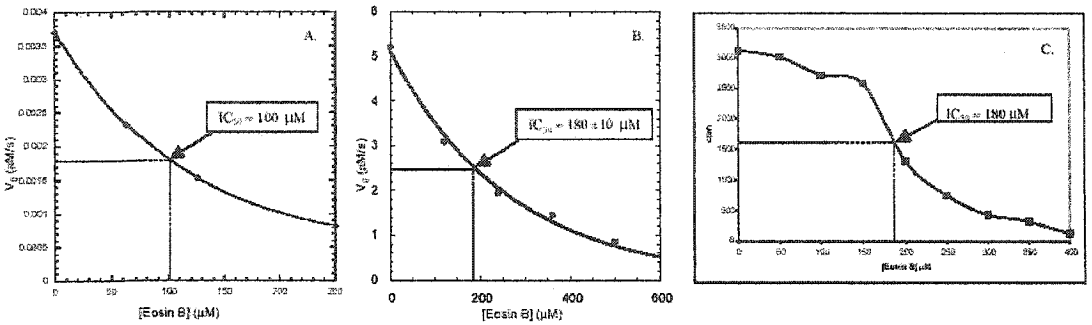

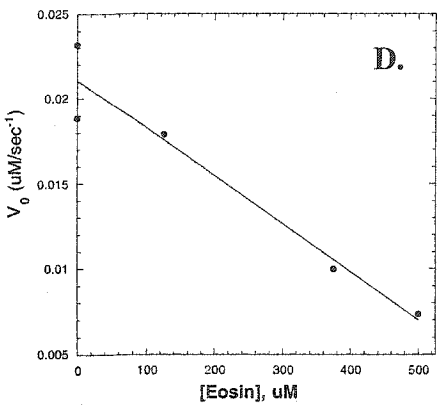

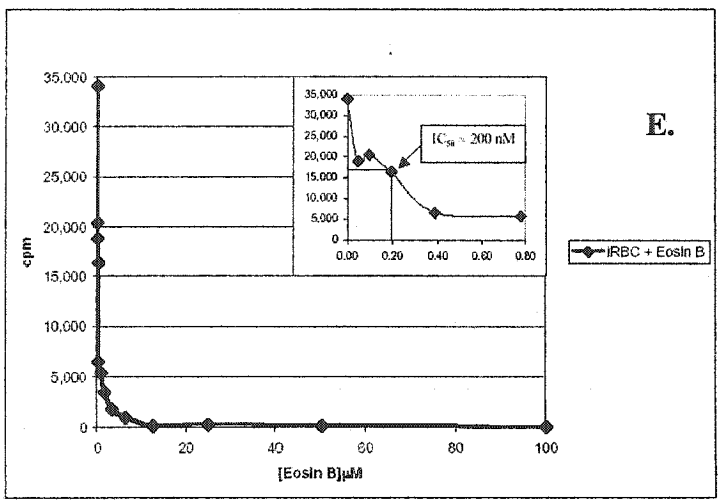

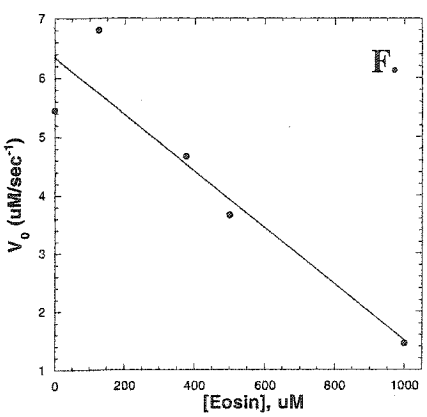

Reproduced with permission of the copyright owner. Further reproduction prohibited without permission.

Transient Kinetic Analysis

Single enzyme turnover experiments, which measure the rate of the chemical conversion of substrate to product at the active site under conditions where enzyme concentration is sufficiently high that substrate binding is not rate-limiting, were performed using a rapid chemical quench apparatus. For each single enzyme turnover experiment, full time courses for *L. major* in the presence and absence of 1 mM eosin B were completed in duplicate, along with t = 0 and t = 60 s controls. Because eosin B was dissolved in dimethyl sulfoxide, an equivalent amount of DMSO (4% of final volume) was added to control reactions. This concentration of DMSO has no effect on the single-turnover reaction rates (data not shown).

To monitor the DHFR reaction, the bifunctional TS-DHFR enzyme (50 μM) was preincubated with a saturating concentration of NADPH (500 μM) and then mixed with a limiting amount of radiolabeled H_2folate (14 or 15 μM). To monitor the TS reaction, the bifunctional TS-DHFR enzyme (50 μM) was preincubated with a saturating concentration of dUMP (500 μM) and then mixed with a limiting amount of radiolabeled CH_2H_4folate (10 or 12.5 μM). The bifunctional TS-DHFR single enzyme turnover experiment was set up similar to that for TS, except that saturating NADPH (500 μM) was added as well as dUMP. All reported concentrations are final, after mixing.

Eosin B was found to inhibit both the TS and DHFR reactions, but TS was inhibited more strongly (Table 5.2). As predicted, the inhibition of the bifunctional reaction by eosin B is equivalent to inhibition of TS alone because the rate of product formation by TS is significantly slower than that of DHFR in *L. major*. The data are presented in Table 5.2 as the percent of activity remaining; the ratio of the rate constant

Reproduced with permission of the copyright owner. Further reproduction prohibited without permission.

obtained in the presence of 1 mM eosin B divided by that with DMSO alone. In experiments examining the bifunctional TS-DHFR reaction, no H_2folate accumulation above background was observed.

To address the question of whether the inhibition observed in the single enzyme turnover experiments described above was because of competition with substrates at the active site, the effects of varying the substrate concentration were examined. Due to the predicted binding to R283 near the TS folate binding domain, we were most concerned that eosin B may be competing with folate substrates. When either 3 or 62 μM CH_2H_4folate was reacted with 250 μM *L. major* TS-DHFR in the presence of 1 mM eosin B, 33-40% activity remained. In the case of the DHFR reaction, equivalent reaction rates were obtained when 4 or 40 μM H_2folate was reacted with 100 μM *L. major* TS-DHFR in the presence of 1 mM eosin B. The fact that a 20-fold change in CH_2H_4folate concentration and a 10-fold change in H_2folate concentration had no effect on the level of inhibition by eosin B at enzyme concentrations where binding of substrate is not rate-limiting, implies that eosin B binds outside of both the TS and DHFR folate binding pockets.

Species Variations in Inhibition by Eosin B

Because one long-term goal of this research is to develop a therapy specific for protozoal bifunctional TS-DHFR, eosin B was tested against TS-DHFR from the evolutionarily divergent but clinically relevant apicomplexan protozoa, *T. gondii*, *P. falciparum*, and *C. hominis*, and against human and *E. coli* monofunctional TS and DHFR for comparison. Steady-state TS-DHFR time courses detailed above, for the

Reproduced with permission of the copyright owner. Further reproduction prohibited without permission.

Table 5.2. Species dependence of eosin B inhibition on the TS-DHFR, TS, and DHFR reactions, and effects of eosin B on two *L. major* mutants. Data are reported as percent activity remaining: rate of the reaction in the presence of 1 mM eosin B divided by the rate with DMSO alone. All values where an error margin is included represent the average results from 2 to 3 paired time courses. In ΔTS, the *L. major* TS domain has been deleted (DHFR only). NA= Not applicable; NE= Not evaluated.

Species/Enzyme	TS-DHFR	TS	DHFR
L. major	24 ±3 %	23±3 %	35±0 %
T. gondii	19 %	NE	28±8 %
E. coli	NA	37±0 %	91±0%
Human	NA	18±0%	12±4 %
***L.Major* Mutants**			
R283E	80%	NE	30%
ΔTS	NA	NA	16%

Reproduced with permission of the copyright owner. Further reproduction prohibited without permission.

reaction of *P. falciparum* or *C. hominis* with eosin B revealed IC_{50} values of 380 μM and 620 μM, respectively (Table 5.1). In a steady-state DHFR reaction (1.5 μM enzyme; 500 μM H_2folate) *C. hominis* was found to have 60% of DHFR activity in the presence of 500 μM eosin B, compared to an equivalent volume of DMSO alone.

Single turnover experiments were set up as detailed above for *L. major* (50 μM enzyme, 1 mM eosin B or 4% DMSO, 500 μM dUMP and/or NADPH, with ~10 μM radiolabeled CH_2H_4folate or H_2folate). The bifunctional TS-DHFR as well as the individual TS and DHFR reactions of *L. major* and *T. gondii* were similarly inhibited by addition of 1 mM eosin B (Table 5.2).

The *E. coli* TS reaction was slightly less inhibited than that of *L. major*. The striking finding was, however, that whereas ~35% DHFR activity remains with both bifunctional enzymes in the presence of 1 mM eosin B, *E. coli* DHFR is almost entirely unaffected by 1 mM eosin B (91% activity remaining; Table 5.2). Whereas the TS enzyme is highly conserved across species (Arg 283 is homologous to Arg 372 in *T. gondii* and Lys 285 in *C. hominis*), the relatively low sequence conservation in DHFR makes sequence alignments inconclusive. Structural alignment of *L. major* with a homology model of *T. gondii* TS-DHFR, however, reveals a similar overall structure in the region of Glu 151, with *T. gondii* residue Glu 177 located very near to and in the same orientation as Glu 151 (coordinates of nearly complete crystal structure kindly provided by Dr. Amy C. Anderson, Dartmouth College). By contrast, an examination of the aligned crystal structures reveals that the loop structure of *E. coli* in the vicinity of Glu 151 is significantly different from that in *L. major*, and the closest acidic residue,

Reproduced with permission of the copyright owner. Further reproduction prohibited without permission.

Asp 90, is oriented in a different direction from Glu 151. Glu 151 is also perpendicular to the nearest acidic residue in *C. hominis*, Glu 139.

Effects of Eosin B on the *L. major* R283E and E151Q Mutants

Because eosin B was predicted by the docking program to interact with Arg 283 (R283) in the TS domain of *L. major* TS-DHFR (see Fig. 5.0B), eosin B was tested against the charge reversal mutant, R283E. Whereas mutation of Arg 283 alone produced an enzyme with only 40% of wild-type TS-DHFR activity, addition of 1 mM eosin B only inhibited the mutant enzyme slightly such that >80% activity remains. This sharply contrasts to what was seen with the wild-type enzyme where, under the same reaction conditions, 1 mM eosin B strongly inhibits the wild-type enzyme, such that ~20% activity remains (Fig. 5.2A). Furthermore, the Arg 283→ Glu substitution had very little effect on the ability of eosin to inhibit the DHFR reaction, consistent with the docking prediction (Fig. 5.2B). Effects of eosin B on the *L. major* R283E mutant are summarized in Table 5.2.

DOCK also predicts that Glu 151 in the *L. major* DHFR domain participates in an electrostatic interaction with eosin B. Another docking program, GLIDE, predicts that eosin B interacts with the Glu 151 backbone (Marina Udier Blaglovic, personal communication). An E151Q charge neutralization mutant was created to test these predictions. Cindy Doan in our lab evaluated this mutant and found that it has similar TS-DHFR activity to wild-type *L. major*, and inhibition by eosin B is uncompromised, suggesting a backbone interaction.

Reproduced with permission of the copyright owner. Further reproduction prohibited without permission.

Comparative Enzyme Inhibition by Eosin Analogs

To evaluate the contributions of structural components of eosin B to its inhibitory properties, eosin B was compared with 3 analogs: fluorescein, phenolphthalein, and a tetra-bromo derivative of eosin B (Fig. 5.3). Fluorescein, the unliganded precursor to eosin B lacking the halogen and nitro groups, was found to be ~8-fold less potent than eosin B itself. At a concentration of 1 mM eosin B, the rate of the TS-DHFR reaction was only 25% that in the absence of inhibitor. In contrast, at 1 mM fluorescein no inhibition was observed, and at 4 mM, a rate that was 50% of the TS-DHFR reaction rate with no inhibitor added could be achieved (Fig. 5.4).

Phenolphthalein, which also resembles the cyclic form of eosin B in that it contains phenolic and benzoic acid moieties (Fig. 5.3), has been reported to be a 5 μM TS monofunctional enzyme inhibitor. Structural studies have shown by X-ray crystallography that it binds at the *Lactobacillus casei* TS active site in a region close to but not overlapping with folate binding [111]. It is important to note, however, that the docking predictions were made with the open tautomer of eosin B and this is also the form favored by our experimental conditions, near neutral pH [115].

If phenolphthalein is binding at a different site than eosin B, it would not make contact with the conserved Arg residue, so we predicted that it should be just as effective at inhibiting the R283E mutant as the wild-type enzyme. Indeed, unlike eosin B in which sensitivity to inhibition was lost by the R283E mutation, phenolphthalein inhibited this mutant to the same degree as the wild-type enzyme: only 30% of TS-DHFR activity remained when 40 μM phenolphthalein was added to 33 μM R283E (data not shown). No inhibition of DHFR activity was observed under similar conditions.

Reproduced with permission of the copyright owner. Further reproduction prohibited without permission.

Fig. 5.2. Effects of eosin B on the *L. major* R283E mutant TS-DHFR and DHFR reactions. In the absence of eosin B, R283E has 40% wild-type TS-DHFR activity. The rate of the R283E TS-DHFR reaction is virtually unchanged in the presence of 1 mM eosin B, whereas 1 mM eosin B significantly inhibits the wild-type TS-DHFR reaction (*A*). The R283E DHFR reaction rate is equivalent to that of the wild-type enzyme; 1 mM eosin B reduces the rate of both the R283E and wild-type *L. major* DHFR reactions by ~70% (*B*). All reaction time courses were followed to 60 s, but only early time points are plotted for visual clarity.

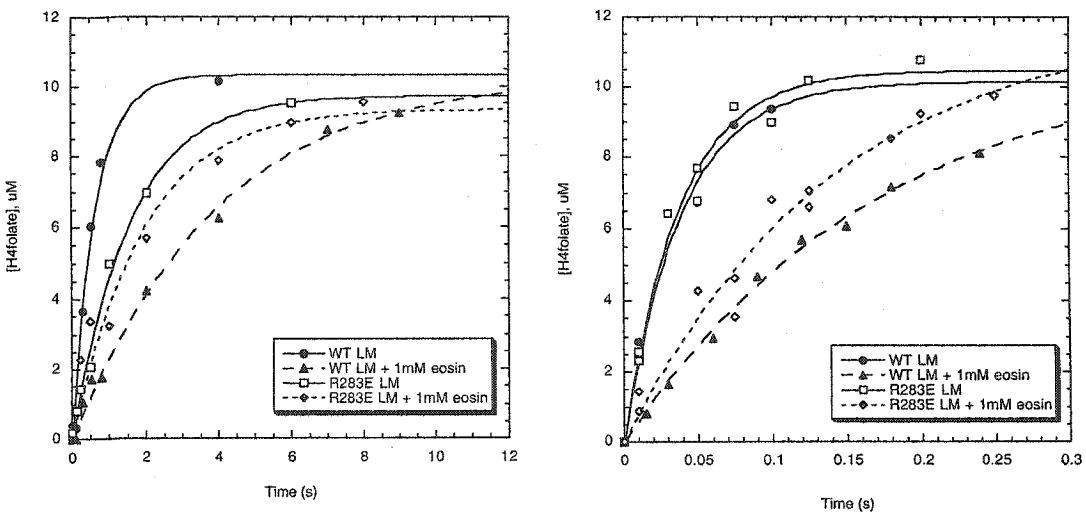

Reproduced with permission of the copyright owner. Further reproduction prohibited without permission.

Fig 5.3. Structures of eosin B tautomers and derivatives. *A*, tautomeric forms of eosin B; *B*, fluorescein; *C*, phenolphthalein; *D*, tetra-bromo derivative of eosin B.

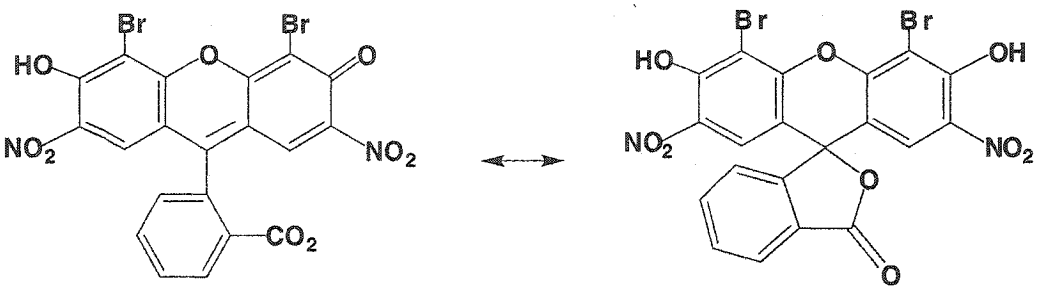

A.

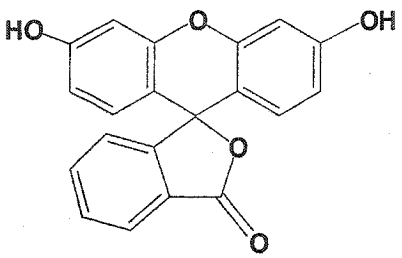

B.

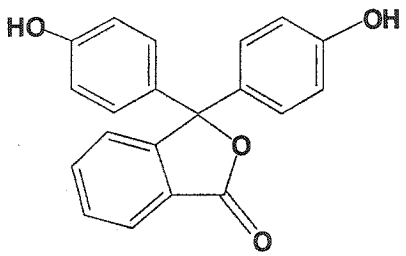

C.

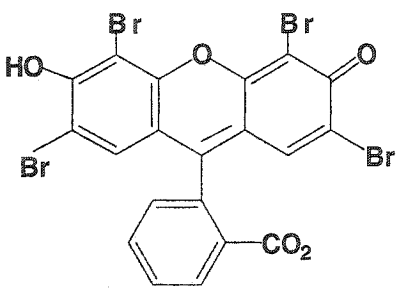

D.

Reproduced with permission of the copyright owner. Further reproduction prohibited without permission.

Fig. 5.4. ***L. major*** **TS-DHFR inhibition by 1 or 4 mM fluorescein as compared with 1 mM eosin B.** 4 mM fluorescein inhibits wild-type *L. major* approximately half as well as 1 mM eosin B; no inhibition was observed with 1 mM fluorescein.

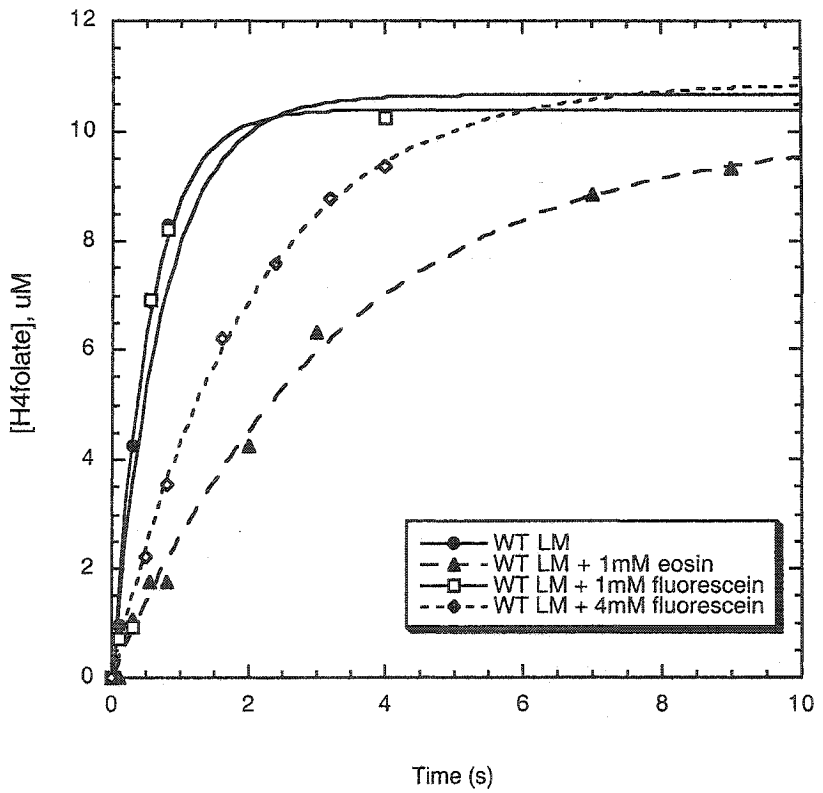

Reproduced with permission of the copyright owner. Further reproduction prohibited without permission.

The tetra-bromo derivative of eosin B, where the nitro-groups were replaced by bromines, was predicted to be a better inhibitor because the bromo-groups are smaller and expected to have more favorable interactions with the greasy pocket. The tetra-bromo derivative of eosin B was found to be an approximately 2-fold better inhibitor of *L. major* and *T. gondii* TS-DHFR than eosin B in single enzyme turnover experiments. In steady-state experiments where either 0.1 μM or 1 μM *L. major* TS-DHFR was reacted with 100 μM CH_2H_4folate in the presence or absence of 62.5 μM of the tetra-bromo derivative, approximately 40% inhibition was observed at both enzyme concentrations.

The tetra-bromo eosin $IC_{50}$with *C. hominis* TS-DHFR was determined in steady-state spectroscopic experiments with 240 μM NADPH and dUMP, 160 μM CH_2H_4folate, and 3 concentrations of *C. hominis* TS-DHFR: 3.1 μM, 310 nM, and 62 nM. Rates in the absence of inhibitor were proportional to enzyme concentration, but tetra- bromo eosin IC_{50} values were found to be dependent on enzyme concentration. The IC_{50} of tetra-bromo eosin was 180 μM with 3.1 μM *C. hominis* TS-DHFR; 17 μM with 310 nM enzyme; and approximately 1 μM with 62 nM enzyme (20% of activity remains in the presence of 1.6 μM tetra-bromo eosin). The fact that inhibition is dependent on *C. hominis* enzyme concentration suggests that it is not specific and may be at least partially due to aggregate-formation [116].

Parasitology: Effects of Eosin in Cell Culture[7]

The next logical step was to test whether eosin B could affect parasite replication in cell culture. Three parasites were tested: *L. major*, *P. falciparum* and *T. gondii*. Eosin

[7] Testing of eosin B in *T. gondii* and *P. falciparum* parasite cell culture was performed by Dr. I. Coppens and K. Massimine, respectively, then both in Dr. K. A. Joiner's lab at Yale University. Figures 5.5, 5.6, 5.7, and 5.8 were created by I. C. and K. M.

Reproduced with permission of the copyright owner. Further reproduction prohibited without permission.

B was found to be a weak (5 mM IC_{50}) inhibitor in *L. major* parasites (Valeska Stempliuk and Dr. Stephen Beverley, Washington University; data not shown). The sensitivity of eosin B was more significant on the apicomplexan parasites, *P. falciparum* and *T. gondii*.

Wild-type *P. falciparum* growth in cell culture was assessed by measuring the incorporation of [^{3}H] hypoxanthine into growing ring-stage parasites. It was observed that the amount of [^{3}H] hypoxanthine taken up decreased with increasing eosin B concentration, indicating a clear decrease in malarial DNA synthesis leading to parasite death. Death was attributable to drug pressure since 1) smear analysis demonstrated that eosin B does not alter red blood cell morphology and 2) DMSO concentrations used to dissolve the eosin B did not have an inhibitory effect on parasite growth. Remarkably, eosin B was found to inhibit erythrocytic *P. falciparum* growth with an IC_{50} value of 200 nM (Fig. 5.1E; Table 5.1). Preliminary data suggests that eosin B is also active against an anti-folate resistant *P. falciparum* strain (HB3).

Both *P. falciparum* and *T. gondii* parasites multiply in a parasitophorous vacuole, whose membrane contains proteinaceous pores [118, 119] that allow the passive bidirectional diffusion of small molecules <1,300- 1,400, in accord with the molecular weight of eosin B (624 g/mole). Eosin's hydrophobicity (Log*P* = 6.476), also suggests that the neutral form of the drug likely gains initial access to host cells through simple membrane diffusion. It was seen that an eosin B concentration of 180 μM reduces *T. gondii* replication inside host cells by 50%, as measured by [^{3}H]uracil incorporation (Fig. 5.1C); matching the IC_{50} value obtained in steady-state biochemical assays (Fig. 5.1B; Table 5.1). This is notable because parasite host cells were unaffected up to a drug concentration of 400 μM as assayed by [^{3}H]thymidine incorporation.

Reproduced with permission of the copyright owner. Further reproduction prohibited without permission.

Leucovorin (folinic acid) was added in an attempt to selectively "rescue" host cells exposed to eosin B. Surprisingly, inhibition of parasite replication was also compromised in the presence of leucovorin (Fig 5.8). The finding that 10 μM leucovorin reverses the inhibition of replication induced by low doses of eosin B provides strong evidence that TS-DHFR is the target of eosin in *T. gondii*, and is also the first indication for a folate transporter in *T. gondii*, discussed in the next section.

Thymidine rescue was not attempted to further establish that TS-DHFR is the target of eosin B in parasites. It is well established that *P. falciparum* lacks the machinery for pyrimidine nucleoside salvage [141], and therefore addition of thymidine does not reverse the effects of known TS inhibitors [142]. In the case of *T. gondii*, recent research suggests the existence of a high affinity, nonspecific nucleoside transporter [143], but thymidine uptake was not detected in subsequent studies using intracellular *T. gondii* parasites [144].

Eosin B localization was visualized by exploiting the auto-fluorescence properties of the dye in fluorescence microscopy studies. Eosin B initially accumulates within the nucleus and mitochondria of uninfected mammalian cells (Fig. 5.5 A, panels a-b). After 20 min exposure, eosin B is mainly sequestered within host cytoplasmic vesicles, identified as lysosomes by chloroquine treatment (Fig. 5.5 A, panels c-d). The time required for trapping within lysosomes may account for an observed delay of eosin B delivery to the parasites.

By 30 min incubation of *T. gondii* infected host cells with eosin B, drug accumulation is found exclusively in the vacuolar space (Fig. 5.5 B, panel a). After 2 h incubation, parasites became accessible to eosin B (Fig. 5.5 B, panel d). The kinetics of eosin B (320 nM) delivery to *T. gondii* over a period of 4 h was further evaluated by fluorimetry (Fig. 5.5

Reproduced with permission of the copyright owner. Further reproduction prohibited without permission.

C). The time course of drug accessibility was confirmed to be biphasic: a very limited amount of eosin B accumulation within parasites is detectable in first the 90 min, after which time the drug gains accessibility to the parasites.

The eosin B distribution within extracellular *T. gondii* parasites was also analyzed. After 1 h incubation, the eosin B staining was primarily in the perinuclear region (Fig. 5.6 a), as indicated by a partial co-localization with the nuclear dye, Hoechst (Fig. 5.6 b-c). Eosin B staining was also comparable to the nuclear pattern of TS-DHFR, revealed by specific antibodies in either immunofluorescence (Fig. 5.6 d) or immunogold EM (Fig. 5.6 e) studies[8]. Co-localization of the site of eosin B accumulation and *T. gondii* TS-DHFR cannot, however, be used as evidence that this enzyme is the drug target.

The long-term cytopathic effects of eosin B on *T. gondii* were examined at the ultrastructural level (Fig. 5.7). Electron microscopy studies revealed that treatment with 180 μM eosin B induces rupture of the *T. gondii* plasma membrane (Fig. 5.7 a) leading to a leakage of the cytosolic contents of the parasite into the vacuolar space after 24 h (Fig. 5.7 b). The cytoplasm of parasites contains autophagic vacuoles and an unusual abundance of large vacuoles of unidentified nature (Fig. 5.7 a). In addition, both the endoplasmic reticulum (Fig. 5.7 b) and the mitochondria are dilated. The spherical contour of mitochondria and the dilatation of their inner cristae suggest a loss of osmoregulatory properties (Fig. 5.7 a-b). Parasite cytopathic alterations were enhanced after 48 h of eosin B incubation (Fig. 5.7 c). Importantly, host mammalian organelles demonstrated no perceptible morphologic changes with 180 μM eosin B. In the presence of toxic concentrations of eosin B (> 720 nM), however, alterations of mammalian

[8] Rabbit anti-TS-DHFR antibodies were produced in the laboratory of Dr. David Roos, University of Pennsylvania; immunoassays were performed by Leah M. Fohl in that laboratory

Reproduced with permission of the copyright owner. Further reproduction prohibited without permission.

Fig. 5.5 Delivery of eosin B to the parasitophorous vacuole. *A*, Fluorescence microscopy of fibroblasts incubated with eosin B. Fibroblasts incubated with 320 nM eosin B for 1 min (panels a-b) or 20 min (panels c-d) prior to microscopy observation. *B*, Fluorescence microscopy with intravacuolar parasites incubated with eosin B. Infected fibroblasts incubated with 320 nM of eosin B for 301 min (panel a) or 4 h (panel b) before microscopy observation. *C*, Kinetics of fluorescence intensity associated with extracellular parasites isolated from HFF cells. After incubation in the presence of eosin B at 320 nM for various times, parasites were isolated from the host cells, adjusted to a density of $5x10^6$/ml and analyzed by fluorimetry. Results represent the means of 3 points over 2 separate experiments.

Reproduced with permission of the copyright owner. Further reproduction prohibited without permission.

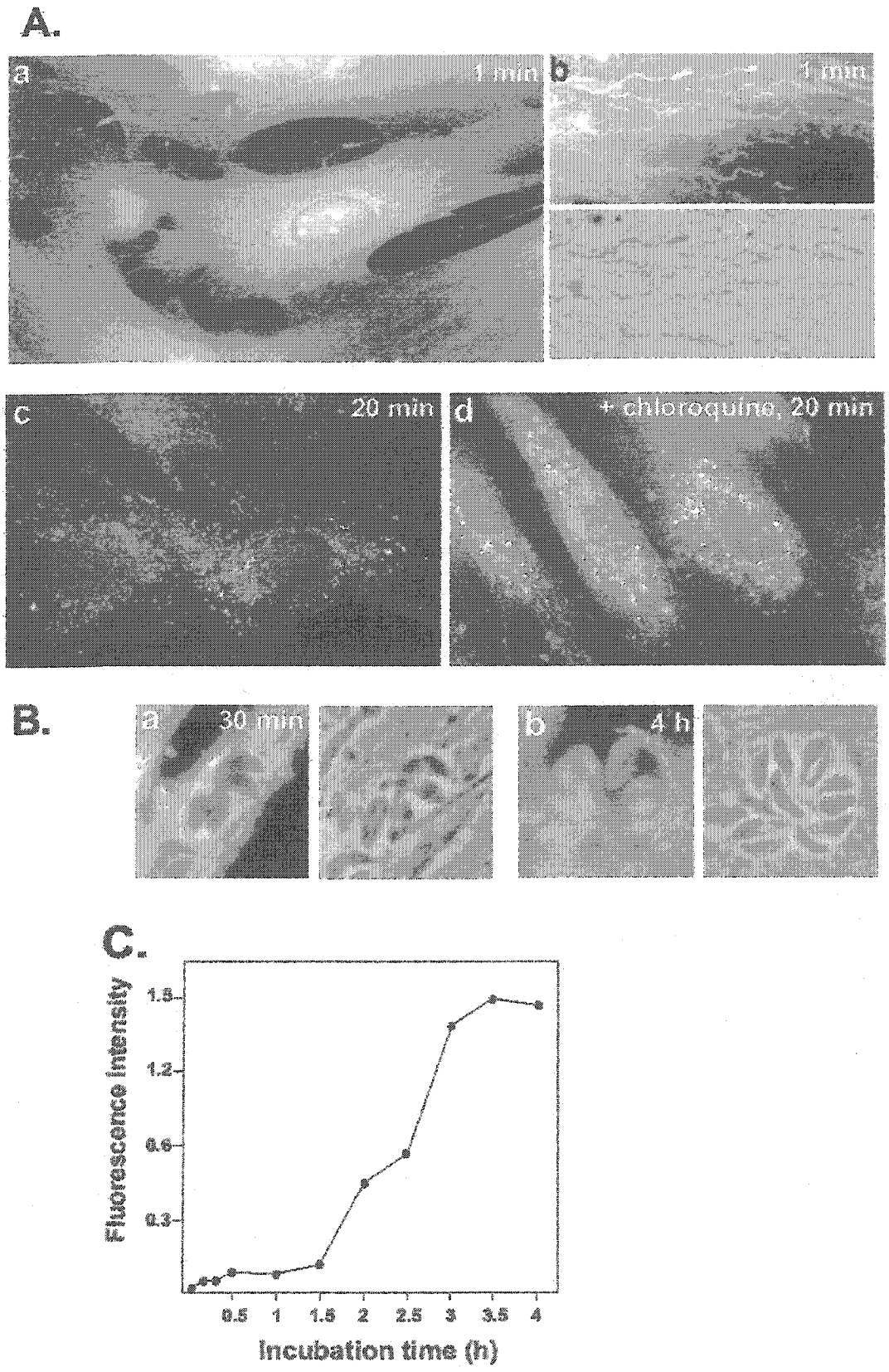

Fig. 5.5

Reproduced with permission of the copyright owner. Further reproduction prohibited without permission.

Fig. 5.6 Accumulation of eosin B in the nuclear area. Fluorescence microscopy of extracellular parasites incubated with eosin B (*a*) or Hoechst (*b*), plus merge (*c*) or intravacuolar parasites labeled with anti-TS-DHFR antibodies (*d-e*); n, nucleus.

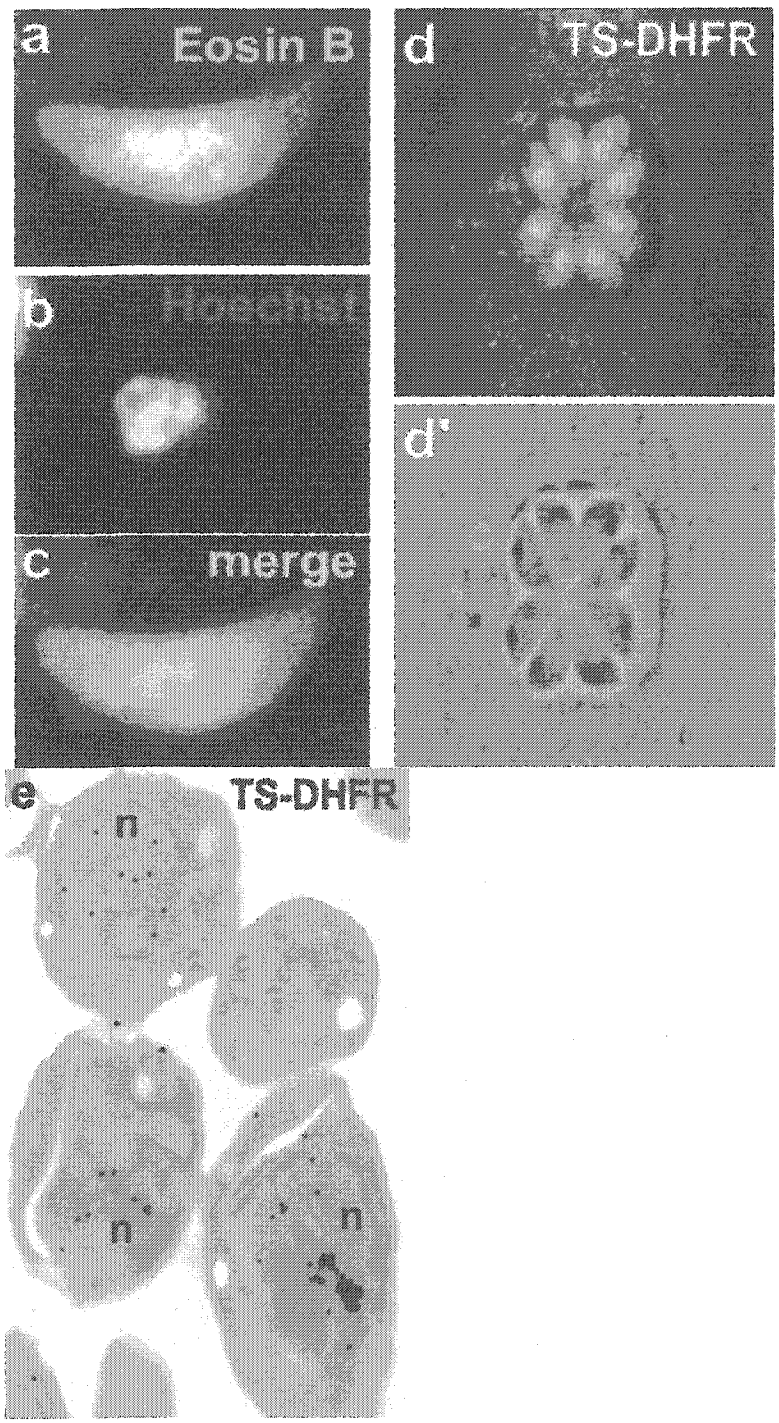

Reproduced with permission of the copyright owner. Further reproduction prohibited without permission.

Fig. 5.7 Cytopathic effects of eosin B on *T. gondii*. Transmission electron microscopy of *T. gondii* incubated in the presence of 320 nM eosin B for 24 h (panels a- b) or 48 h (panel c), or 720 nM of eosin B for 24h (panels d-e). In panel a, arrowheads pinpoint the rupture of the plasma membrane (PM) of an extracellular parasite. a, autophagic vacuole; ER, reticulum endoplasmic; hER, host reticulum endoplasmic; hm, host mitochondrion; m, mitochondrion; n, nucleus; PV, parasitophorous vacuole; PVM, parasitophorous vacuole membrane. Bars are 0.2 μm.

Reproduced with permission of the copyright owner. Further reproduction prohibited without permission.

Fig. 5.7

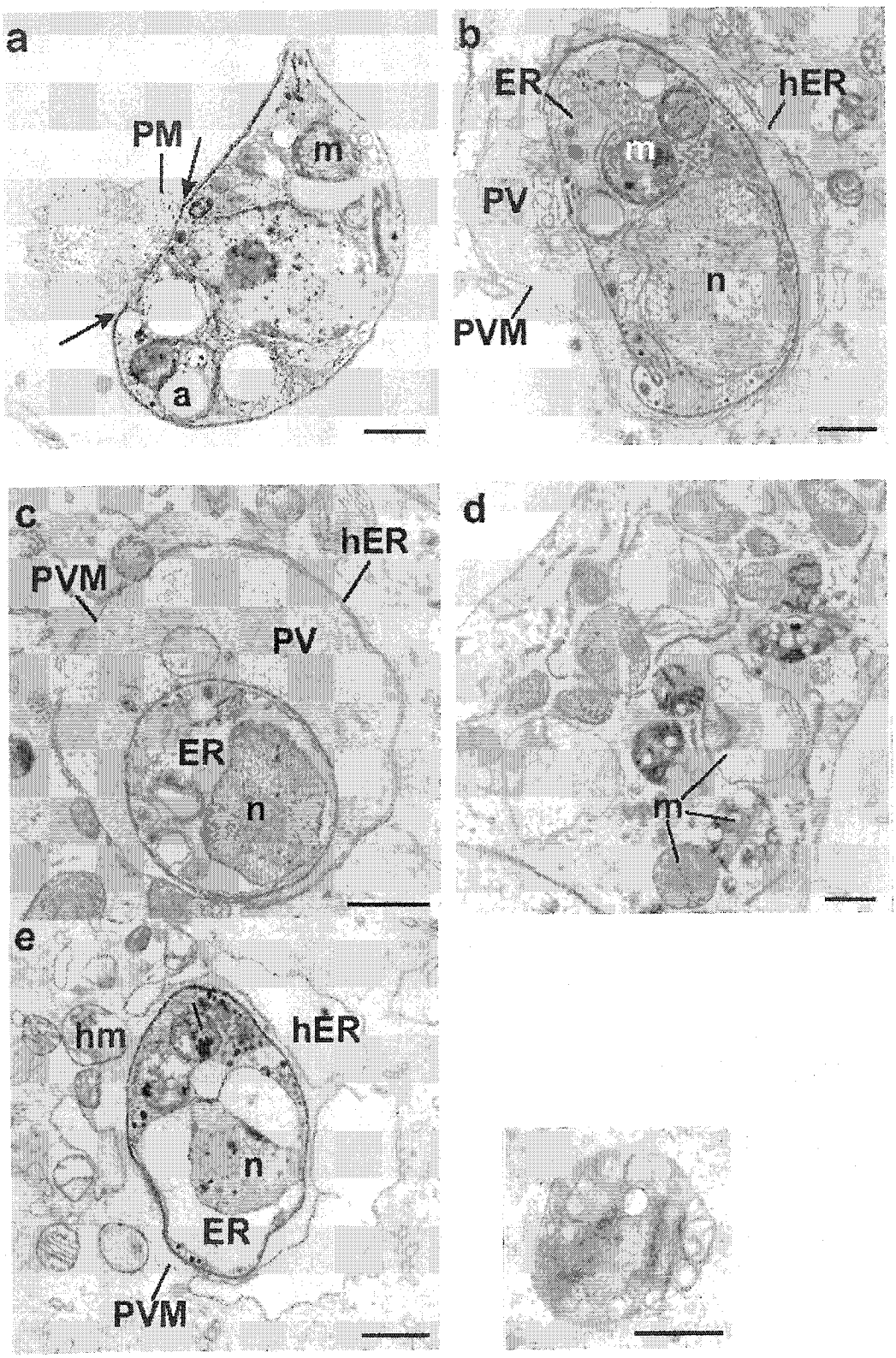

Reproduced with permission of the copyright owner. Further reproduction prohibited without permission.

mitochondria (Fig. 5.7 d and inset) as well as a dramatic swelling of the endoplasmic reticulum were observed (Fig. 5.7 e). In the case of *P. falciparum*, eosin accumulation appears to be cytoplasmic and the drug is clearly excluded from the food vacuole. Electron microscopy studies indicate overall *P. falciparum* organelle disruption in the presence of eosin B (data not shown).

Evidence for a Folate Transporter in *T. gondii* Parasites

T. gondii is known to practice *de novo* folate synthesis and has long been thought to lack mechanisms for exogenous folate uptake [120]. Accordingly, the reduced folate, leucovorin is often co-administered with high-dose antifolate chemotherapy to selectively protect host cells by bypassing the need for TS-DHFR [121]. We therefore investigated the effects of eosin B co-administered with leucovorin to decrease host cell toxicity and were surprised to find that this compound can partially reverse the effects of eosin B on *T. gondii* in cell culture. These findings provide (i) further evidence that TS-DHFR is the target of eosin B in *T. gondii* parasites and (ii) preliminary evidence of a mechanism for exogenous folate internalization by *T. gondii* (Fig 5.8, [122]).

The capacity of [^{3}H]folic acid and [^{3}H]folinic acid to transverse the *T. gondii* cell membrane were further investigated. The steady state accumulation of these compounds conformed to Michaelis-Menten kinetics, with apparent K_m values of 1.4 and 4.1 μM and apparent V_{max} values of 3.01 and 2.97 pmol/min/10^7 parasites for folate and leucovorin, respectively. HPLC analysis of the cell pellet after a 10 min incubation with either [^{3}H]folic or [^{3}H]folinic acid revealed radiolabeled peaks co-eluting with non-radiolabeled folic or folinic acid standards, respectively (Fig. 5.9). HPLC conditions designed to separate

Reproduced with permission of the copyright owner. Further reproduction prohibited without permission.

Fig. 5.8 Reversal of drug toxicity by leucovorin. *A*, Host (HFF) cells incubated with 400 μM, 500 μM, or 600 μM eosin B ± 10 μM leucovorin prior to assaying for radioactive thymidine incorporation. *B*, Intracellular T. gondii parasites (RH) incubated with 200 μM or 300 μM eosin B ± 10 μM leucovorin for 4 h prior to assaying for radioactive uracil incorporation.

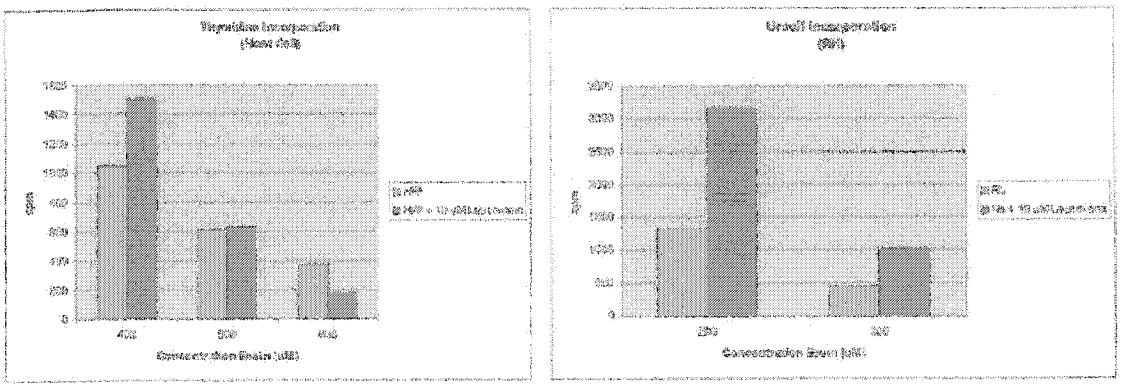

Reproduced with permission of the copyright owner. Further reproduction prohibited without permission.

Fig. 5.9 HPLC evidence for transport of intact folic acid and folinic acid into *T. gondii* parasites. When *T. gondii* parasites are incubated for 10 min with tritiated folic acid, HPLC traces from filtered cell pellets reveal a 16.5 min peak co-eluting with the non-radiolabeled folic acid standard (A). When incubated with tritated folinic acid, an 11 min peak, co-eluting with the non-radiolabeled folinic acid standard, is observed (B). There is a 30 s delay between the UV and radioactivity detectors.

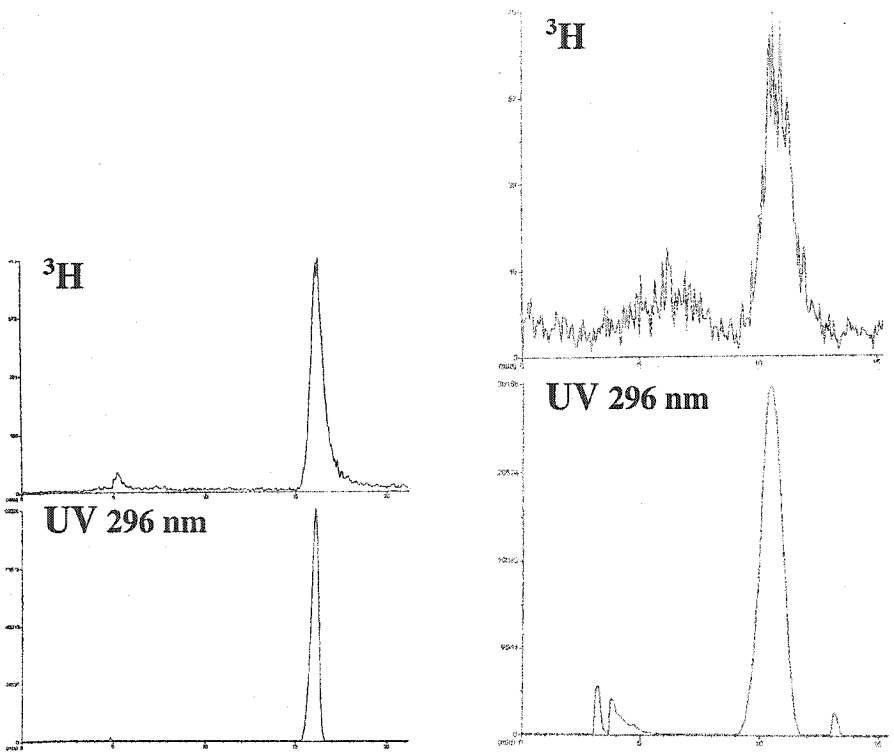

Reproduced with permission of the copyright owner. Further reproduction prohibited without permission.

polyglutamated folates (0.1M phosphate buffer, pH 6; 1% acetonitrile, 1.3 ml/min [123]); along with a $PteGlu_5$ standard (retention time= 13.5 min, 280 nm) revealed no detectable polyglutamation. These results confirm the uptake of intact folates rather than breakdown products of these compounds, and suggest that there is no folate metabolism in the parasites over the course of the experiment, making a concentrative transport mechanism reasonable.

At physiologic temperature (37°C), *T. gondii* accumulates folates in a biphasic manner: rapid uptake for the first five minutes followed by slower accumulation. Temperature dependence is observed, with greatly reduced rates of accumulation at low temperatures. A Q_{10} value of 6.77 was obtained, reflecting an active transport mechanism [124]. An activation energy of 76 kJ/mol was determined by linear regression from the negative slope of the Arrhenius plot. Transport of radiolabeled folate substrates was inhibited by high doses of corresponding non-radiolabeled substrates, demonstrating saturability of the transporter. Folate and leucovorin uptake is competitively inhibited by the folate analog methotrexate, but not by adenosine (known to utilize a different transporter [93]), suggesting a specific carrier for folate transport. Pulse-labeling indicates that, like other folate transporters, that from *T. gondii* is bi-directional. In summary, these findings suggest the presence of a rapid, high affinity, temperature/energy dependent, saturable, specific and bi-directional transporter for folate compounds in *T. gondii*[9].

[9] Additional details and primary data for results summarized in this section can be found in [122]. With the exception of HPLC analysis, experiments in this section were performed by Dr. Isabelle Coppens and Kristen Massimine.

Reproduced with permission of the copyright owner. Further reproduction prohibited without permission.

DISCUSSION

Molecular docking was used to target the shallow groove connecting the TS and DHFR active sites of the *L. major* bifunctional enzyme; the surface originally hypothesized to form an electrostatic channel for the substrate intermediate, H_2folate. Eosin B, predicted by NWU DOCK to interact with Arg 283 in the TS domain and Glu 151 in the DHFR domain of the *L. major* bifunctional enzyme, was found to have an IC_{50} value of 100 μM. Although such a level of inhibition is modest by drug standards, first round lead compounds from virtual screening often inhibit in this range; modification can improve these leads by several orders of magnitude [82, 110, 125, 126]. Because targeting the non-active site of a molecule for inhibition requires a more in-depth understanding of the interplay between mechanism and structure than targeting the active site, we sought to address these issues prior to attempting generation of more potent and specific inhibitors.

A non-active site TS-DHFR inhibitor could act by interfering with channeling of H_2folate from TS to DHFR, protein conformational changes constituting TS-DHFR domain-domain communication, or both. As discussed below, a number of experiments did provide evidence that eosin B is a non-active site inhibitor, capable of inhibiting both TS and DHFR. Because the proposed binding site for eosin B is located in the shallow groove region containing the putative electrostatic channel, one might anticipate that a small molecule bound in this region, or mutations that alter charge, might interfere with the transit of H_2folate from the TS to the DHFR active site. Accordingly, one might predict that the kinetics would reflect a build-up of the H_2folate intermediate in solution. Consistent with the mutagenesis studies presented in the previous chapter, however,

Reproduced with permission of the copyright owner. Further reproduction prohibited without permission.

using a transient kinetic analysis, a single enzyme turnover experiment examining the TS-DHFR reaction did not show a difference in H_2folate accumulation in the presence or absence of eosin B. As a likely alternative to inhibition of substrate channeling, eosin B may exert its effect by interfering with domain-domain communication, or the series of protein conformational changes induced by ligand binding at one active site that affects activity at the active site of the other enzyme.

The finding that eosin B only marginally inhibits the *L. major* R283E charge reversal mutant supports the suggestion that eosin B does in fact, interact with Arg 283, a residue located in the shallow groove targeted with the docking program. Whereas phenolphthalein is known by X-ray crystallography to bind to the TS active site, it inhibits R283E to the same degree as wild-type *L. major* TS-DHFR. This observation suggests that the binding sites for eosin B and phenolphthalein are distinct, and is not surprising because phenolphthalein is most similar to the cyclic form of eosin B while the docking predictions and our experimental conditions (pH 7.5-8) employ the open form [115]. Nonetheless, the finding indicates that the decreased ability of eosin to bind R283E is unlikely to be because of a remote effect, such as a change in the active site conformation, as a result of the non-active site mutation. The fact that TS is a highly conserved enzyme and position 283 is completely conserved as a basic residue (arginine or lysine) across enzyme species could account for the similar TS inhibition observed with the bifunctional and monofunctional enzymes tested. Arg 283 is homologous to Arg 372 in *T. gondii* and Lys 285 in *C. hominis*.

Conversely, whereas there is structural similarity between *L. major* and *T. gondii* TS-DHFR in the region of Glu 151, limited structural conservation exists with *E. coli*

Reproduced with permission of the copyright owner. Further reproduction prohibited without permission.

DHFR and the closest acidic residue, Glu 90, is oriented in a different direction from Glu 151, possibly explaining the poor inhibition of eosin in the *E. coli* enzyme. Eosin B is also a poor inhibitor of the apicomplexan enzyme, *C. hominis*, with an IC_{50} of 620 μM for the TS-DHFR reaction. This is not unexpected when one considers structural differences between *L. major* and the apicomplexa TS-DHFR enzymes, particularly evident with *C. hominis* TS-DHFR, the well-defined binding groove in *L. major* being replaced by a shallow scooped region in the apicomplexa enzymes. Furthermore, Glu 151 is parallel to Glu 177 in *T. gondii* , but perpendicular to the nearest acidic residue in *C. hominis*, Glu 139.

Efforts are underway to definitively elucidate the site of binding of eosin through co-crystallization of eosin B with *T. gondii* TS-DHFR. Co-crystals of *T. gondii* TS-DHFR and eosin B were grown by Dr. Amy C. Anderson's group at Dartmouth College in the presence of both TS and DHFR ligands, with eosin B at a concentration of 1 mM to insure full occupancy of the binding site. The space group (C222), unit cell (a=143.7, b=187.1, and c=123.6; a= b= g=90°) and crystallization conditions of the co-crystal are similar to those of native TS-DHFR. The crystals appear reddish in color, confirming the presence of eosin. Unfortunately the crystals were very small and initial evaluation at the synchrotron indicated that the diffraction was too weak to discern the details of eosin B binding.

Whereas Arg 283 and Glu 151 appear to make key contacts with the hydroxyl groups on eosin B, comparative inhibition by the scaffold molecule, fluorescein, predicts that the hydroxyl groups are not the only functional groups on the molecule that are important for binding. The hydroxyl groups are present on both the scaffold molecule and

Reproduced with permission of the copyright owner. Further reproduction prohibited without permission.

eosin B, but eosin B is an 8-fold better inhibitor of *L. major* TS-DHFR than is fluorescein. This suggests that the 4',5'-dibromo and 2'7'-dinitro groups on eosin B also promote binding, either directly or indirectly, by increasing the hydrophobicity of the inhibitor. Reviewing the structure, the one functional group that does not appear to participate in energetically favorable interactions is the 5' bromine. This bromine does, however, lie close to a hydrophilic pocket near the conserved basic loop in the DHFR domain, and therefore may be ideally positioned for modification. Understanding structural characteristics that contribute to inhibition by eosin B should allow for structure-based design of analogs with greater potency and specificity for the bifunctional enzyme in the future (see Part B of this chapter).

The evaluation of the mode of action of eosin B using spectroscopic techniques is difficult because, at the concentrations necessary to see inhibition, the dye absorbs light, making fluorescence and absorbance studies unfeasible because of inner-filter effects. Transient kinetic studies indicate that eosin B is not competitive with monoglutamyl folate substrates (either CH_2H_4folate or H_2folate). The finding that eosin B inhibits both the TS and DHFR reactions without competing for either folate substrate provides kinetic evidence, supporting the structural predictions of DOCK and results with the R283E mutant, that eosin B binds outside of the active sites of both TS and DHFR.

One aspect of eosin B with which we were concerned was its potential ability to form aggregates in solution that could inhibit many enzymes nonspecifically. Indeed, there is a precedent for fluorinated dyes acting as nonspecific inhibitors [116]. Several lines of evidence suggest, however, that eosin B is, in fact, inhibiting *L. major* TS-DHFR specifically. First, IC_{50} values for aggregate-based inhibition are very sensitive to changes

Reproduced with permission of the copyright owner. Further reproduction prohibited without permission.

in enzyme concentration. With eosin B, on the other hand, steady-state inhibition was unaffected by 10-fold increases in the concentration of *L. major* TS-DHFR (from 0.1 to 1 μM enzyme). If eosin B were forming large aggregates capable of binding up enzyme, the same concentration of aggregates should have been formed in either case, as the same eosin B concentration was used, but a much greater percent inhibition would be observed at low enzyme concentration. Instead ~50% inhibition was seen at both enzyme concentrations. Second, a point substitution, Arg 283→Glu, diminished the inhibition of eosin by over an order of magnitude, consistent with the docking prediction of a classical 1:1 complex being formed in this region. Finally, in the pre-steady-state kinetics, a ratio of inhibitor:enzyme of 20:1 was used, whereas aggregation-based nonspecific inhibitors appear to require ratios of over 1000:1 (inhibitor:enzyme). Nonspecific inhibition therefore seems unlikely to explain the activity of eosin versus TS-DHFR. Conversely, it appears that inhibition of *C. hominis* TS-DHFR by the tetra-bromo derivative of eosin B is likely to be due, at least in part, to aggregate formation. Aggregation by the tetra-bromo derivative of eosin B has not yet been confirmed by light scattering measurements.

Evidence that eosin B is specifically targeting TS-DHFR has been further obtained by cell culture experiments with *T. gondii*. *T. gondii* replication is reduced by 50% at a drug concentration of 180 μM, similar to the IC_{50} of eosin in steady-state biochemical assays with *T. gondii* TS-DHFR protein. Furthermore, growth inhibition induced by eosin B is reduced by administration of leucovorin, a chemical that is used as an antidote to compounds that block the conversion of folic acid to folinic acid. Additionally, concern over potential toxicity related to nonspecific inhibition by eosin B is lessened by the finding that no adverse effects were observed in rats fed diets

Reproduced with permission of the copyright owner. Further reproduction prohibited without permission.

containing up to 2% eosin B, leading to FDA approval of eosin B for use in drugs and cosmetics [137].

Differences in folate metabolic pathways as well as drug uptake or stability may account for the poor inhibition of *L. major* by eosin B in cell culture [127]. *L. major* is known to encode P-glycoprotein family members including MDR and MRP homologs, and also contains a large vacuole and acidic compartments not present in other parasites. Eosin B was found to inhibit *P. falciparum* growth with an IC_{50} value of 200 nM, a concentration approximately 1000-fold less than that which is needed to block *T. gondii* replication. A plausible explanation for this finding may be related to a difference in drug accessibility to the parasite enzyme. The most striking difference between the parasites is their host cell. *P. falciparum* invades mature erythrocytes, which lack intracellular organelles and which are devoid of metabolic activities. In contrast, *T. gondii* can replicate within nucleated cells replete with full biosynthetic machinery. Whereas eosin B may have a relatively direct access to the enzyme target of *P. falciparum*, the drug might be trapped in the different compartments of the *T. gondii* host cell, reducing the amount of drug available for the parasite. Toxic metabolites of eosin B may be also generated by the cells, causing a loss of host cell viability and, as a consequence, reduction of parasite replication. The IC_{50} of 380 μM found subsequently in biochemical assays, however, suggests that eosin B is likely binding additional targets in *P. falciparum* parasite cell culture. Nevertheless, eosin B has potential as a lead molecule for antimalarial drug development, particularly since it was also found to have activity against drug resistant strains of *P. falciparum.*

Reproduced with permission of the copyright owner. Further reproduction prohibited without permission.

In principle, non-active site binding regions offer unique opportunities to discover specific inhibitors. Often, however, such sites lack the tightly defined geometrical and functional constraints of active sites and as such are difficult to target. Here we were able to use molecular docking to target the shallow groove region between the TS and DHFR active sites in the *L. major* bifunctional enzyme. Several lines of evidence suggest that eosin B binds outside of the two active sites. The effects of the Arg 283 Glu point substitution are, moreover, consistent with the docking prediction. Whereas mutation of basic residues in the shallow groove region, including Arg 283, does not appear to affect domain-domain communication, or at least TS catalysis, eosin B binding in this region affects both TS and DHFR activity, presumably by inducing or preventing key conformational changes. This, coupled with the fact that no build-up of H_2folate was observed, suggests that eosin B exerts its effects on TS and DHFR via interference with domain-domain communication rather than electrostatic channeling.

Comparative inhibition by eosin B analogs has yielded structural information that should allow for design of more potent and specific inhibitors of protozoal TS-DHFR and could produce novel therapies specific for parasitic infections, including toxoplasmosis and malaria, particularly drug-resistant malaria. Eosin B has already been shown to be an inhibitor of *T. gondii* in cell culture at concentrations where host cells are unharmed. As such, findings with eosin B represent an important step toward establishing proof-of-principle that the non-active site, shallow groove region of the bifunctional TS-DHFR enzyme can serve as a molecular target that when inhibited, results in parasite death.

A second major finding of these studies is the existence of a *T. gondii* folate transporter, exhibiting characteristics consistent with a recently cloned and characterized

Reproduced with permission of the copyright owner. Further reproduction prohibited without permission.

high-affinity folate transporter gene from *Leishmania tarentolae* [128]. Sequence-homology searches using the *L. tarentolae* gene have revealed folate transporter candidate genes in the *T. gondii* and *P. falciparum* genomes. Kristen Massimine is currently in the process of attempting to clone and heterologously express these genes. Whereas *Leishmania* species are folate auxotrophs, relying on salvage for survival, why do redundate mechanisms for obtaining folates exist in apicomplexa parasites? An additional topic of future investigation is relative contributions of *de novo* folate synthesis and folate salvage at different stages of the cell cycle and under conditions of minimal or abundant endogenous starting materials for *de novo* synthesis or exogenous folates.

Reproduced with permission of the copyright owner. Further reproduction prohibited without permission.

Part B. Non-Active Site Inhibition of Apicomplexan TS-DHFR

Eosin B was found through a molecular docking screen targeted at a non-active site region in *L. major* TS-DHFR. Given the structural and mechanistic differences between TS-DHFR from *L. major* and the apicomplexa protozoa, it should not be surprising that eosin B is a less potent inhibitor of these enzymes. Eosin B does inhibit both TS and DHFR activity to some extent with *T. gondii* and *C. hominis* TS-DHFR, however, and in *T. gondii* eosin B qualifies as a respectable lead compound from a first-pass docking screen, particularly since it also has activity in parasite cell culture [104]. We plan to functionalize this compound to improve potency and selectivity as a non-active site inhibitor of *T. gondii* TS-DHFR, as well as perform additional docking screens targeted at the corresponding non-active site region in the *T. gondii* crystal structure. In the case of *C. hominis*, the crystal structure was recently solved, so we are exploring new potential non-active site inhibitor binding targets at the DHFR interface and adjacent to the cross-over helix, and have targeted these sites using the computational program, *GLIDE v.2.5*, coupled with databases of compounds with medicinal properties.

It should be noted that even a compound that binds specifically to a non-active site region of TS-DHFR but does not result in inhibition of enzyme activity is useful for drug development. Such a compound may be used as an anchor, tethered to a known active site inhibitor, to create a bifunctional inhibitor with improved potency and selectivity. The concept and advantages of a bifunctional inhibitor are discussed as follows.

Reproduced with permission of the copyright owner. Further reproduction prohibited without permission.

1. A Bifunctional Inhibitor for *T. gondii* TS-DHFR

A bifunctional enzyme with multiple active and non-active site binding pockets is the perfect substrate for creation of a bifunctional inhibitor. This involves design of a molecule that connects two ligands specific for two proximal binding sites on an enzyme surface with a flexible linker arm. Bifunctional inhibitors are advantageous because they have the theoretical and demonstrated ability to combine ligands to produce an inhibitor with greater than additive binding affinity. This is due to the concept of additive binding free energies and the multiplicative relationship for binding affinities ($\Delta G = -RT\ln K$). For example, if 2 molecules specific for 2 different binding sites each have binding free energies of 6 kcal/mole (K_i = 100 μM), are joined together by a completely neutral linker, they have a theoretical binding energy of 12 kcal/mole (additive) but a theoretical binding affinity of 10 nM (multiplicative). This strategy has been successfully exploited in several enzyme systems including FKBP, stromolysin, and BCL-2. [129-131] and has become a major technology engine for biotechnology companies. In the case of drug development targeted at parasitic infections, bifunctional inhibitors have an additional advantage: effectively a combination drug therapy, the bifunctional inhibitor should be more effective at preventing the rapid emergence of drug resistant parasite strains.

We are awaiting the solution of the *T. gondii* TS-DHFR enzyme co-crystallized with eosin B before attempting to synthesize a bifunctional inhibitor connecting eosin B (or another compound binding to the same non-active site region) and a DHFR active-site inhibitor. Nonetheless, we have put thought into the design of such an inhibitor. Reviewing the eosin B structure, the one functional group that does not appear to participate in energetically favorable interactions is the 5' bromine. Since this bromine

Reproduced with permission of the copyright owner. Further reproduction prohibited without permission.

lies close to a hydrophilic pocket near the conserved basic loop in the DHFR domain however, it is ideally positioned for modification.

The DHFR active site is the favored position for the active-site inhibitor moiety of the bifunctional inhibitor since DHFR is less conserved than TS, affording greater specificity for the parasite enzyme (and hopefully few side-effects for the human patient). We initially planned to use methotrexate as our DHFR ligand, but methotrexate binds to most DHFR enzymes with tight affinity and it was decided that an inhibitor with greater selectivity but weaker affinity would be preferable. Experimentally, it is more straightforward to demonstrate proof-of-concept (multiplicative binding affinity) for a bifunctional inhibitor composed of two parts that exhibit relatively weak binding. Consequently, we opted for the DHFR ligand trimethoprim, which has a 44-fold selectivity for *T. gondii* relative to mammalian DHFR and binds with an IC_{50} value around 2.7 μM. Based upon estimated binding constants of 180 μM for eosin B and 2.7 μM for trimethoprim, the bifunctional inhibitor would have a theoretical upper bounds K_d value of ~4.8 x 10^{-10} M or 480 pM.

Molecular modeling suggests that building from one of the methoxy groups on the aromatic ring of trimethoprim would allow for attachment via the position occupied by the 5' bromine in eosin B. A polyether linkage was chosen due to its flexibility, relatively high hydrophilicity, availability in modular units, and ease of synthesis. The length of the polyethylene glycol linker was chosen to preserve the preferred gauche conformation for the O-C-O dihedral angle and to avoid unfavorable van der Waals contacts with the protein. Our modeling suggests an optimal linker length of 13 polyethylene glycol units (Marina Udier Blagovic, personal communication). A synthetic protocol was developed

Reproduced with permission of the copyright owner. Further reproduction prohibited without permission.

by Guang Xiu Dai in our lab, using a strategy that we have already successfully applied to create bifunctional inhibitors of HIV-1 reverse transcriptase (linking a non-nucleoside and nucleoside inhibitor). The eosin B-trimethoprim bifunctional inhibitor docked into the *T. gondii* protein is shown in Fig. 5.10.

Fig 5.10 Bifunctional inhibitor for *T. gondii* TS-DHFR. The DHFR inhibitor, trimethoprim is connected to eosin B via a polyethylene linker.

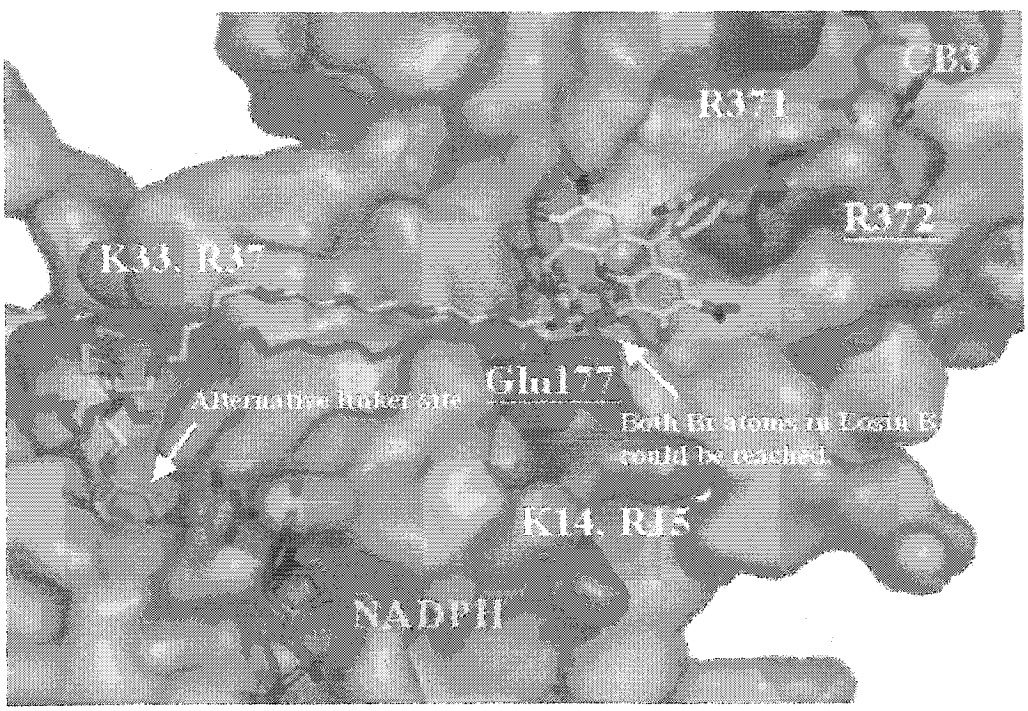

Reproduced with permission of the copyright owner. Further reproduction prohibited without permission.

2. A New Docking Site in *C. hominis* TS-DHFR

With the solution of the *C. hominis* TS-DHFR crystal structure, we had the opportunity to look for new potential non-active site binding pockets in the apicomplexa enzyme. We were particularly interested in the region surrounding the cross-over helix, as this helix packs against the DHFR active site of the opposite half of the dimer, making close contacts with catalytic residues. A well-defined cavity was discovered at the *C. hominis* linker-DHFR interface, adjacent to the cross-over helix (Fig 5.11). Marina Udier Blagovic, in Dr.William Jorgenson's lab at Yale University, found and targeted this cavity using the recently developed second generation docking program, *GLIDE v.2.5* [89], in conjunction with the *C. hominis* TS-DHFR crystal structure. There are several advantages to the *GLIDE* program, including that it accounts for solvation effects and entropic factors, incorporates a systematic search of ligand flexibility, and applies filters to screen for molecules that have drug-like properties and avoid chemical functionalities known to be associated with toxicity. Libraries available for virtual or *in silico* screening include the ACD (Available Chemicals Directory), MDDR (MDL Drug Data Report), Maybridge Database, and CMC (Comprehensive Medicinal Chemistry) Database, consisting of over 350,000 molecules, as well as a propriety database from Schrödinger Chemicals.

The propriety database from Schrödinger Chemicals and the CMC Database have been screened, and two commercially available compounds from the Schrödinger propriety database as well as 7 of the 15 highest scoring compounds (lowest predicted binding energy) from the CMC database were ordered. These compounds were tested at 1 mM, or the highest concentration where no precipitate was observed and not resulting in

Reproduced with permission of the copyright owner. Further reproduction prohibited without permission.

inner-filter effect (light-blocking) in TS-DHFR and DHFR steady-state spectroscopic experiments (Table 5.3)[10]. The two Schrödinger propriety database compounds, F1092-1772 and F0917-7119, were highly lipophilic, posing a challenge to enzymatic assays. In preliminary spectroscopic experiments conducted in the presence of 5% DMSO, however, F1092-1772 was found to be a ~100 μM IC_{50} inhibitor of the *C. hominis* DHFR reaction, and F0917-7119 was found to be a ~100 μM IC_{50} of the TS-DHFR reaction.

Preliminary spectroscopic experiments indicated that, of the 7 CMC compounds tested, two, streptonigrin and flavin mononucleotide (FMN) have activity against *C. hominis* TS-DHFR: the predicted positions of these compounds within the binding site are shown in Fig. 5.12. Since both compounds are colored (streptonigrin is brownish-black and FMN is yellow), inner-filter effects limited the concentration at which the compounds could be tested. Therefore, the compounds were also tested at 1 mM in rapid chemical quench experiments with radiolabeled substrates (50 μM *C. hominis* TS-DHFR; 11 μM H_2folate or 13 μM CH_2H_4folate). At 1 mM, both compounds were found to inhibit the DHFR reaction; the TS-DHFR reaction was strongly inhibited by FMN but not inhibited by streptonigrin.

In further steady-state spectroscopic assays, FMN was found to be a 20 μM IC_{50} inhibitor of *C. hominis* TS-DHFR that does not compete with CH_2H_4folate: inhibition was unchanged in the presence of 15.6 μM-156 μM CH_2H_4folate. The *T. gondii* TS-DHFR reaction is also inhibited, but at 20 μM FMN, 88% of Human TS activity remains, suggesting selectivity for the bifunctional enzyme. The streptonigrin and FMN IC_{50}

[10] Oladapo Babatunde, a Yale undergraduate student, contributed to collection of the preliminary data presented in this section and will continue to work on this project. He created Table 5.3. Figures 5.10, 5.11 B, and 5.12 were created by Marina Udier Blagovic.

Reproduced with permission of the copyright owner. Further reproduction prohibited without permission.

values for the *C. hominis* DHFR reaction were found to be 240 μM and 400 μM, respectively (Table 5.4). Inhibition by the compounds was unchanged in the presence of H_2folate concentrations ranging from 16 μM to 160 μM, suggesting that neither inhibitor competes with H_2folate. Both compounds exhibited similar inhibition of the *T. gondii* TS-DHFR reaction. FMN was found to be a 21 μM inhibitor of the *P. falciparum* TS-DHFR reaction; streptonigrin and FMN were found to be 235 μM and 390 μM inhibitors of the *P. falciparum* DHFR reaction, respectively (Table 5.4).

The inhibitors were also tested against two *C. hominis* cross-over helix mutants: E205L and R210M. While inhibition of the TS-DHFR reaction by FMN was comparable to what was observed with wild-type *C. hominis* (IC_{50} values of 20 μM and 24 μM for E205L and R210M, respectively), inhibition of the DHFR reaction was impaired after mutagenesis. FMN was found to be a ~800 μM inhibitor of E205L and a 770 μM inhibitor of R210M. Streptonigrin was found to be a 350 μM inhibitor of E205L and a 400 μM inhibitor of R210M (Table 5.4). The fact that mutations near the putative inhibitor binding region resulted in decreased inhibitory activity supports the hypothesis that the predicted binding location is correct. A PubMed search did not reveal the compounds to be known inhibitors of TS or DHFR. Interestingly however, the recently discovered ThyX enzymes, representing a sequence/structurally unrelated alternative for thymidylate synthesis, use FMN as a cofactor [31].

Dr. Amy C. Anderson's group at Dartmouth College is currently attempting to co-crystallize streptonigrin and FMN with *C. hominis* TS-DHFR to confirm the predicted binding location. We also plan to assay for activity in parasite cell culture. Other libraries will be screened, and additional compounds will be ordered and tested both for ability to

Reproduced with permission of the copyright owner. Further reproduction prohibited without permission.

inhibit enzyme activity and for binding alone. Binding can be detected by changes in intrinsic enzyme fluorescence following addition of the compound; in a spin-column binding assay, where the small molecule will come through the column if it is bound to enzyme or by micro-calorimetry. Compounds that bind specifically but do not inhibit will be considered for use as an anchor for the creation of a bifunctional *C. hominis* TS-DHFR inhibitor.

If the binding location is confirmed in *C. hominis*, it is likely to be similar in *P. falciparum* TS-DHFR and co-crystallization with the compounds could aid in resolving the portion of the linker region that is disordered in electron density. Of additional interest, molecular docking may help elucidate the mechanism of translational autoregulation in *P. falciparum* TS-DHFR. Unlike with human DHFR, the *P. falciparum* mRNA binds a non-active site region [34, 36]. Yuvaniyama *et al.* [8] put forth the idea that the *P. falciparum* mRNA may bind in a groove between a DHFR insertional helix and the junctional region; a region near to our potential molecular docking target in *C. hominis.* [49]. Translational autoregulation requires a mechanism to situationally allow for binding and release of mRNA; therefore, if mRNA binds to a non-active site, this site is likely to be closely regulated by what is happening at the enzyme active sites. By extension, if an active site and a non-active site region are tightly coupled, disruption of the non-active site with a small molecule inhibitor may disrupt activity. If this hypothesis is correct, the mRNA binding region could represent a viable non-active site therapeutic target.

Reproduced with permission of the copyright owner. Further reproduction prohibited without permission.

Fig 5.11 New docking site in *C. hominis* TS-DHFR. Overview of a new docking site in *C. hominis* TS-DHFR with inhibitor in red, *A*; close-up of site with inhibitor in green and DHFR ligand in white, *B*.

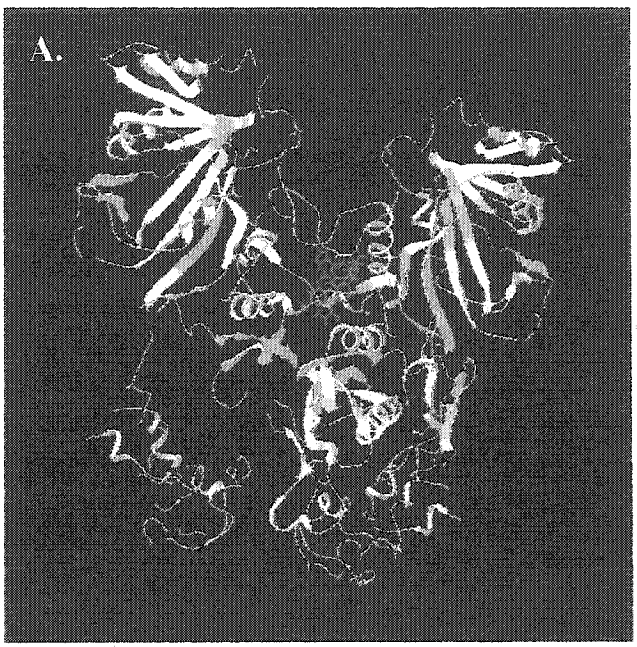

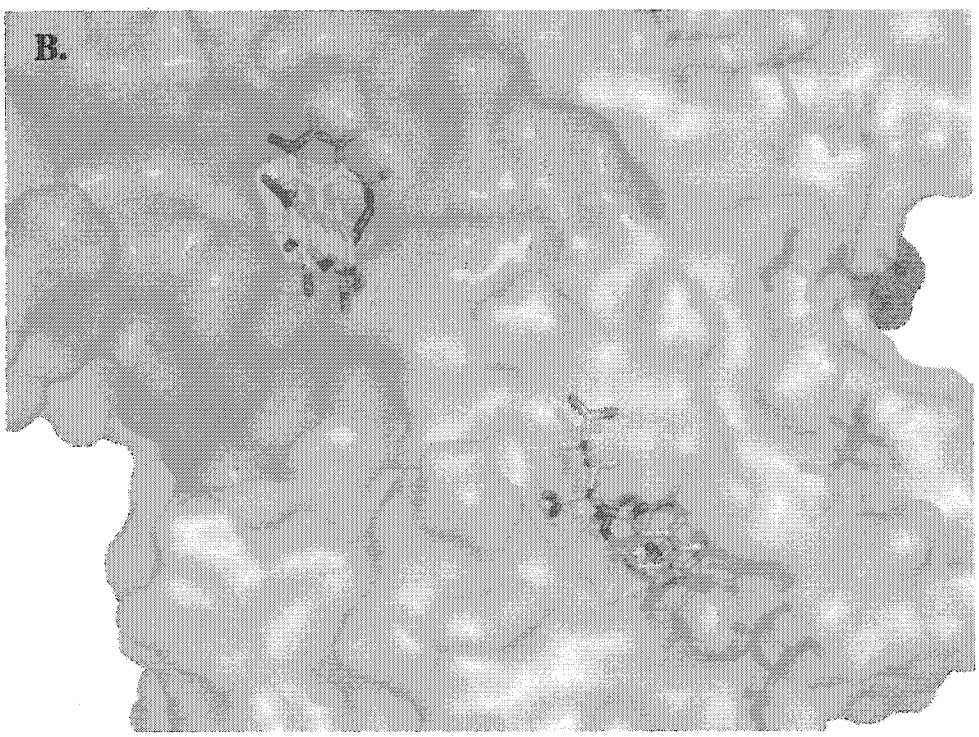

Reproduced with permission of the copyright owner. Further reproduction prohibited without permission.

Table 5.3 Glide Hits tested. Structures obtained using *GLIDE v. 2.5* and the CMC database (*A*) or Schrödinger propriety database (*B*) that were screened as possible non-active site inhibitors of *C. hominis* TS-DHFR.

Compound Name / Compound Formula	Structure	Glide Score
Digoxin / $C_{41}H_{64}O_{14}$	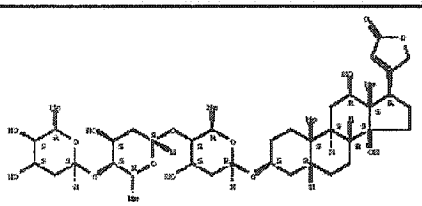	-9.75
Chitobiose / $C_{16}H_{28}N_2O_{11}$	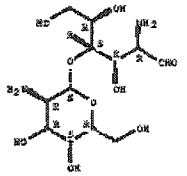	-8.78
Ketoconazole / $C_{26}H_{28}Cl_2N_4O_4$	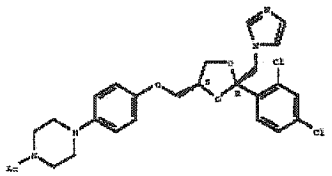	-8.41
Tobramycin / $C_{18}H_{37}N_5O_9$	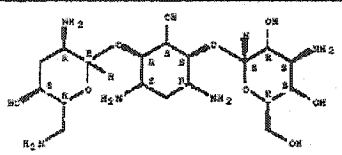	-8.41
Streptonigrin / $C_{25}H_{22}N_4O_8$	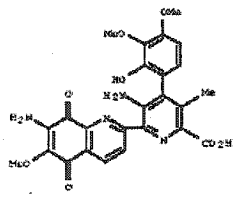	-8.32
Flavin Mononucleotide / $C_{17}H_{21}N_4O_9P$	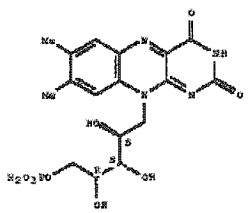	-8.08
N-Acetyllactosamine / $C_{14}H_{25}NO_{11}$	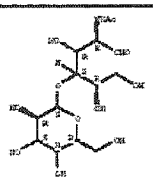	-7.96 **A.**

Reproduced with permission of the copyright owner. Further reproduction prohibited without permission.

Table 5.3

F1092-1772 / $C_{20}H_{16}FN_5O$	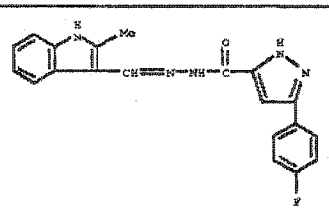
F0917-7119 / $C_{23}H_{24}N_6OS$	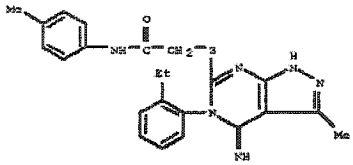

B.

Table 5.4 IC_{50} Values (μM) for Enzyme inhibition by Flavin Mononucleotide and Streptonigrin

Species	FMN TS-DHFR	FMN DHFR	Streptonigrin DHFR
C. hominis			
Wild-type	20	400	240
E205L	20	~800	350
R210M	24	770	400
P. falciparum	21	235	390

Reproduced with permission of the copyright owner. Further reproduction prohibited without permission.

Fig 5.12 Predicted binding orientations of streptonigrin and flavin mononucleotide in a non-active site pocket of *C. hominis* TS-DHFR. Zoomed out view of streptonigrin in binding site, *A*; zoomed in view of flavin mononucleotide in the binding site, *B*. Inhibitors in green; active site ligands in blue.

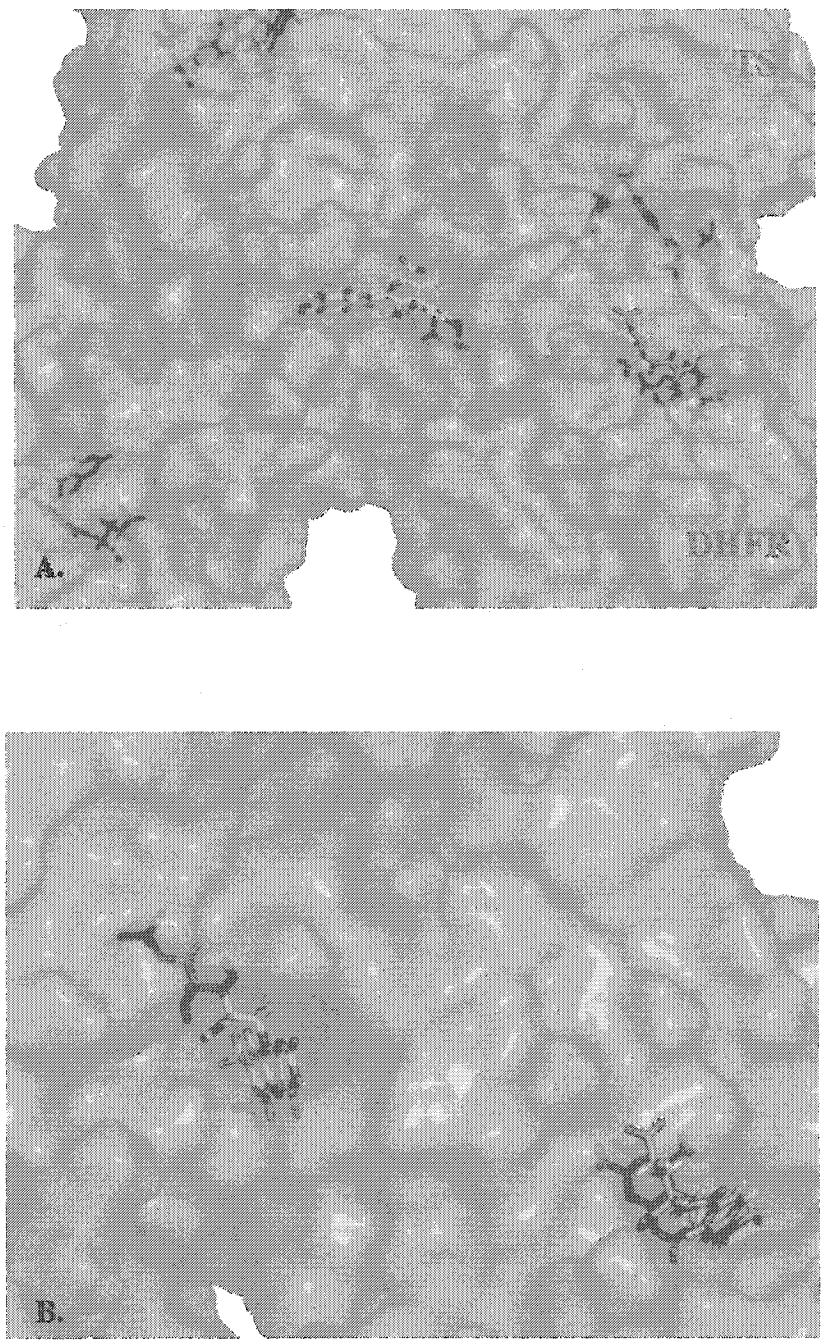

Reproduced with permission of the copyright owner. Further reproduction prohibited without permission.

Chapter Six

Conclusions and Future Directions

Reproduced with permission of the copyright owner. Further reproduction prohibited without permission.

A major finding of this research is that the significant structural differences between the recently crystallized apicomplexan TS-DHFR enzymes, from *C. hominis* and *P. falciparum*, and the well-known kinetoplastid structure (*L. major*) translate as significant mechanistic differences between parasite classes and among parasites within the same class. These data are presented in Chapter 3, "Kinetic Characterization of Bifunctional TS-DHFR from the Apicomplexan Protozoa *Cryptosporidium hominis*" [132]. Part A of the chapter focuses on three aspects of *C. hominis* TS-DHFR: determination of TS-DHFR kinetic mechanism, substrate channeling behavior, and domain-domain communication.

Unexpectedly, the unique mechanistic features of *C. hominis* TS-DHFR involve the highly conserved TS domain. At 45 s^{-1}, *C. hominis* TS activity is 10 to 40-fold faster than other TS enzymes studied and a new kinetic mechanism was required to simulate *C. hominis* TS behavior, including incorporation of the slow conformational change observed following binding of the folate analog, PDDF. Additionally, while there is HPLC evidence for a *C. hominis* TS intermediate, no pre-steady-state burst in consumption of the cofactor, CH_2H_4folate, was observed. Perhaps most striking, a large accumulation of H_2folate produced at TS and a lag in product formation at DHFR were observed. These observations make *C. hominis* TS-DHFR the first bifunctional TS-DHFR enzyme studied for which there is clear evidence against H_2folate substrate channeling.

The apicomplexan TS-DHFR enzymes characterized differ from *L. major* in that, whereas there are multiple lines of evidence for domain-domain communication with *L.*

Reproduced with permission of the copyright owner. Further reproduction prohibited without permission.

major TS-DHFR (ligand binding at TS affecting DHFR activity and vice-versa), no such effects were found with *C. hominis* or *T. gondii*. The apicomplexan TS-DHFR enzymes are similar in that they exhibit maximal DHFR activity even when TS is in an unliganded state (130 s^{-1} and 180 s^{-1}, respectively), with no further acceleration upon complex formation at TS. This differs from *L. major* in which DHFR rate is relatively slow at 6.4 s^{-1}, but is accelerated to 120 s^{-1} following ternary complex formation at TS [56]. The proximity of the *C. hominis* cross-over helix to the DHFR active site in the opposite half of the dimer, however, suggests the possibility of a different form of communication among apicomplexan TS-DHFR enzymes. The possibility of communication across the dimer interface, rather than TS and DHFR active sites, will be a topic of continuing exploration.

A preliminary mechanistic analysis of a third apicomplexan protein, TS-DHFR from *P. falciparum*, is presented in Part B of the chapter. *P. falciparum* TS-DHFR follows the pattern of the other apicomplexan enzymes in that the DHFR rate is fast even in the absence of TS ligands. This enzyme is like *T. gondii* TS-DHFR in that the TS rate is relatively slow and there is no evidence against substrate channeling (little accumulation of H_2folate in the TS-DHFR reaction). At least under the conditions tested, no burst in CH_2H_4folate was observed. Further characterization of *P. falciparum* TS-DHFR will be a subject of future research in the lab.

In Chapter 4, "Probing Electrostatic Channeling and Domain-Domain Communication in Bifunctional TS-DHFR Using Site-Directed Mutagenesis" [96], we used site-directed mutagenesis to test the hypothesis that substrate channeling in the bifunctional TS-DHFR enzyme from *L. major* occurs via electrostatic interactions

Reproduced with permission of the copyright owner. Further reproduction prohibited without permission.

between the negatively charged H_2folate produced at TS and a series of lysine and arginine residues on the surface of the protein. Accordingly, 12 charge reversal or charge neutralization mutants were made, with up to 6 putative channel residues changed at once. The mutants were assessed for impaired channeling using two criteria: a lag in product formation at DHFR and an increase in H_2folate accumulation. Surprisingly, none of the mutations produced changes consistent with impaired channeling, so our findings do not support the electrostatic channeling hypothesis. Burst experiments confirmed that the mutants also did not interfere with intermediate formation at TS, suggesting that domain-domain communication was also unaffected. One mutant, K282E/R283E, was found to be TS-dead because of an impaired ability to form the covalent enzyme-CH_2H_4folate -dUMP complex prerequisite for chemical catalysis.

In the second part of this chapter, site-directed mutagenesis was used to probe domain-domain communication by apicomplexan TS-DHFR. Forcing *T. gondii* TS to remain in an obligate "open" conformation via C-terminal deletion (V610Am) was found to have no effect on domain-domain communication: full DHFR activity was observed in the presence and absence of TS ligands. Additionally, while very slow, the *T. gondii* C-terminal mutant was not TS dead and no TS intermediate was detected. Two *C. hominis* cross-over helix mutants, E205L and R210M, were also created. Point mutation of helix residues participating in hydrogen bonding interactions with the DHFR domain of the other half of the dimer, was found not to have a significant effect on enzyme activity or communication. The effects making of multiple point mutations or removing portions of the cross-over helix on enzyme kinetics, communication between the TS and DHFR

Reproduced with permission of the copyright owner. Further reproduction prohibited without permission.

domains, and between the two halves of the homodimeric enzyme will be a topic of further investigation.

In Chapter 5, "Use of Molecular Docking to Identify Non-Active Site Inhibitors of TS-DHFR" [104], molecular docking was successfully used to target the shallow groove between the two active sites of the *L. major* bifunctional enzyme. One of the predicted inhibitors, eosin B, was found to inhibit both the *L. major* TS and DHFR catalytic activities, without competing with substrates, suggesting that the non-active site region, unique to bifunctional enzymes, represents a valid therapeutic target. When Arg 283, a key residue to which eosin B is predicted to bind, is mutated to glutamate, eosin B only minimally inhibits the TS-DHFR reaction.

Consistent with the mutagenesis results presented in Chapter 4, binding of eosin B in the putative channeling region did not produce an accumulation of H_2folate. Therefore, rather than impeding a conformational associated with substrate channeling, we now believe that the most likely mechanism of inhibition by eosin B is via interference with conformational changes associated with domain interactions.

Eosin B was found to be a 180 μM IC_{50} inhibitor of the *T. gondii* TS-DHFR reaction in both biochemical and cell culture assays. Partial reversal of eosin inhibition by leucovorin led to the identification of folate transporter activity in *T. gondii*. Kristen Massimine in Dr. Joiner's lab is currently attempting to clone and heterologously express candidate folate transporter genes from *T. gondii* and *P. falciparum*. Dr. Amy C. Anderson's group is currently in the process of attempting to co-crystallize eosin and *T. gondii* TS-DHFR. Once this is accomplished, we plan to functionalize eosin B to improve potency and selectivity for the *T. gondii* enzyme. We also have plans to link eosin to an

Reproduced with permission of the copyright owner. Further reproduction prohibited without permission.

established DHFR active site inhibitor to develop a bifunctional inhibitor for the *T. gondii* bifunctional TS-DHFR enzyme. Eosin B was found to be a weaker inhibitor of *P. falciparum* and *C. hominis* TS-DHFR in biochemical assays. In cell culture however, eosin was a 100 nM IC_{50} antagonist of *P. falciparum* proliferation; worth pursuing even if the drug is hitting additional targets.

With *C. hominis*, a new non-active site region, between the DHFR domain and the cross-over helix, was targeted using the docking program,GLIDE. Two of the predicted inhibitors, streptonigrin and flavin mononucleotide, were found to have activity against *C. hominis* TS-DHFR. Preliminary data suggests that inhibition of DHFR activity is impaired by mutation of the cross-over helix (E205L or R210M), consistent with the predicted binding location. If the binding location is confirmed by co-crystallization, these inhibitors (or other molecules found to bind without inhibiting activity) will be functionalized and creation of a bifunctional inhibitor will be considered. Co-crystalization may also aid in resolution of the disordered portion of the linker region in the *P. falciparum* TS-DHFR structure.

The non-active site region targeted in *C. hominis* TS-DHFR is near the proposed mRNA binding site in *P. falciparum* [8]. It is unknown whether *C. hominis*, *T. gondii*, or *L. major* participate in translational repression, but this is a topic of future investigation. Other mechanistic questions which could have implications for the development of non-active site inhibitors include the mechanism of TS half-sites reactivity (random or sequential?) and the role of the third and final enzyme in the catalytic cycle, SHMT. It is possible that SHMT complexes with the bifunctional TS-DHFR enzyme, or otherwise

Reproduced with permission of the copyright owner. Further reproduction prohibited without permission.

modulates TS-DHFR enzymatic activity. SHMT is also a potential target for drug design [133].

A final direction worth pursuing is the significance of folylpolyglutamate versus folylmonoglutamate substrates. Folylmonoglutamate substrates were used in this study due to the relative ease of synthesizing tritiated forms, and because the precedent in the literature is almost exclusive use of monoglutamyl folates. In nature however, folates typically possess 3-9 γ-linked glutamyl moieties in a distribution that is somewhat species dependent [6]. There is evidence to suggest that inclusion of the polyglutamyl group may impact mechanistic and functional conclusions. It is well established that there is ordered binding at TS, with dUMP binding first, followed by the monoglutamyl form of CH_2H_4folate. A study using folylpolyglutamate substrates, however, demonstrated that the polyglutamyl folates have higher affinity for TS, abolishing the order of binding and inducing a conformational change in the absence of dUMP [98]. Residues comprising the *L. casei* binding site for the polyglutamyl portion of folylpolyglutamate correspond to Lys 282, Arg 283, and Arg 287 in *L. major* TS-DHFR [134], residues originally hypothesized to participate in electrostatic channeling and which, when mutated, impair TS activity. It has been shown that the interaction between TS and the polyglutamyl groups is primarily electrostatic [135], although we do not have evidence for electrostatic channeling by *L. major* TS-DHFR with monoglutamylfolate substrates, it may be worthwhile to repeat analysis of the mutants with polyglutamyl substrates.

High or growing rates of infection, emerging resistance, ineffective therapies, and unacceptable side-effects prove that there is an urgent need both for new therapies and new therapeutic targets for the treatment of protozoal infections. While it is possible to

Reproduced with permission of the copyright owner. Further reproduction prohibited without permission.

develop active site inhibitors in the absence of detailed mechanistic and structural information via such methodologies as high throughput screening, a more subtle and thorough understanding is necessary to identify and evaluate potential non-active site targets and inhibitors. Mechanistic features unique to bifunctional TS-DHFR which may be exploited in the development of non-active site inhibitors include: substrate channeling, TS-DHFR domain-domain communication, communication between halves of the homodimeric bifunctional enzyme, and coupled TS-DHFR translational autoregulation. This research provides important insights into the mechanistic and structure-function features of bifunctional TS-DHFR from four clinically relevant protozoal parasites. These studies, as well as the recently solved TS-DHFR crystal structures, also serve to stress significant differences between bifunctional TS-DHFR enzymes. The molecular docking results represent an important step toward establishing proof-of-principle that non-active site regions of bifunctional TS-DHFR can serve as effective molecular targets. We anticipate that non-active site inhibitors, specific for the bifunctional enzyme, will ultimately be developed for use in combination with active site therapies.

Reproduced with permission of the copyright owner. Further reproduction prohibited without permission.

References

1. Chu, E., Callender, M.A., Farrell, M.P. and Schmitz, J.C. (2003) Thymidylate synthase inhibitors as anticancer agents: from bench to bedside, *Cancer Chemother Pharmacol. 52*, S80-9.

2. Beverley, S. M., Ellenberger, T. E. and Cordingley, J. S. (1986) Primary structure of the gene encoding the bifunctional dihydrofolate reductase-thymidylate synthase of Leishmania major, *Proc Natl Acad Sci U S A. 83*, 2584-8.

3. Roos, DS. (1993) Primary structure of the dihydrofolate reductase-thymidylate synthase gene from Toxoplasma gondii, *J Biol Chem. 268*, 6269-80.

4. Grumont, R.,Washtien, W. L., Caput, D. and Santi, D. V. (1986) Bifunctional thymidylate synthase-dihydrofolate reductase from Leishmania tropica: sequence homology with the corresponding monofunctional proteins, *Proc Natl Acad Sci U S A. 83*, 5387-91.

5. Grumont, R., Sirawaraporn, W. and Santi, D. V. (1988) Heterologous expression of the bifunctional thymidylate synthase-dihydrofolate reductase from Leishmania major, *Biochemistry. 27*, 3776-84.

6. Knighton, D. R., Kan, C. C., Howland, E., Janson, C. A., Hostomska, Z., Welsh, K. M., and Matthews, D. A. (1994) Structure of and kinetic channelling in bifunctional dihydrofolate reductase-thymidylate synthase, *Nat Struct Biol. 1*, 186-94.

7. Vasquez, J.R., Gooze, L., Kim, K., Gut, J., Petersen, C. and Nelson, R.G. (1996) Potential antifolate resistance determinants and genotypic variation in the bifunctional dihydrofolate reductase-thymidylate synthase gene from human and bovine isolates of Cryptosporidium parvum, *Mol Biochem Parasitol. 79*, 153-65.

8. Yuvaniyama, J., Chitnumsub, P., Kamchonwongpaisan, S., Vanichtanankul, J., Sirawaraporn, W., Taylor, P., Walkinshaw, M. D. and Yuthavong, Y. (2003) Insights into antifolate resistance from malarial DHFR-TS structures, *Nat Struct Biol. 10*, 357-65.

9. O'Neil, R. H., Lilien, R. H., Donald, B. R., Stroud, R. M., and Anderson, A. C. (2003) Phylogenic classification of protozoa based on the structure of the linker domain in the bifunctional enzyme, dihydrofolate reductase-thymidylate synthase, *J Biol Chem. 278*, 52980-7.

10. Roland, A. R. (1996) *Opportunistic Complications of HIV. 5*. 81-107.

11. Luft, B. J. and Remington, J. S. (1992) Toxoplasmic encephalitis in AIDS, *Clin*

Reproduced with permission of the copyright owner. Further reproduction prohibited without permission.

Infect Dis. 15, 211-22.

12. Ferreira, M. S. and Borges, A.S. (2002) Some aspects of protozoan infections in immunocompromised patients—a review, *Mem. Inst. Oswaldo Cruz. 97*, 443-57.

13. Nelson, R. and Rosowsky, A. (2001) Dicyclic and tricyclic diaminoprimidine derivatives as potent inhibitors of Cryptosporidium parvum dihydrofolate reductase: structure-activity and structure-selectivity correlations, *Antimicrob Agents Chemother. 45*, 3293-303.

14. Mead, J.R. (2002) Cryptosporidiosis and the challenges of chemotherapy, *Drug Resistance Updates. 5*, 47-57.

15. Tzipori, S. (1998) Cryptosporidiosis: Laboratory Investigations and Chemotherapy, *Adv. Parasit. 40*, 187-221.

16. Guerrant, R. (1997) Cryptosporidiosis: An Emerging, Highly Infectious Threat, *Emerging Infect. Diseases. 3*, 51-7.

17. Current, W., Reese, N., Ernst, J., Bailey, W., Heyman, M. and Weinstein, W. (1983) Human Cryptosopridiosis in Immunocompetent and Immunodeficient Persons, *New Eng. J. Med*, 1252-7.

18. Cordell, R. and Addiss, D. (1994) Cryptosporidiosis in child care settings: a review of the literature and recommendations for prevention and control, *Pediatr Infect Dis J. 13*, 310-7.

19. Frick, C. and Crabb, J. (1998) Water-borne cryptosporidiosis: detection methods and treatment, *Adv. Pasit. 40*, 237-74.

20. Neill, M., Rice, S., Ahmad, N., and Flanigan, T (1996) Cryptosporidiosis: an unrecognized cause of diarrhea in elderly hospitalized patients, *Clin. Infect. Dis. 22*, 167-70.

21. Dillingham, R.A., Lima, A.A., and Guerrant, R.L. (2002) Cryptosporidiosis: epidemiology and impact, *Microbes Infect. 4*, 1059-66.

22. Hill, D. and Dubey, J. P. (2002) Toxoplasma gondii: transmission, diagnosis and prevention, *Clin Microbiol. Infect. 8*, 634-40.

23. Aspinall, T.V., Joynson, D.H., Guy, E., Hyde, J.E., and Sims, P.F. (2002) The molecular basis of sulfonamide resistance in Toxoplasma gondii and implications for the clinical management of toxoplasmosis, *J Infect Dis. 185*, 1637-43.

24. Georgiev, V. S. (1994) Mangement of toxoplasmosis, *Drugs. 48*, 179-88.

Reproduced with permission of the copyright owner. Further reproduction prohibited without permission.

25. Miller, L.H., Baruch, D.I., Marsh, K. and Doumbo, O.K. (2002) The pathogenic basis of malaria, *Nature. 415*, 673-9.

26. Cowman, A. F. (2001) Functional analysis of drug resistance in Plasmodium falciparum in the post-genomic era, *Int J Parasitol. 31*, 871-8.

27. Ridley, R.G. (2002) Medical need, scientific opportunity and the drive for antimalarial drugs, *Nature. 415*, 686-93.

28. Stechmann, A. and Cavalier-Smith, T. (2002) Rooting the eukaryote tree by using a derived gene fusion, *Science. 297*, 89-91.

29. Stroud, R. M. (1994) An electrostatic highway, *Nat Struct Biol. 1*, 131-4.

30. Johnson, E.F., Hinz, W., Atreya C.E., Maley, F. and Anderson, K.S. (2002) Mechanistic characterization of Toxoplasma gondii thymidylate synthase (TS-DHFR)-dihydrofolate reductase. Evidence for a TS intermediate and TS half-sites reactivity, *J Biol Chem. 277*, 43126-36.

31. Myllykallio, H., Lipowski, G., Leduc, D., Filee, J., Forterre, P., and Liebl, U. (2002) An alternative flavin-dependent mechanism for thymidylate synthesis, *Science. 297*, 105-7.

32. Chu, E., Takimoto, C.H., Voeller, D., Grem, J.L., Allegra, C.J. (1993) Specific binding of human dihydrofolate reductase protein to dyhydrofolate reductase messenger RNA in vitro, *Biochemistry. 32*, 4756-60.

33. Chu, E. and Allegra, C.J. (1996) The role of thymidylate synthase in cellular regulation, *Adv Enzyme Regul. 36*, 143-63.

34. Tai, N., Ding, Y., Schmitz, J.C. and Chu, E. (2002) Identification of critical amino acid residues on human dihydrofolate reductase protein that mediate RNA recognition, *Nucleic Acids Res. 30*, 4481-8.

35. Liu, J., Schmitz, J.C., Lin, X., Tai, N., Yan, W., Farrell, M., Bailly, M., Chen, T. and Chu, E. (2002) Thymidylate synthase as a translational regulator of cellular gene expression, *Biochim Biophys Acta. 1587*, 174-82.

36. Zhang, K. and Rathod, P. K. (2002) Divergent regulation of dihydrofolate reductase between malaria parasite and human host, *Science. 296*, 545-7.

37. Hardy, L.W., Finer-Moore, J.S., Montfort, W.R., Jones, M.O., Sant, D.V., and Stroud, R.M.. (1987) Atomic structure of thymidylate synthase: target for rational drug design, *Science. 235*, 448-55.

38. Maley, F., Pedersen-Lane, J. and Changchien, L. (1995) Complete restoration of

Reproduced with permission of the copyright owner. Further reproduction prohibited without permission.

activity to inactive mutants of Escherichia coli thymidylate synthase: evidence that E. coli thymidylate synthase is a half-the-sites activity enzyme, *Biochemistry. 34*, 1469-74.

39. Saxl, R. L., Changchien, L.-M., Hardy, L. W., and Maley, F. (2001) Parameters affecting the restoration of activity to inactive mutants of thymidylate synthase via subunit exchange: further evidence that thymidylate synthase is a half-of-the-sites activity enzyme, *Biochemistry. 40*, 5275-82.

40. Danenberg, P.V. and Danenberg, K.D. (1978) Effect of 5, 10-methylenetetrahydrofolate on the dissociation of 5-fluoro-2'-deoxyuridylate from thymidylate synthetase: evidence for an ordered mechanism, *Biochemistry. 17*, 4018-24.

41. Spencer, H. T., Villafranca, J.E. and Appleman, J. R. (1997) Kinetic scheme for thymidylate synthase from Escherichia coli: determination from measurements of ligand binding, primary and secondary isotope effects, and pre-steady-state catalysis, *Biochemistry. 36*, 4212-22.

42. Carreras, C.W. and Santi, D.V. (1995) The catalytic mechanism and structure of thymidylate synthase, *Annu Rev Biochem. 64*, 721-62.

43. Anderson, A.C., O'Neil, R.H., DeLano ,W.L. and Stroud, R.M. (1999) The structural mechanism for half-the-sites reactivity in an enzyme, thymidylate synthase, involves a relay of changes between subunits, *Biochemistry. 38*, 13829-36.

44. Galivan, J.H., Maley, G.F. and Maley, F. (1976) The effect of substrate analogs on the circular dichroic spectra of thymidylate synthetase from Lactobacillus casei, *Biochemistry. 15*, 356-62.

45. Danenberg, K.D. and Danenberg, P.V. (1979) Evidence for a sequential interaction of the subunits of thymidylate synthetase, *J Biol Chem. 254*, 4345-8.

46. Donato, H. Jr., Aull, J.L., Lyon, J.A., Reinsch, J.W., and Dunlap, RB (1976) Formation of ternary complexes of thymidylate synthetase as followed by absorbance, fluorescence, and circular dichroic spectra and gel electrophoresis, *J Biol Chem. 251*, 1303-10.

47. Moore, M.A., Ahmed, F. and Dunlap, R.B. (1986) Trapping and partial characterization of an adduct postulated to be the covalent catalytic ternary complex of thymidylate synthase, *Biochemistry. 25*, 3311-7.

48. Perry, K.M., Carreras, C.W., Chang, L.C., Santi, D.V., and Stroud, R.M. (1993) Structures of thymidylate synthase with a C-terminal deletion: role of the C-terminus in alignment of 2'-deoxyuridine 5'monophosphate and 5,10-

Reproduced with permission of the copyright owner. Further reproduction prohibited without permission.

methylenetetrahydrofolate, *Biochemistry. 32*, 7116-25.

49. Rathod, P.K. and Phillips, M.A. (2003) Prized malaria drug target nailed, *Nat Struct Biol. 10*, 316-8.

50. Stone, S.R. and Morrison, J.F. (1984) Catalytic mechanism of the dihydrofolate reductase reaction as determined by pH studies, *Biochemistry. 23*, 2753-8.

51. Stone, S.R. and Morrison, J.F. (1982) Kinetic mechanism of the reaction catalyzed by dihydrofolate reductase from Escherichia coli, *Biochemistry. 21*, 3757-65.

52. Thillet, J., Adams, J.A. and Benkovic, S.J. (1990) The kinetic mechanism of wild-type and mutant mouse dihydrofolate reductases, *Biochemistry. 29*, 5195-202.

53. Cayley, P.J., Dunn, S.M., and King, R.W. (1981) Kinetics of substrate, coenzyme, and inhibitor binding to Escherichia coli dihydrofolate reductase, *Biochemistry. 20*, 874-9.

54. Fierke, C., Johnson, K. A., and Benkovic, S.J. (1987) Construction and evaluation of the kinetic scheme associated with dihydrofolate reductase from Escherichia coli, *Biochemistry. 26*, 4085-92.

55. Liang, P-H. and Anderson, K.S. (1998) Kinetic reaction scheme for the dyhydrofolate reductase domain of the bifunctional thymidylate synthase-dihydrofolate reductase from Leishmania major, *Biochemistry. 37,* 12206-12.

56. Liang, P-H. and Anderson, K.S. (1998) Substrate channeling and domain-domain interactions in bifunctional thymidylate synthase-dihydrofolate reductase, *Biochemistry. 37*, 12195-205.

57. Hyde, C.C., Ahmed, S.A., Padlan, E.A., Miles, E.W. and Davies, D.R. (1988) Three-dimensional structure of the tryptophan synthase alpha 2 beta 2 multienzyme complex from Salmonella typhimurium, *J Biol Chem. 263*, 17857-71.

58. Ovadi, J. (1991) Physiological significance of metabolic channelling, *J Theor Biol. 152*, 1-22.

59. Anderson, K. S., Miles, E. W. and Johnson, K. A. (1991) Serine modulates substrate channeling in tryptophan synthase. A novel intersubunit triggering mechanism, *J Biol Chem. 266*, 8020-33.

60. Anderson, K.S., Kim, A.Y., Quillen, J. M., Sayers, E., Yang, X-J. and Miles, E. W. (1995) Kinetic characterization of channel impaired mutants of tryptophan

Reproduced with permission of the copyright owner. Further reproduction prohibited without permission.

synthase, *J Biol Chem. 270*, 29936-44.

61. Schlichting, I., Yang, X-J., Miles, E. W., Kim, A.Y., and Anderson, K. S. (1994) Structural and kinetic analysis of a channel-impaired mutant of tryptophan synthase, *J Biol Chem. 269*, 26591-93.

62. Thoden, J., Holden, H., Wesenberg, G., Raushel, F. and Rayment, I. (1997) Structure of carbamoyl phosphate synthetase: a journey of 96 A from substrate to product, *Biochemistry. 36*, 6305-16.

63. Anderson, K. S. (1999) Fundamental mechanisms of substrate channeling, *Methods Enzymol. 308*, 111-45.

64. Crawford, I. P. and Johnson, L. M. (1963) Mutants of E. coli defective in the B protein of tryptophan synthetase, *Genetics. 48*, 725-36.

65. Meek, T. D., Garvey, E. P., and Santi, D. V. (1985) Purification and characterization of the bifunctional thymidylate synthetase-dihydrofolate reductase from methotrexate-resistant Leishmania tropica, *Biochemistry. 24*, 678-86.

66. Ripoll, D.R., Faerman, C.H., Axelsen, P.H., Silman, I. and Sussman, J. L. (1993) An electrostatic mechanism for substrate guidance down the aromatic gorge of acetylcholinesterase, *Proc Natl Acad Sci U S A. 90*, 5128-32.

67. Koppenol, W.H. and Margoliash, E. (1982) The asymmetric distribution of charges on the surface of horse cytochrome c. Functional implications., *J Biol Chem. 257*, 4426-37.

68. Tan, R.C., Truong, T. N., McCammon, J. A., and Sussman, J. L. (1993) Acetylcholinesterase: electrostatic steering increases the rate of ligand binding, *Biochemistry. 32*, 401-3.

69. Getzoff, E.D., Tainer, J.A., Weiner, P.K., Kollman, P.A., Richardson, J.S. and Richardson, D.C. (1983) Electrostatic recognition between superoxide and copper, zinc superoxide dismutase, *Nature. 306*, 287-90.

70. Getzoff, E.D., Cabelli, D.E., Fisher, C.L., Parge, H.E., Viezzoli, M.S., Banci, L. and Hallewell, R.A. (1992) Faster superoxide dismutase mutants designed by enhancing electrostatic guidance, *Nature. 358*, 347-51.

71. Elcock, A. H., Potter, M. J., Matthews, D. A., Knighton, D. R. and McCammon, J.A. (1996) Electrostatic channeling in the bifunctional enzyme dihydrofolate reductase-thymidylate synthase, *J Mol Biol. 262*, 370-4.

72. Elcock, A.H., Huber, G.A., and McCammon, J.A. (1997) Electrostatic channeling

Reproduced with permission of the copyright owner. Further reproduction prohibited without permission.

of substrates between enzyme active sites: comparison of simulation and experiment, *Biochemistry. 36*, 16049-58.

73. Blakley, R.L. (1960) Crystalline dihydropteroylglutamic acid, *Nature. 188*, 231-2.

74. Matthews, C.K. and Huennekens, F.M. (1960) Enzymatic preparation of the l, L-diastereoisomer of tetrahydrofolic acid, *J. Biol. Chem. 235*, 3304-3308.

75. Curthoys, N.P., Scott, J. M. and Rabinowitz, J. C. (1972) Folate coenzymes of Clostridium acidi-urici. The isolation of (l)-5,10-methenyltetrahydropteroyltriglutamate, its conversion to (l)-tetrahydropteroyltriglutamate and (l)-10-(14 C)formyltetrahydropteroyltriglutamate, and the synthesis of (l)-10-formyl-(6,7- 3 H 2)tetrahydropteroyltriglutamate and (l)-(6,7- 3 H 2)tetrahydropteroyltriglutamate, *J Biol Chem. 247*, 1959-64.

76. Dawson, R. M. C., Elliott, W. H. and Jones, K. M. (1969) *Data for Biochemical Research*, Oxford University Press, Oxford, UK.

77. Kallen, R. G. and Jencks, W. P. (1966) The dissociation constants of tetrahydrofolic acid, *J Biol Chem. 241*, 5845-50.

78. Barshop, B. A., Wrenn, R.F. and Frieden, C. (1983) Analysis of numerical methods for computer simulation of kinetic processes: development of KINSIM--a flexible, portable system, *Anal Biochem. 130*, 134-45.

79. Lorber, D. M. and Shoichet, B. K. (1998) Flexible ligand docking using conformational ensembles, *Protein Sci. 7*, 938-50.

80. Shoichet, B. K., Bodian, D. L. and Kuntz, I. D. (1992) Molecular docking using shape-descriptors, *J. Comput. Chem. 13*, 380-97.

81. Meng, E. C., Shoichet, B. K. and Kuntz, I. D. (1992) Automated docking with grid-based energy evaluation, *J. Comput. Chem. 13*, 505-24.

82. Shoichet, B. K. and Kuntz, I. D. (1993) Matching chemistry and shape in molecular docking, *Protein Eng. 6*, 723-32.

83. Gilson, M. K. and Honig, B. (1991), The inclusion of electrostatic hydration energies in molecular mechanics calculations, *J. Comput. Aided Mol. Des. 5*, 5-20.

84. Rashin, A. A. (1990), Hydration phenomena, classical electrostatics, and the boundary element method, *J. Phys. Chem. 94*, 1725-33.

85. Gilson, M. K. and Honig, B. H. (1987) Calculation of electrostatic potentials in an

Reproduced with permission of the copyright owner. Further reproduction prohibited without permission.

enzyme active site, *Nature. 330*, 84-6.

86. Guner, O. F., Hughes, D. W. and Dumont, L. M. (1991) An integrated approach to three-dimensional information management with MACCS-3D, *J Chem Inf Comput Sci. 31*, 408-14.

87. Meng, E. C., Gschwend, D. A., Blaney, J. M., and Kuntz, I. D. (1993) Orientational sampling and rigid-body minimization in molecular docking, *Proteins. 17*, 266-78.

88. Ferrin, T. E., Huang, C. C., Jarvis, L. E., and Langridge, R. (1988), The Midas display system, *J. Mol. Graph. 6*, 13-27, 36-7.

89. Friesner, R. A., Banks, J. L., Murphy, R., Halgren, T. A., Klicic, J., Mainz, D., Repasky, M., Knoll, E., Shaw, D., Shelley, M., J., P., Sander, L. and Shenkin, P. (2003) *J Med Chem*, in press.

90. Roos, D. S., Donald, R. G., Morrissette, N. S. and Moulton, A. L.(1994) Molecular tools for genetic dissection of the protozoan parasite Toxoplasma gondii, *Methods Cell Biol. 45*, 27-63.

91. Nakaar, V., Samuel, B. U., Ngo, E. O. and Joiner, K. A. (1999) Targeted reduction of nucleoside triphosphate hydrolase by antisense RNA inhibits Toxoplasma gondii proliferation, *J Biol Chem. 274*, 5083-7.

92. Desjardins, R. E., Canfield, C. J., Haynes, J. D. and Chulay, J. D. (1979) Quantitative assessment of antimalarial activity in vitro by a semiautomated microdilution technique, *Antimicrob Agents Chemother. 16*, 710-8.

93. Schwab, J.C., Afifi Afifi, M., Pizzorno, G., Handschumacher, R.E. and Joiner, K.A. (1995) *Toxoplasma gondii* tachyzoites possess an unusual plasma membrane adenosine transporter, *Mol Biochem Parasitol. 70*, 59-69.

94. Morrissette, N.S., Bedian, V., Webster, P. and Roos, D.S. (1994) Characterization of extreme apical antigens of Toxoplasma gondii, *Exp Parasitol. 79*, 445-59.

95. Karsten, V., Qi, H., Beckers, C.J., Reddy, A., Dubremetz, J.F., Webster, P. and Joiner, K.A. (1998) The protozoan parasite Toxoplasma gondii targets proteins to dense granules and the vacuolar space using both conserved and unusual mechanisms, *J Cell Biol. 41*, 1323-33.

96. Atreya, C.E., Johnson, E.F., Williamson, J., Chang, S-Y., Liang, P-H. and Anderson, K.S. (2002) Probing electrostatic channeling in protozoal bifunctional thymidylate synthase-dihydrofolate reductase using site-directed mutagenesis, *J Biol Chem. 278*, 28901-11.

Reproduced with permission of the copyright owner. Further reproduction prohibited without permission.

97. Trujillo, M., Donald, R. G. K., Roos, D. S., Greene, P. J. and Santi, D.V. (1996) Heterologous expression and characterization of the bifunctional dihydrofolate reductase-thymidylate synthase enzyme of Toxoplasma gondii, *Biochemistry. 35*, 6366-74.

98. Kamb, A., Finer-Moore, J.S. and Stroud, R.M. (1992) Cofactor triggers the conformational change in thymidylate synthase: implications for an ordered binding mechanism, *Biochemistry. 31*, 12876-84.

99. Finer-Moore, J. S., Montfort, W. R. and Stroud, R.M. (1990) Pairwise specificity and sequential binding in enzyme catalysis: thymidylate synthase, *Biochemistry. 29*, 6977-86.

100. Dev, I. K., Dallas, W. S., Ferone, R., Hanlon, M., McKee, D. D. and Yates, B. B. (1994) Mode of binding of folate analogs to thymidylate synthase. Evidence for two asymmetric but interactive substrate binding sites, *J Biol Chem. 269*, 1873-82.

101. Finer-Moore, J. S., Santi, D. V. and Stroud, R. M (2003) Lessons and conclusions from dissecting the mechanism of a bisubstrate enzyme: thymidylate synthase mutagenesis, function, and structure, *Biochemistry. 42*, 248-56.

102. Wattanarangsan, J., Chusacultanachai, S., Yuvaniyama, J., Kamchonwongpaisan, S. and Yuthavong, Y. (2003) Effect of N-terminal truncation of Plasmodium falciparum dihydrofolate reductase on dihydrofolate reductase and thymidylate synthase activity, *Mol Biochem Parasitol. 126*, 97-102.

103. Shallom, S., Zhang, K., Jiang, L. and Rathod, P. K. (1999) Essential protein-protein interactions between Plasmodium falciparum thymidylate synthase and dihydrofolate reductase domains, *J Biol Chem. 274*, 37781-6.

104. Atreya, C.E., Johnson, E.F., Irwin, J.J., Dow, A., Massimine, K.M., Coppens, I., Stempliuk, V., Beverley, S., Joiner, K.A., Shoichet, B.K. and Anderson, K.S. (2002) A molecular docking strategy identifies Eosin B as a non-active site inhibitor of protozoal bifunctional thymidylate synthase-dihydrofolate reductase, *J Biol Chem. 278*, 14092-100.

105. Anderson, K.S. and Johnson, K.A (1990) Detection of enzyme intermediates: lessons from EPSP synthase, *Chem Rev. 90*, 1131-49.

106. Variath, P., Liu, Y., Lee, T. T., Stroud, R. M. and Santi, D. V (2000) Effects of subunit occupancy on partitioning of an intermediate in thymidylate synthase mutants, *Biochemistry. 39*, 2429-35.

107. Dwyer, D. S. (2001) Electronic properties of the amino acid side chains contribute to the structural preferences in protein folding, *J Biomol Struct Dyn. 18*, 881-92.

Reproduced with permission of the copyright owner. Further reproduction prohibited without permission.

108. Shoichet, B. K., Leach, A. R., and Kuntz, I. D. (1999) Ligand solvation in molecular docking, *Proteins. 34*, 4-16.

109. Su, A. I., Lorber, D. M., Weston, G. S., Baase, W. A., Matthews, B. W. and Shoichet, B. K. (2001) Docking molecules by families to increase the diversity of hits in database screens: computational strategy and experimental evaluation, *Proteins. 42*, 279-93.

110. Tondi, D., Slomczynska, U., Costi, M. P., Watterson, D. M., Ghelli, S. and Shoichet, B. K. (1999) Structure-based discovery and in-parallel optimization of novel competitive inhibitors of thymidylate synthase, *Chem Biol. 6*, 319-31.

111. Shoichet, B. K., Stroud, R. M., Santi, D. V., Kuntz, I. D. and Perry, K. M. (1993) Structure-based discovery of inhibitors of thymidylate synthase, *Science. 259*, 1445-50.

112. Jones, T. R., Webber, S. E., Varney, M. D., Reddy, M. R., Lewis, K. K., Kathardekar, V., Mazdiyasni, H., Deal, J., Nguyen, D., Welsh, K. M., Webber, S., Johnston, A., Matthews, D. A., Smith, W. W., Janson, C. A., Bacquet, R. J., Howland, E. F., Booth, C. L., Herrmann, S. M., Ward, R.W., White, J., Bartlett, C. A. and Morse, C. A. (1997) Structure-based design of substituted diphenyl sulfones and sulfoxides as lipophilic inhibitors of thymidylate synthase, *J Med Chem. 40*, 677-83.

113. Bolin, J. T., Filman, D. J., Matthews, D. A., Hamlin, R. C. and Kraut, J. (1982) Crystal structures of Escherichia coli and Lactobacillus casei dihydrofolate reductase refined at 1.7 Å resolution. I. General features and binding of methotrexate, *J Biol Chem. 257*, 13650-62.

114. Reich, S. H., Fuhry, M. A., Nguyen, D., Pino, M. J., Welsh, K. M., Webber, S., Janson, C. A., Jordan, S. R., Matthews, D. A., Smith, W. W. *et al.* (1992) Design and synthesis of novel 6,7-imidazotetrahydroquinoline inhibitors of thymidylate synthase using iterative protein crystal structure analysis, *J Med Chem. 35*, 847-58.

115. Waheed, A. A., Rao, K. S. and Gupta, P. D. (2000) Mechanism of dye binding in the protein assay using eosin dyes, *Anal Biochem. 287*, 73-9.

116. McGovern, S. L., Caselli, E., Grigorieff, N. and Shoichet, B. K. (2002) A common mechanism underlying promiscuous inhibitors from virtual and high-throughput screening, *J Med Chem. 45*, 1712-22.

117. Li, J. B., Zhu, T. H., Cramer, C. J. and Truhlar, D. G.(1998) A new class IV charge model for extracting accurate partial charges from wave functions, *J. Phys. Chem. 102*, 1820-31.

Reproduced with permission of the copyright owner. Further reproduction prohibited without permission.

118. Schwab, J. C., Beckers, C. J., and Joiner, K. A. (1994) The parasitophorous vacuole membrane surrounding intracellular Toxoplasma gondii functions as a molecular sieve, *Proc Natl Acad Sci U S A. 91*, 509-13.

119. Desai, S. A. and Rosenberg, R. L. (1997) Pore size of the malaria parasite's nutrient channel, *Proc Natl Acad Sci U S A. 94*, 2045-9.

120. Allegra, C.J., Kovacs, J.A., Drake, J.C., Swan, J.C., Chabner, B.A. and Masur, H.1987) Potent in vitro and in vivo antitoxoplasma activity of the lipid-soluble antifolate trimetrexate, *J Clin Invest. 79*, 478-82.

121. Masur, H., Polis, M. A., Tuazon, C. U., Ogata-Arakaki, D., Kovacs, J. A., Katz, D., Hilt, D., Simmons, T., Feuerstein, I. and Lundgren, B. (1993) Salvage trial of trimetrexate-leucovorin for the treatment of cerebral toxoplasmosis in patients with AIDS, *J Infect Dis. 167*, 1422-6.

122. Massimine, K.M., Atreya, C. E., Anderson, K. S., Joiner, K. A. and Coppens, I. (2003) Toxoplasma gondii is capable of exogenous folate transport, *Molec. Biochem. Parasit.*, submitted.

123. Krungkrai, J., Webster, H.K., Yuthavong, Y (1989) De novo and salvage biosynthesis of pteroylpentaglutamates in the human malaria parasite, Plasmodium falciparum., *Mol Biochem Parasitol. 32*, 25-37.

124. Sirotnak, F.M. and Tolner, B. (1999) Carrier-mediated membrane transport of folates in mammalian cells, *Annu Rev Nutr. 19*, 91-122.

125. Gradler, U., Gerber, H. D., Goodenough-Lashua, D. M., Garcia, G. A., Ficner, R., Reuter, K., Stubbs, M. T. and Klebe, G. (2001) A new target for shigellosis: rational design and crystallographic studies of inhibitors of tRNA-guanine transglycosylase, *J. Mol. Biol. 306*, 455-67.

126. Schneider, G. and Bohm, H. J. (2002) Virtual screening and fast automated docking methods, *Drug Discov Today. 7*, 64-70.

127. Hardy, L.W., Matthews, W., Nare, B., and Beverley, S.M. (1997) Biochemical and genetic tests for inhibition of Leishmania pteridine pathways, *Exp Parasitol. 87*, 157-69.

128. Richard, D., Kundig, C., and Ouellette, M (2002) A new type of high affinity folic acid transporter in the protozoan parasite Leishmania and deletion of its gene in methotrexate-resistant cells, *J Biol Chem. 277*, 29460-7.

129. Hajduk, P. J., Meadows, R. P. and Fesik, S. W. (1997) Discovering high-affinity ligands for proteins, *Science. 278*, 497-9.

Reproduced with permission of the copyright owner. Further reproduction prohibited without permission.

130. Muchmore, S.W., Sattler, M., Liang, H., Meadows, R.P., Harlan, J.E., Yoon, H.S., Nettesheim, D., Chang, B.S., Thompson, C.B., Wong, S.L., Ng, S.L. and Fesik, S.W. (1996) X-ray and NMR structure of human Bcl-xL, an inhibitor of programmed cell death, *Nature. 381*, 335-41.

131. Shuker, S., Hajduk, P., Meadows, R. P. and Fesik, S. (1996) Discovering high-affinity ligands for proteins: SAR by NMR, *Science. 274*, 1531-4.

132. Atreya, C. E. and Anderson, K. S. (2003) Kinetic Characterization of Bifunctional Thymidylate Synthase-Dihydrofolate Reductase (TS-DHFR) from Cryptosporidium hominis: A Paradigm Shift for TS Activity and Channeling Behavior, *J Biol Chem,* submitted.

133. Alfadhli, S. and Rathod, P.K. (2000) Gene organization of a Plasmodium falciparum serine hydroxymethyltransferase and its functional expression in Escherichia coli, *Mol Biochem Parasitol. 100*, 283-91.

134. Maley, G.F., Maley, F. and Baugh, C.M. (1982) Studies on identifying the folylpolyglutamate binding sites of Lactobacillus casei thymidylate synthetase, *Arch Biochem Biophys. 216*, 551-8.

135. Kisliuk, R.L., Gaumont, Y., and Baugh, C.M. (1974) Polyglutamyl derivatives of folate as substrates and inhibitors of thymidylate synthetase, *J Biol Chem. 249*, 4100-3.

136. Hardy, L.W., Graves, K.L. and Nalivaika, E. (1995) Electrostatic guidance of catalysis by a conserved glutamic acid in Escherichia coli dTMP synthase and bacteriophage T4 dCMP hydroxymethylase, *Biochemistry 34*, 8422-32.

137. Federal Register (1982) *Rules and Regulations 53845*, Vol. 47, No. 230.

138. Montfort, W.R., Perry, K.M., Fauman, E.B., Finer-Moore, J.S., Maley, G.F., Hardy, L., Maley, F., and Stroud, R.M. (1990) Structure, multiple site binding, and segmental accommodation in thymidylate synthase on binding dUMP and an anti-folate, *Biochemistry, 29*, 6964-77.

139. Carreras, C. W., Climie, S. C. and Santi, D. V. (1992) Thymidylate synthase with a C-terminal deletion catalyzes partial reactions but is unable to catalyze thymidylate formation, *Biochemistry, 31*, 6038-44.

140. Cody, V., Galitsky, N., Luft, J. R., Pangborn, W., Rosowsky, A. and Queener, S. F. (2002) Structure-based enzyme inhibitor design: modeling studies and crystal structure analysis of Pneumocystis carinii dihydrofolate reductase ternary complex with PT653 and NADPH, *Acta Crystallogr D Biol Crystallogr, 58*, 946-54.

Reproduced with permission of the copyright owner. Further reproduction prohibited without permission.

141. Reyes, P., Rathod, P.K., Sanchez, D.J., Mrema, J.E., Rieckmann, K.H., and Heidrich, H.G. (1982) Enzymes of purine and pyrimidine metabolism from the human malaria parasite, Plasmodium falciparum, *Mol Biochem Parasitol*, *5*, 275-90.

142. Jiang, L., Lee, P.C., White, J., and Rathod, P.K. (2000) Potent and selective activity of a combination of thymidine and 1843U89, a folate-based thymidylate synthase inhibitor, against Plasmodium falciparum. *Antimicrob Agents Chemother*, *44*, 1047-50.

143. De Koning, H.P., Al-Salabi, M.I., Cohen, A.M., Coombs, G.H., and Wastling, J.M. (2003) Identification and characterisation of high affinity nucleoside and nucleobase transporters in Toxoplasma gondii. *Int J Parasitol*, *33*, 821-31.

144. Al Safarjalani,O.N., Naguib, F.N., and El Kouni, M.H. (2003) Uptake of nitrobenzylthioinosine and purine beta-L-nucleosides by intracellular Toxoplasma gondii. *Antimicrob Agents Chemother*, *47*, 3247-51.

Reproduced with permission of the copyright owner. Further reproduction prohibited without permission.